UNIVERSITÀ
DEGLI STUDI
FIRENZE

DOTTORATO DI RICERCA IN
SCIENZE CHIMICHE

CICLO XXIX

COORDINATORE Prof. PIERO BAGLIONI

Automated Multispectral 3D Image-based Modeling for Cultural Heritage applications

Settore Scientifico Disciplinare CHIM/12

Dottoranda
Dott. Emanuela Grifoni

Tutor
Prof. Stefano Legnaioli

Coordinatore
Prof. Piero Baglioni

Anni 2014/2017

Hic et Nunc

Table of Contents

Abbreviations List

AOTF	*Acousto-Optical Tunable Filter*
APS	*Advanced Photo System type-C*
AR	*Augmented Reality*
BFD	*Back Focus Distance*
BSM	*Blind Separation Methods*
CAVE	*Computer Automatic Virtual Environment*
CCD	*Charge-Coupled Device*
CH	*Cultural Heritage*
ChromaDI	*Chromatic Derivative Imaging*
CIE	*International Commission on Illumination*
CMOS	*Complementary Metal-Oxide Semiconductor*
CRI	*Color Rendering Index*
CT	*Computerized Tomography*
CVF	*Circular Variable Filters*
DEM	*Digital Elevation Model*
DLT	*Direct Linear Transformation*
DSLR	*Digital Single-Lens Reflex*
DSP	*Digital Signal Processor*
EDX	*Energy Dispersive X-ray*
EDXRF	*Energy Dispersive X-ray Fluorescence*
EFL	*Equivalent Focal Length*
EM	*Electromagnetic*
EOP	*Exterior Orientation Parameters*
EXIF	*Exchangeable image file format*
FFL	*Flange Focal Length*
FHW	*Foundation of the Hellenic World*
GAP	*Google Art Project*
HSI	*Hyperspectral Imaging*
IBM	*Image Based Modeling*
ICA	*Independent Component Analysis*
ICOM	*International Council of Museums*
ICP	*Iterative Closest Point*
ICT	*Information and Communications Technology*
InGaAs	*Indium Gallium Arsenide*
InSb	*Indium Antimonide*
IOP	*Interior Orientation Parameters*
IR	*Infrared*
IRFC	*Infrared False Color*
IR-M	*Infrared-Model*
KM	*Kubelka-Munk (Theory)*

LCTF	*Liquid Crystal Tunable Filter*
LVF	*Circular Linear Filters*
MCA	*Multi-Channel Analyzer*
MCT	*Mercury-Cadmium-Telluride*
MMI	*Maximixation of Mutual Information*
MS	*Multispectral*
MSI	*Multispectral Imaging*
MUG	*MUseum Generator*
MVS	*Multi-View Stereo*
NDT	*Non-Destructive Technique*
NIR	*NearInfrared*
NIT	*Non-Invasive Technique*
OE	*Ontology Engineering*
PCA	*Principal Component Analysis*
PRISMS	*Portable Remote Imaging System for Multispectral Scanning*
QE	*Quantum Efficiency*
RBM	*Range Based Modeling*
RGB	*Red Green Blue*
RGB-M	*Red Green Blue – Model*
RMS	*Root Mean Square*
SDD	*Silicon Drift Detector*
SfM	*Structure from Motion*
SIFT	*Scale Invariant Feature Transform*
SLR	*Single-Lens Reflex*
SMIRR	*Scanning Multispectral IR Reflectography*
SN	*Samples per node*
SOM	*Self-Organizing Map*
SPD	*Spectral Power Distribution*
SUMUS	*SUperfici MUltiSpettrali (project)*
SWIR	*Short Wave Infrared*
TGS	*HyperMuseum Theme Generator System*
ToF	*Time of Flight*
UCS	*User Coordinate System*
USI	*Ultraspectral Imaging*
UV	*Ultraviolet*
V-MUST.NET	*V-Must Thematic Network*
VIS	*Visible*
VR	*Virtual Reality*
WDXRF	*Wavelength Dispersive Analysis*
XRF	*X-Rays induced Fluorescence*

The view on immediate reality
has become a chimera
in the land of technology

W. Benjamin

Introduction

Project genesis

The historicized and confirmed shifting from analogue to digital technology has clearly revolutionized in every sense the art space. Each period has looked at the works of art with their own technical, environmental, and cultural interfaces. Once, André Malraux argued that since the introduction of the photography «the history of art (had been) the history of what (could) be photographed» (Malraux, 1957). Nowadays we might say that the history of art of the near future will be the history of what can be digitalized.

In recent years, the documentary survey of Cultural Heritage (CH) has experienced an enormous boost also thanks to the implementation and optimization of *Digital Photogrammetry*: the branch of the science of representation by which it became possible to determine the objective knowledge of reality starting from its digital representation.

The *Reality-Based 3D Modeling* was born from the convergence of photogrammetry — which has the measured object's documentation as its purpose — and *Computer Vision* — which aims to the automatism in computer-assisted generation of fine geometric and appearance detailed three-dimensional models.

While keeping in mind that the object of the studies on the tangible CH «is the artwork, physical material and concrete» (Bruschi, 1978), the scope of these technologies — generically referred as *Digital Imaging* — is to bring documentation, preservation and restoration of CH to a more computational oriented approach. Thanks to the large processing capacity, these applications can increment, supplement or partially replace the traditional heritage recording systems. They improve and extend the deductible information, so to revolutionize the practices of acquisition, analysis, and data dissemination.

With CH 3D modeling as an ordinary practice, the very realistic products obtained in a permanent digital form will be surely passed down to future generations for: historical documentation, cross-comparison, monitoring of shape & colors, simulation of aging deterioration, virtual reality/computer graphics applications, computer aided restoration, multimedia museum exhibitions, etc. (Remondino, 2011).

The only negative note is that, despite the large number of very impressive 3D results obtained by different research groups over the past decade, the systematic and targeted use of 3D surveying and modeling in the CH field is not yet employed as a default approach. This depends on the fact that it is an *in fieri* research, that still lacks of any form of standardization, therefore the operators must still take confidence with the switching from the previous technique to the new one.

As claimed by some scholars, the revolutionary impact of what is called *Virtual Reality* (VR) is multiplying considerably the learning rules. The conversion of an artwork in a digital format as an *Augmented Reality* (AR) object emphasizes in a broad sense its esthetical and physical knowledge because the AR interactive and perceptual process spreads its message and content. The learning process that takes place through the alternation of real and virtual phases develops redundancy and spatial contextualization of the information.

Generally, the use of 3D RBM is consolidated for all those works of art that are inherently three-dimensional, such as sculptures, archaeological artifacts and contexts. On the contrary, the most widespread tendency is to consider the paintings as two-dimensional objects on which apply all the different imaging techniques ignoring the depth information. The planar nature of a painting partly justifies this approach. However, the reverse side of the paintings can be highly informative and in some cases the deviation from the planarity both of the support and of the surface are relevant factors for conservators. Consequently, the detection of the punctual location of the painting layers is a current issue, so it arises the need to push forward the painting survey until obtaining a better spatially resolved imaging system in different bands of the electromagnetic spectrum (EM).

The 2D Multispectral (MS) digitization and the 3D modeling of easel paintings are common non-contact acquisition techniques that collect complementary information (spectral and spatial). Integrating the analysis of radiometric contents using 2D multispectral images and the 3D morphometric details of a painting in a single coordinate system can obviously enhance the potential insights into data analysis. Indeed, the usefulness to get a 3D model morphometrically correct and well detailed in the Infrared (IR) spectral band, in order to obtain a multiplicity of structural and spectral information in a single digital representation has been proved. It overcomes the limitations of traditional photography and help conservators, diagnosticians and art historians to broaden the range of deductive ability.

Over the last years, many research groups tried to develop three-dimensional recording techniques in different spectral bands. Usually, most of these already proposed combined systems lacks flexibility because they acquire data related to the same object or scene by different sensors or in different modes that require complex and time-consuming operations of registration. With the advent of the new 3D Data capture image-based methodologies, new scenarios that avoid the hardworking phase of registration are opening up.

Trying to bring together in a single solution all the instances above mentioned, a specific variant of 3D RBM integrated with the *Multispectral Imaging* (MSI) technique will be here introduced. As it will be described in the next sections, the 3D modeling procedure directly based on multispectral images that we propose is a good compromise in terms of flexibility, portability, cost and precision. The conceptual assumption is that the MSI is an extension of Color Imaging. Thus, the *Structure from Motion* (SfM) strategy is a much more flexible and easy way to render the different spectral bands, because there is no need neither to proceed to the registration nor to necessarily know the calibration parameters of the devices used. This has been possible thanks to the use of commercial, and open source software together with a multispectral digital camera covering the *Near Infrared* (NIR) band up to 1050 nm.

With this same method, it is also possible to get in output a single 3D model starting from a variety of input data such as: color images, UV Induced Fluorescence images, Thermal images, etc. In addition, analytical data such as X-Ray Fluorescence (XRF) can be easily registered directly on the 3D model.

Because of their suitability for the specific needs of the technical testing, a 14^{th} panel painting signed by Barnaba from Modena — preserved in the Museum of San Matteo in Pisa— and a 15^{th} panel painting — preserved in the Bellomo Museum in Siracusa — have been chosen as test panels for the method.

Essay Structure

The dissertation is divided into five parts. The first chapter contextualizes the thesis in the wide field of the documentation of Cultural Heritage: drawing inspiration from the pivotal W. Benjamin's essay, a critical discourse is hereby proposed on how *the works of art* is recorded, modeled, visualized and communicated *in the age of its digital reproduction*. The two chapter sections trace the history of the artistic documentation from the time of analogical photography up to the era of Digital Photogrammetry, and of the art content dissemination from the idea of the imaginary museum up to the current virtual museum. Considering 3D digitization as a conservation tool in itself, the birth of the art diagnostics as modern discipline is briefly mentioned.

The second chapter of this essay defines its theoretical framework. Assuming that all the surveying techniques used to carry out the research work are non-contact and non-destructive, I will report the theoretical basis of the Multispectral Imaging, of the Digital Photogrammetry, and of the X-Ray Fluorescence analysis (XRF), because each of these techniques have respectively provided information on the investigated works of art referring to spectral, morphometric and compositional data.

The third chapter is a review of the recent state of the art practices developed about the integration of 3D and MS data for CH, with particular reference to the combined acquisition systems used by different laboratories. Through the literature review, it is possible to identify the reason why the method that I propose could actually represent a valid and original alternative to the existing systems. In this same section, I also mentioned some of the case studies that have been addressed by my research team during the course of my Ph.D.

The fourth chapter is the core of my thesis work, with the development of an automated Photogrammetric and MS procedural modeling. The chapter focuses on the two case studies selected, and it describes all the methodologies, software packages and tools used. The general workflow implemented is systematically dissected: from the first data acquisition phase, to the data processing; from the dense point cloud creation until the textured model building. To verify the quality of the results and the reproducibility of the method, a quantitative evaluation approach for 3D models distance computing has been used.

In the fifth chapter, the XRF results are reported. This compositional analysis has been performed on the painting in order to obtain a qualitative characterization of the artist's palette and to have a set of data directly geo-referenceable on the 3D model.

Lastly, some conclusions are drawn and future perspectives are proposed.

1

Background.

The Work of Art in the Age of its Digital Reproduction

1.1 Documenting the Cultural Heritage. From photography to digital photogrammetry

Nowadays we can reasonably sustain that the increasingly widespread use of automated methodologies for 2D and 3D data acquisition, together with the Computerized Visual Analysis of the paintings, is a *de facto* representation of what might be considered as an epochal milestone.

Something similar happened as a consequence of the introduction of photographic practice in the field of the documentation of CH, between the end of the 19^{th} and the first decades of the 20^{th} century (Walsh, 2007). In fact, as initially happened with the products of the photographic technique, the technologically advanced diagnostic documentation methodologies are now going to profoundly change Art History in its operative habits. In the past, the attributive techniques were particularly favored, while today the needs of conservation, exhibition and communication are instead more easily fulfilled. It was indeed with the first applications of photographic techniques — real technological link with the 19^{th} *Connoisseurship* — that gave birth to the discipline of the art diagnostics as intended in its modern sense.

The transition between those two centuries was a very crucial historical moment for Italy, where the first signals of a novel generation of art historians and scientists who used photography and its branches as an indispensable tool to their job emerged, i.e. to do research, didactics, and preservation. However, the debate on the programmatic use of photography for the study and documentation of works of art developed simultaneously across Europe (Recine, 2006).

Starting from John Ruskin's statement, according to which the photographic medium «(has been) the most marvellous invention [...] capable of saving some evidence from the great public of wreckers» (Ruskin, 1846, 2010), we remind the first photographically illustrated book to be published commercially by W. H. Fox Talbot (poetically titled *The Pencil of Nature*, 1844 – 1846), (Signorini, 2007), and the important contribution of Giovanni Morelli. He was the first to use the medium of photography as a rigorous tool of investigation. Indeed, his "experimental investigative method", also called *scientific attributionism*, was based on the identification and recognition of formal isolated and unaware calligraphic details of a pictorial composition, more precisely validated by the use of the photographs (Cardinali, 2002). We might say that these three personalities and their respective influences well summarize the field in which photography has played and continues to play a key role: the global reading of an artistic document, analyzed as a formal *datum* in its material structure and released in its textual message.

Around 1870 the first small-medium photographic enterprises started a process of transformation of photography as a good of mass consumption. By then, Munsell, Alinari, Brogi, Ponti, and some foreign photographers who operate mainly in Italy such as James Anderson, became among the most important in the field of reproduction. In addition, the Ministry of Education gave start to the first photographic census of the Italian monuments. At the same time and with the same goal, the art historian Pietro Selvatico Estense drew up a project titled *Proposta per la riproduzione fotografica dei principali monumenti d'Italia*, which aimed at the formation of an utopian photographic museum. Through the collation of photographs, this museum would have to retrace the monumental history of Italy and constitute a more general visual history of art for educational purposes. In this regard, P. Selvatico intended the photography as an "excellent intermediary" for the visual education of the public, in full agreement with his contemporary Francesco Dall'Ongaro, who defined it as the most democratic of all the *translation* techniques. The theoretical basis of the *Proposal* was already enucleated in his essay *Sui vantaggi che la fotografia può portare all'arte*, a speech about the advantages of photography in art education and knowledge of CH. According to T. Serena (1997), the importance of Selvatico's more recent project, however, is conferred by the overcoming of the purely instrumental idea of photography, since it referred to issues of documentation in relation to the new ethics of preservative restoration. He had the merit of codifying the standards of representation and the grammar of normative interpretation by considering photography as the technological progress of traditional engraving techniques and directing the photographer's work according to the visual prerogatives of art historians. Selvatico was also the first to set up a real photographic "scientific" campaign even though the first official plan to use photographs to document the artwork's state of degradation before its restoration dates back only to 1889 (Costantini, 1986).

Before speaking about how the concept regarding a photographic museum has inspired André Malraux's later visionary idea of museum *without* *walls*, it is relevant to remember some other prominent figures and to retrace some other major milestones. Adolfo Venturi (1856-1941) and Bernard Berenson (1865-1959)[i] are among these. A. Venturi had the merit of setting up the first Art History course in an Italian University (1890). He also draw up the monumental and masterful *Storia dell'Arte Italiana*, published between 1901 and 1940 by Ulrico Hoepli with 11 volumes containing more than 18.000 photographs. He was a convinced user of the photographic medium as a scientific aid in the critical reading of the figurative text: famous is the speech he gave at the academic year opening (1904/1905) about the methodological approach «to view and to re-view», by initiating a philological method continued with Pietro Toesca, Lionello Venturi and Roberto Longhi. According to the opinion of the latter,

> «[...] without any means of overemphasis we might say that what concerns the rapid spread of art knowledge the invention of photography had a cultural significance slightly less than that of press [...]. Many historians today are ashamed to admit that much of their work is based on the photographs».

It is known that many historians, in the course of their academic careers, ended by collecting tens of thousands of photographs which were then transferred to archives, foundations, and photographic libraries — nowadays also on line — like those belonging to Luca Beltrami (1854-1933)[ii], Giuseppe Fiocco (1884-1972)[iii], Carlo Ludovico Ragghianti (1910-

[i] The photographic archive of B. Berenson is available at the web page: <http://web-archive.itatti.harvard.edu/berenson-library/collections/fototeca-photograph-archive>

[ii] Beltrami's collection is part of the Civic Photographic Archive of Milan. It is available at the web page: <http://archiviofotografico.milanocastello.it/it/content/storia>

[iii] The photographic archive of G. Fiocco is preserved at the Giorgio Cini Foundation, including about 730,000 photographs. Among these is also incorporated the Fund Berenson from Villa i Tatti, available at the web page: <http://www.cini.it/fototeca>. See also (Furlan, 2005).

1987)[iv], Giuliano Briganti (1918-1992)[v] and Federico Zeri (1921-1998)[vi]. We should not forget that already in 1892, the first Institute for Conservation and Promotion of documentary photography — the *National Photographic Cabinet* founded by the engineer Gargiolli — was active in Rome.

By all this, we deduce that art criticism — at least from A. Venturi — is a photographically induced and long monochromatically founded phenomenon, suffering the limits of its own working tools (black and white printing, two-dimensionality, subjectivity in shooting, etc.) (Smargiassi, 2015). From the picture presented above it is evident that each epoch has looked at the works of art with their own technical, environmental, cultural interfaces.

The newly born discipline of the art diagnostics lays its roots on those years (De Ruggeri, 2002; Marabelli, 2006; Cardinali & De Ruggeri, 2013). One of the first example was the Gräff's report at the *International Conference for the Study of scientific methods applied to the examination and the conservation of paintings* held in Rome in 1930. In his speech, Gräff related its attributive discoveries made by the systematic use of magnifying lenses, binocular microscope, raking light and photographic pictorial details shooting. His activity might be therefore considered the trait union between the Morellian attributive method through investigating procedures and the birth of the art diagnostic methods. In the same period, the early use of macro and microphotography made its way.

In a few years, such international meeting was followed by the foundation of some pioneering diagnostic laboratories, like the one in Moscow (1918),

[iv] The photographic archive of Ragghianti is available at the web page: <http://www.fondazioneragghianti.it/fototeca-2>

[v] <http://fototecabriganti.comune.siena.it:8085/>

[vi] <http://www.fondazionezeri.unibo.it/it/fototeca/fototeca-zeri>

the British Museum Research Laboratory (1919) and the Fogg Art Museum laboratory at the Harvard University (1925). The latter began to use radiography to identify the absorption degree of paint pigments. In the last instance, we can say that this gave birth to the Diagnostic Imaging. However, it was obvious from the beginning that the radiographic image showed some significant reading difficulties: the complex stratigraphy of a painting returned on a two-dimensional image did not help the data interpretation about the spatial depth position of each element.

In 1949, the restorer Augusto Vermeheren tried to solve this problem realizing a rudimental stereo-strati-radiographic equipment (fig. 1a): an X-rays tube, positioned on a sliding carriage, walked to a circumference arc track, allowing both the pendulum movement and the fixed positioning in two equally spaced points (Vermehren, 1952). The stereo-radiography was based on the possibility of reproducing the three-dimensional appearance of the structure of an object, acquiring X-rays of the same area on two separate plates with two irradiations from different positions.

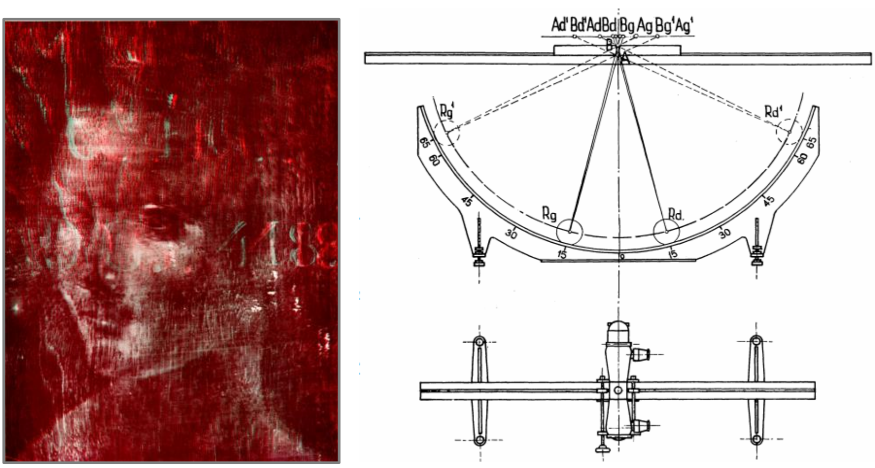

a) b)

Fig. 1 a)The stereo-radiographic image of a painting by Vermehren;
b) the sketch of the stereo-radiographic system.
Figure credits: (Vermehren, 1952).

The device combined the characteristics of both the strati-radiography and the stereo-radiography (Padfield, 2002). Pease (1946), Loose (1964) and Kozlowski (1960) later used the same method, with a few changes and improvements. The technological improvement of such a system is known as the *Computed Tomography* (CT), a technique ordinarily used for the structural study of works of art.

The need to obtain a better spatially resolved imaging system in different spectral bands in order to analyze the paint layers and their punctual location is still an open problem. In the wake of the primitive system set up by Vermeheren, many research groups in recent years — as we shall see in the following chapters — have tried to develop three-dimensional recording techniques in different spectral bands.

The succeeding developments that provided a huge contribution to the deep knowledge of the CH and to the affirmation of Diagnostic Imaging as a crucial technique for critical reading of the work of art are a chronicle of our times. This Ph.D project aims to be part of this attempt and it tries to give a speculative and practical contribution in this direction.

1.2 Collecting the Cultural Heritage. From the Museum "Without walls" to the Virtual Museum

As mentioned in the previous pages, the idea about a photographic museum that would provide a vast iconographic repertoire for education, comparative and documentary purposes according to a serial exposure model, is conceptually not far from André Malraux's visionary idea of museum "without walls". In 1947 the French novelist, art historian, and revolutionary politician published the *Imaginary Museum*, which along with Aby Warburg's figurative *Mnemosyne Atlas* (Mazzucco, 2011 and 2012), Hanne Darboven's *Cultural History 1980–1983 (*Dietrich, 1997) and Gerhard Richter's still ongoing *Atlas project* (Hage, 2016)[vii], was the forerunner of that "Virtual Museum" which is all-pervading our current digital age.

> The grandest consequence of photography is that it gives us the feeling of being able to have the whole world on our mind, as an anthology of images. Collect photographs is to collect the world (Sontag, 2004).

Susan Sontag's statement appears to refer exactly to Malraux's intent. In his dissertation, Malraux argued that since the introduction of the photography «the history of art for the last hundred years (had been) the history of what (could) be photographed» (Malraux, 1957) and that photographic reproduction allowed juxtaposing works of art from all places and times just in the space of an illustrated book:

> We, however, have far more great works available to refresh our memories than those, which even the greatest of museums, could bring together. For a "Museum Without Walls" (*musée imaginaire*) is coming into being, and it will carry infinitely farther that revelation of the world of art, limited perforce, which the "real" museums offer us within our walls (Malraux, 1957, p. 12).

In this statement, it is clear the abstract reference to Paul Valery, also cited — not coincidentally — by Walter Benjamin in the preface of his seminal essay *The Work of Art in the Age of Mechanical Reproduction* (1936):

> Art works will acquire a kind of ubiquity. [...] They will no longer exist only in themselves, but all of them will exist wherever there is someone. [...] One must expect that such innovations will transform the whole technique of the arts,

[vii] Begun in 1964. See generally throughout the complete work and publications referring to it on the artist's website <https://www.gerhard-richter.com/en/art/atlas>

> will consequently have an effect on creation itself, will go as far, perhaps, as to modify the very notion of art (Valery, La Conquete de l'ubiquite, 1934).

Malraux reiterated also W. Benjamin's thesis according to which the photographic reproduction decontextualizes and emancipates the work of art because it can «detect aspects of the original that are only accessible to the lens, which is adjustable and able to choose their point of view at will, but not to the human eye» (Benjamin, 2011). Therefore, just looking at the art from different points of view, in the last forty years of his life Malraux "dismounted" works of art from their original context and then reassemble montages of them in his book, thanks to the new exposure mode acquired by the photographic medium. Through this practice, he analyzed the changing role of photographic medium in allowing the works of art to be universally accessible on a new format and not more firmly constrained into the exhibition rooms of a museum. In a speech pronounced the 21st of June 1936, at the General Secretariat of the *International Association of Writers for the Defense of Culture*, he said:

> Now, the art of the masses is always an art of truth. Gradually the masses have ceased to go to art, to meet her on the walls of the cathedrals; but it so happens that, today, if the masses are not going to art, the fatal nature of technologies means that art is going to the masses. [...] From thirty years, every art has invented its reproduction tools: radio, cinema, photography. The destiny of art goes from a unique masterpiece, irreplaceable, to the masterpiece reproduced, up to the work done for its own reproduction to such an extent that the original no longer exists (Malraux, 1936).

Today the current digital technology is realizing all of this. A. M. Battro (2010) which was one of the first to provide the definition of "Virtual Museum", well summarized that the digital technology firstly separated photography from its paper support, then it promoted the extended projection of color images with high fidelity and, nowadays it is making the public free to navigate in virtual spaces, in real time, out of forced corridors and predetermined paths of art galleries (Huhtamo, 2010).

The shifting from analogue to digital technology has clearly revolutionized the art space, in every sense (Enhuber, 2015). Therefore, if it is right what Benjamin claimed in 1936, according to which

> [...] bringing things spatially and humanly is an indispensable need of the masses, as it is their tendency to overcoming the uniqueness of any data through the receipt of its reproduction

and that

> the technological reproducibility of the artworks changes the relation of the masses to the art (Benjamin, 2011),

we can certainly say that the increasing number of virtual visitors (or remote hosts) compared to the "real visitors" attests the current spontaneous trend to consult massively digital platforms for virtually enjoying artworks.

Consequently, all over the world many famous museums in the last twenty years have begun to digitize their own collections and to put exhibitions online in 3D virtual tour, in order to democratize art, making it easily accessible for a wider public and enriching the art consumer's experience, participation, and engagement. That is exactly what the industrialization of photographic technology did while democratizing all experiences by translating them into images, and to a full extent realizing the original promise in the photograph of the debuts (Sontag, 2004). Many researchers have debated on the role of new media in the museum, on the impact of the digital revolution in contemporary society, and on the effects of the digitalization of art space in accessibility and consumption of art (Hazan, 2007; Witcomb, 2007; Enhuber, 2015).

Computing is having a profound effect on how museums manage and make visible their collections. This can be defined as the new "Cultural (digital) Revolution", that is a point in space-time in which coalition of science, technology, and art is openly combined. This social phenomenon — which for someone is son of globalization — can be intended instead as a kind of attitude whereby each scientist and every citizen of a country may also feel citizens of the world, thanks to the cyber-heritage linking arts and cultures in an intercultural understanding (Liritzis, et al., 2015).

For what concern Europe, the ENUMERATE Core Survey 3 (Nauta & Heuvel, 2015) is very significant in providing a reliable baseline of statistical data about various aspects of digitization, digital preservation and online access to cultural heritage in Europe. Highlights of the report's findings are that the 84% of cultural institutions have a digital collection (fig. 2) even if just the 23% of the heritage collections is digitized; academic research is perceived as the most important reason to provide digital access to the collection (8,6%), followed by educational use of the collection (8,1%) and sales and commercial licensing (3%), at least (fig. 3).

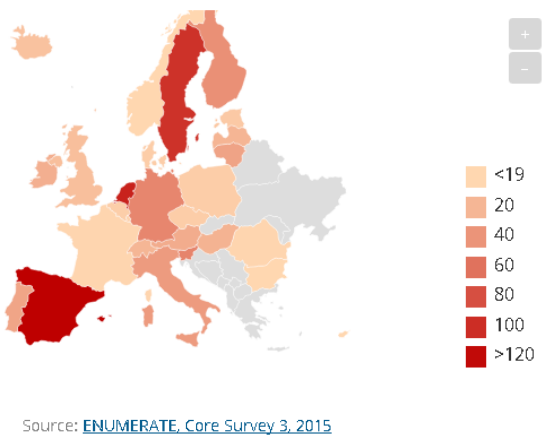

Fig. 2
Institutions with digital collections - responses per country (Enumerate Core Survey 3, 29/5/2015).
Figure credits: (http://pro.europeana.eu/enumerate/digital-heritage-indicators/institutions-with-digital-heritage-collections).

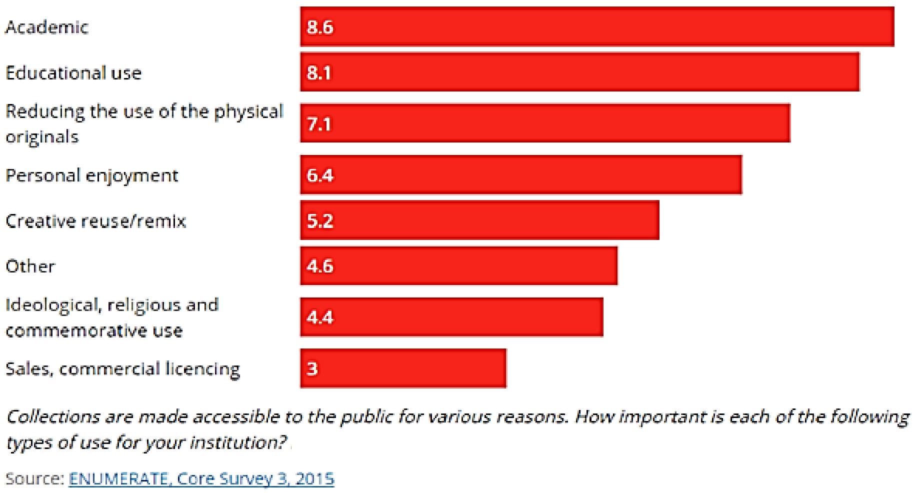

Fig. 3 The histogram plot shows the importance of different types of use of digital collections.
Figure credits: (http://pro.europeana.eu/enumerate/digital-heritage-indicators/importance-of-types-of-use-of-digital-collections).

Among the best-known multimedia digitization projects — referring both to museums than to other kind of institutions — there are certainly: the pioneering and ongoing *Tate Insight*[viii], the *Europeana Project*[ix] and *Google Art Project* (GAP) (Hart, 2011; Proctor, 2011).

The first one is on line since 1998. It is a comprehensive database of indexed images about over 65.000 artworks, thanks to which it is also possible to display many fragile work usually not exhibited for preservation reasons. The second one is the EU digital platform for cultural heritage. The European Commission launched it in 2008. It includes more than 50 million of digitized objects from libraries, archives, audio-visual archives, and museums. It currently brings together more than 2.200 collaborating institutions. The last one is a notable example for digitizing art space. It was launched in 2011 by the Google Cultural

[viii] <http://www.tate.org.uk/about/projects/insight-digitisation-tate-collection>
[ix] <http://www.europeana.eu/>

Institute. Upgraded in 2012 in a second generation-platform, it has so far digitized over 50.000 artworks, which are currently available online thanks to the collaboration with more than 150 institutions in 40 countries. In this case, the most innovative contribution is provided by the specific project called *Art Project Gigapixels*[x]. Using the professional panoramic heads CLAUSS RODEON VR Head HD and CLAUSS VR Head ST (St. John, 2016)[xi], Google Art team is able to create gigapixel images, whose super high-resolution allows users to zoom into brushstroke-level detail, magnifying finer points not appreciable to the naked eye at the distance that an exhibition imposes (fig. 4).

Evidently, this will be a promising and an intriguing tool for professional artistic and conservative documentation, useful for art lovers but mostly for specialists in the field, such as scholars, museum personnel, art historians, diagnosticians and restorers. The detailed inspection of such images could extend the traditional and conventional qualitative investigation of high quality artworks — what macrophotography "once" did — working as powerful base for sophisticated computer-based methods for paintings analysis, e.g. statistical pattern recognition and unsupervised extraction of visible features techniques (texture, outline shape, *craquelure*, spatial color distribution, etc.) (Lettner, et al., 2004; Lewis, et al., 2004; Legnaioli, et al., 2013; Liu, et al., 2013). Moreover, properly calibrated images (Berns, 2001) might provide an accurate color measurement across the entire surface of the painting to record the state of conservation of the investigated object at the acquisition time (Barni, et al., 2005) and to check the quality of eventual past restoration works, useful for future comparisons. Overall, by paraphrasing Malraux's

---

[x] <https://www.google.com/culturalinstitute/beta/usergallery/art-project-gigapixels/DAJiOwFKTTbQLQ?hl=en>

[xi] <https://www.google.com/culturalinstitute/beta/project/art-camera>

statement, it can be said that *the history of art will be the history of what can be digitized.*

Fig. 4 From left to right four increasing levels of magnification of the high-resolution digitized painting The Merchant Georg Gisze, Hans Holbein the Younger, 1532 (from Google Art Project Gigapixels).
Figure credits: (*https://www.google.com/culturalinstitute/beta/u/0/asset/the-merchant-georg-gisze/VwFTBKeaJVASog*).

Tracing an abstract straight line with what has been said above, therefore the Virtual Museum — broadly speaking — is today the obvious heir of the Malraux's *imaginary museum*. A place able to reduce further both physical and "mental" distance between the works of art exhibited in faraway real museums, conferring ubiquity to the tangible and intangible CH (special ICOM News: *Museums and Intangible Heritage*, 2003), and building a «universal digital memory» (Lévy, 2010).

However, the VM is emerging as complex entity that raises new issues and brings the museum facing new challenges. Several examples demonstrate in fact that the expression "virtual museum" covers a wide range of connotations, spanning from the generic digital applications or Computer Graphics up to VR systems.

«The new museum Web sites are only the first manifestation of the post-Internet museums» (Walsh, 2007). Indeed, some museums are promoting the use of advanced visualization tools that combine high-resolution, immersive projection-based technology (AR) and a 3D illusion of complete sense of presence, within the very physical space of the gallery. This is the case, for example, of one of the first VR application, namely a CAVE (*Computer Automatic Virtual Environment*) installed at the Foundation of the Hellenic World (FHW) in Athens in 1999 (Roussou, 2002).

Some others, not connected to a real museum environment, have even ventured in getting collections exclusively online. Existing solely in cyberspace, they are reversing the terms of the approach and thus they are creating the potential for a "real" tour of virtual museum rather than a virtual tour of "real" museum. Lastly, some systems — such as the pilot *HyperMuseum Theme Generator System* (TGS) (Meersman, De Bruyne, & Stuer, 2001) and the more recent Spanish *Museum Generator* (MUG)[xii] — allow generating automatically in a few minutes new personalized virtual museums in web format. They exploit the *Ontology Engineering* (OE) approach that works selecting a catalog of digital resources with meta-information organized in semantic formats, directly based on the specifications of the single end-user.

As it is evident, the quick boost of computing technology in this direction is very huge and it is not possible in this context to cover all the different applications, because it is not the aim of this Ph.D. thesis.

One of the most notable and excellent project — the *V-Must Thematic Network* (V-MUST.NET)[xiii] coordinated by CNR — has recently tried to outline the subtle above mentioned differences between digital collections, online archives and virtual museums[xiv]. In this regard, it provided a definition of the latter expression, which results to be currently the most complete, accepted and shared by the academic world:

[xii] <http://www.ximdex.com/en/xlabs/mug.html>

[xiii] < http: //www.v-must.net/home>

[xiv] For a bibliographic orientation on the subject, see at least the bibliography compiled by the UNESCO-ICOM Museum Information Centre, revised in September 2010: <http://icom.museum/fileadmin/user_upload/pdf/Bibliographies/20100908_Biblio_Virtual_Museums.pdf>.

> A virtual museum is a digital entity that draws on the characteristics of a museum, in order to complement, enhance, or augment the museum experience through personalization, interactivity, and richness of content. Virtual museums can perform as the digital footprint of a physical museum, or can act independently, while maintaining the authoritative status as bestowed by ICOM in its definition of a museum (Pinna, 2003); (Schweibenz, 2004); (Karp, 2004).
>
> In tandem with the ICOM mission of a physical museum, the virtual museum is also committed to public access; to both the knowledge systems embedded in the collections and the systematic, and coherent organization of their display, as well as to their long-term preservation. (V-Must Thematic Network, March 2014), (Hazan, et al., 2014).

It is worth saying that, although the preconditions for VR are available since 1990s, the cultural, aesthetic, sociological and scientific implications of the use of these technologies for heritage are still in the making. The abundance of publications emerged in recent years, investigating critical cultural theory and global Digital Heritage, attests the actual centrality of the issue (Cameron & Kenderdine 2007; Parry, 2013). Clearly, fundamental hermeneutical questions and the need for a thorough epistemological study on the communication of the virtual, on the learning's rules and on the quality of information developed by these new technologies, are emerging. «The interaction between real ontologies, the empirical perception of material culture (objects), and their virtual ontologies (the digital representations), creates new perspectives in the domain of data processing, data analysis, data sharing, data contextualization, and cultural transmission» (Liritzis, 2015). This is a very relevant topic, because, as M. Forte said, «it concerns *in toto* the next

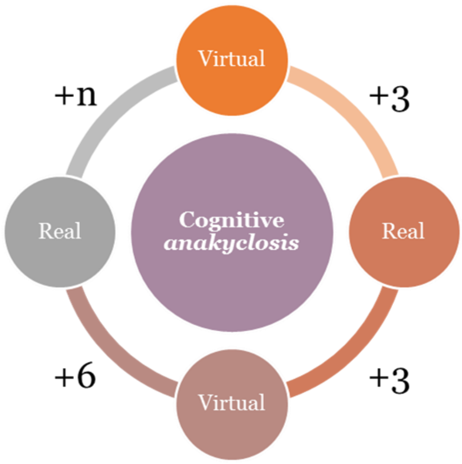

Fig. 5 Cognitive anacyclosis graphic scheme: In the progressive alternation of real and virtual, the learning stages will increase. Figure credits: (Forte, 2004).

generations of cultural communication and the awareness of the new collective memories that will live a nomadic and de-territorialized relationship with information» (Forte, 2004).

I consider very interesting the discourse about "Cognitive Anacyclosis" (*ἀνακύκλωσις, anakýklōsis*) and "Informative Echo" (fig. 5) proposed by this scholar because it well relates — in the last instance — with the aims of this thesis. He argues that the revolutionary impact of the virtual reality is to multiply considerably the learning rules: the conversion of an artwork in a digital format, provided with VR, with its interactive and perceptual process, emphasizes in a broad sense the physical knowledge of the object, because it spreads its message and content. The learning process that takes place through the alternation of real and virtual phases, develops redundancy and spatial contextualization of the information. The latter reframes itself, bouncing in different contexts and adding new levels and new itineraries (Forte, 2004).

A premise so broad — ranging from the discussion about the correlation between the photographic medium, art theory and art diagnostics; the evolution from the post-photographic museum in a post-Internet museum, the switching from the 2D analogical CH surveying in a 2D/3D CH digital surveying; until the evaluation of how this is ontologically influencing the dissemination, the communication and the scientific knowledge of the works of art — it is necessary to contextualize the goal of my thesis.

I would prove the usefulness to get a morphometrically correct and well detailed IR spectral band 3Dmodel (*Multi-source image fusion)*, in order to obtain a multiplicity of structural and spectral information in a single digital representation for broadening the range of deductive inquiry.

Whether this variant will have deemed valid results, it would be considered as a contribution to Diagnostic Imaging, able both of analytically pointing out and enriching with new, revealing dimensions any "text to be queried". This means that the analytical would correspond to that "synthetic summarizing moment", allowing a quick, synoptic and comparative reading of the artwork, which it is the ultimate purpose of Art Diagnostic.

Although the computer-based interpretive products obtained with this methodology are best suited for valid scientific inquiry, they could be enjoyed also by a wider public in museums, directly inside standard web pages or in custom on line galleries, by means of the new interactive visualization systems.

The brightest clarity of the image
did not suffice us,
for this seemed to wish just
as much to reveal something
as to conceal something.
Its revelation seemed to summon us
to teat the veil and to uncover the
mysterious background;
but at the same time
this all-illuminated total visibility
cast a spell over the eyes
and prevented them
from penetrating deeper.

F. Nietzsche

2
Theoretical Framework

2.1 Criteria of the technical approach

All techniques here proposed and used both for the characterization of the artworks selected as case studies, and for the development of three-dimensional MS documentation method, are *non-destructive* (NDTs) and *non-invasive* (NITs). They entail the least possible interaction with the art object, so to ensure its maximum integrity, at the end of being perfectly coherent with the art diagnostics requirements. Generally, the increasing demand of the minimal impact of diagnostic analysis on the constituent material is accompanied with the growing demand of the use of instruments directly *in situ*, to avoid any damaging displacement of the artworks. All our equipment for the data acquisition is portable and not bulky. The data processing partly takes place in real time and mostly in the laboratory.

Before moving to the theoretical discussion of the physical foundations of each techniques, so to have a better understanding of what is involved in their interaction with the artwork, it is necessary to make a distinction between destructive/non-destructive and invasive/non-invasive analysis (fig. 6).

There are slightly differing opinions at this regard, but it is quite accepted the consideration that destructive analysis do not preserve the structural integrity and functionality of the art material, and generally, they require a sampling. Whenever different analyses do not deteriorate the sample, maintaining it available for other analyses, than these techniques can be defined just invasive but non-destructive. On the other hand, non-invasive analyses instead require the condition of not altering the physical and the chemical conditions of the artwork, not interfering with the changing processes between the art object and the environmental (Poldi & Villa, 2006).

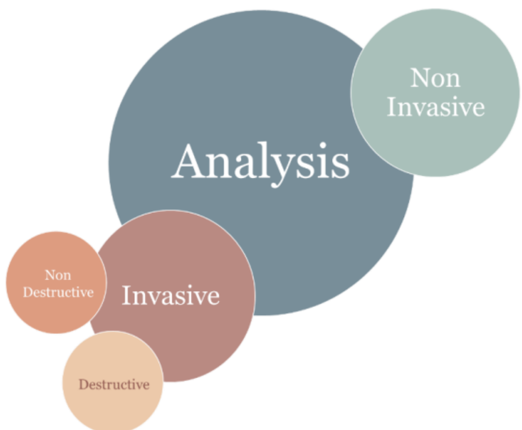

Fig. 6 Relational graph NDTS / NITs analysis.

Thus, the non-invasiveness of a technique corresponds to the capacity to not alter the system from a thermodynamic point of view. According to some scholars, microanalytical techniques that use incident ionizing particles on the artwork's surface providing absorption and re-emission of radiations — such as fluorescence — still involve an exchange of energy and they must be considered, in various ways, NITs.

In my opinion the latter sense is too stringent because these measures are usually punctual and very limited in time so as not to make any significant irreversible change in chemical and physical composition of materials. In summary we can say that Spectral Imaging, Digital Photogrammetry and X-Rays Induced Fluorescence — the techniques that we used — are all contactless surveys that rely on the use of electromagnetic (EM) radiation in all its energy spectrum without being neither destructive nor invasive.

2.2 Spectral Imaging

Spectral Imaging is based on techniques that record different images of an artifact, selectively detecting radiations of different wavelengths (λ) while the object's surface is irradiated with a continuous source that emits radiations in a wide portion of the electromagnetic spectrum (EM) (fig. 7), from Ultraviolet (UV) to Infrared range (IR).

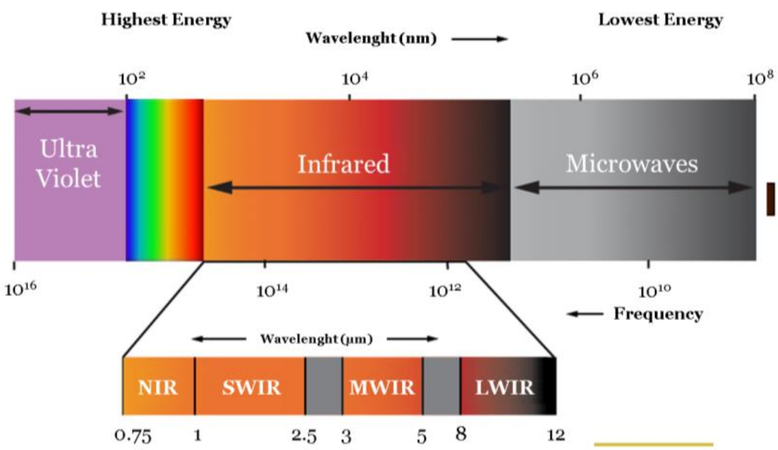

Fig. 7 EM spectrum.

Spectral Imaging was originally defined by Goetz in the late 1980s and discussed for remote sensing and astronomy (Goetz, 2009). It can be divided into *Color* (fig. 8*b*), *Multispectral* (MSI) (fig. 8*d*), *Hyperspectral* (HSI) (fig. 8*e*), and *Ultraspectral Imaging* (USI) according to its spectral resolution, number of bands, width, and contiguousness of bands (Liang, 2012).

MSI systems generally collect data in few and relatively noncontiguous wide spectral bands, typically measured in micrometers or tens of micrometers. While HSI systems can collect hundreds of spectral bands, USI systems can collect even more. Fig. 8*e* shows the concept of the hypercube data captured by a spectral imaging system. The spectral imaging data can be visualized as a three-dimensional (3D) cube or a stack of multiple two-dimensional (2D) images because of its intrinsic structure, in which the cube face is a function of the spatial coordinates and the depth is a function of λ.

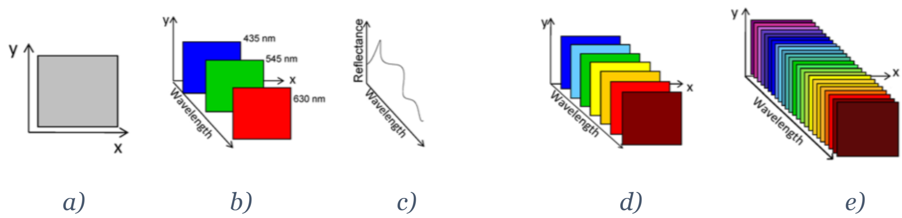

Fig. 8 a) Monochrome image; b) RGB Color Imaging; c) Spectroscopy; d) Multispectral Imaging; e) Hyperspectral imaging.
Figure credits: (Li, et al., 2013).

One of the most important advantages of this technique is that it can acquire reflectance, absorption, or fluorescence spectrum for each pixel of the image depending on the physical, chemical and geometric properties of the illuminated surface, i.e. the painting constituents: pigments, binding media, and varnishes.

By the 1990s, MSI — less than 10 spectral bands — was applied to imaging of old master paintings in museums and galleries (Burmester et al., 1993; Martinez, et al., 1993). Initially it was used to improve color accuracy of the images captured and for qualitative comparison between the bands. Later, Spectral Imaging was used to obtain reflectance spectra for pigment identification (Baronti, et al., 1998; Casini, et al., 1999; Liang, et al., 2005). Most pigment are transparent to NIR λ, hence images in the IR are useful for revealing the underdrawings and *pentimenti* — changes done by the artist himself during the painting creation process — beneath the paint (van Asperen de Boer, 1968; Liang, et al., 2013). A comparison between images in the visible spectral range with those in the NIR — called *reflectograms* — can also reveal damages to the paintings or past interventions as retouching.

The outer layer instead mainly absorbs UV radiations, as a consequence of their higher energetic wave-packets. They can induce fluorescence-emission phenomena (*Visible UV induced Fluorescence*) that differ from material to material and from pigment to pigment according to the chemical composition and the aging degree of the sample. This allows, for instance, to estimate the conservation state of varnishes or to obtain maps of retouching and restoration interventions performed with pigments, which may differ for the type of fluorescence although of the same color class of the original paint.

Comprehensive reviews on spectral imaging applications in art conservation and archaeology can be found in a number of reviews (Fischer & Kakoulli, 2006; Kubik, 2007; Liang, 2012).

2.2.1 Multispectral Acquisition System

Spectrophotometers acquire spectra with nanometric precision in a single spot (1D) while MSI systems acquire data along two spatial dimensions and one spectral dimension in snapshot and sequential modes. Currently, different kinds of systems are available to acquire MS images, ranging from commercial to experimental apparatus as MS scanners and imagers. They are generally categorized based on:

- Different detectors (Photomultiplier tube, Si-based *Charge-Coupled Device* (CCD) or *Complementary Metal-Oxide Semiconductor* (CMOS) used for the 350–1000 nm range, mechanically cooled *Indium Gallium Arsenide* (InGaAs) detector used for the 900–1700 nm range (*Short Wave Infrared* - SWIR) and *Indium Antimonide* (InSb) or *Mercury-Cadmium-Telluride* (MCT) arrays used for the 1000–2500 nm range, etc.).
- Dispersing system (interferometer, dispersive spectrometers often referred to prisms, gratings, or beam splitters used with whiskbroom and pushbroom imaging modes, etc.)
- Filtering technology used (sequential optical filters, electronically tunable filters used in spectral scanning instruments such as: *Acousto-Optical Tunable Filter* (AOTF), *Liquid Crystal Tunable Filter* (LCTF), *Circular and Linear Variable Filters* (CVF and LVF), etc.

The relative response depends on the performance of the imaging device, as well as on the spectral band used.

Waveband selection is mostly achieved by means of a scheme of filters — most often bandpass interference filters — fitted with an IR camera, which records the spatial distribution, and the set of multiband images is stacked as a sequence of acquisitions. To acquire a single image in the range of the filter, in some device — as ours — the filters are mounted on an internal motorized wheel between the lens and the detector. In some others, the filters are sequentially positioned in front of the lens. In these case, the spectral images set need to be registered and various algorithms can be used to compensate geometric distortion, longitudinal aberrations and ghosting introduced by the filters. Furthermore, such systems suffer from systematic errors such as blurring of the MS channels, which affects the reliability of spectral data and require optical calibration. Custom designed filter sets that have the same optical thickness will ensure that the image scale stay the same for different λ. Detector size limits in practice the spatial resolution because of mosaicking.

Many MS acquisition systems have been developed or adapted for the study of CH. For the specific interests of this thesis, we present only two that will be described in detail in the following chapters: the Multi-Vis-NIR scanner developed by CNR-INO's Cultural Heritage Group (SMIRR technique) (Daffara, et al., 2010) mentioned as an example of integrated device (section 3.3) and the DTA ChromaC4 MS camera that we used to carry the testing (section 4.2.1). However, we must also mention the two notable systems developed within large projects that have marked the advancement of this art diagnostic technique: the VASARI project (Martinez, et al., 2002) and the CRISATEL European project (Ribés, et al., 2005). The first one focused on the development of a 12 bands MS acquisition system based on a CCD and a filter-wheel tunable light source. The second one was based on a linear CCD mechanically displaced to acquire 20,000 vertical lines, used in conjunction with a dedicated synchronized lighting system. To cover the 380 nm to 1000 nm range this system used 13 interference filters — 10 in the visible and 3 in the NIR.

2.2.2 Color Imaging

The perceived color of an object is a function of the spectral reflectance of its surface, the spectral distribution of the illumination and the spectral sensitivities of the cones in the eye, at the least. A recorded color image is thus both device and illuminant dependent. When a surface is acquired under a given illuminant, it is impossible to estimate the surface color accurately under another illuminant in the absence of additional information on the spectral reflectance.

In conventional Color Imaging, each pixel is characterized by three components such as Red, Green and Blue. Theoretically, these three components are necessary and sufficient to synthesize any color from a colorimetric point of view, but conventional Color Imaging systems based on three primary colors present a number of limitations that result from their weak spectral resolution. A high spectral resolution allows a better estimation of the surface reflectance. This in turn permits a better characterization of its intrinsic physical properties regardless of the acquisition conditions (illuminant, acquisition device).

It is possible to acquire color-accurate images with conventional trichromatic sensors by working in adapted color spaces such as CIELAB (Berns, 2001). However systems that acquire more than three spectral components permit a better estimation of the reflectance. CIE recommends that MS acquisition systems acquire 31 bands between 400 nm and 700 nm — that is, one channel every 10 nm — but Berns (Berns, et al., 2005) states comparable spectral precision can be obtained using less than 10 bands. There is thus a great variability in the number of bands acquirable by MS acquisition systems.

2.2.3 Multispectral Imaging

The NIR radiation passes through the materials of the pictorial film and it is backscattered from the underlying layers. The IR reflectogram of the painting is created by recording the reflected radiation. The involved physical phenomena are related to the propagation of the IR radiation through the paint layers and they depending on the properties of the pigments, of the binder, together with the background's ability to reflect the incident radiation. Underdrawings made with materials that absorb IR, as metal tip, charcoal and graphite, have high visibility. Ever since the pioneering work of van Asperen de Boer in the 1960s (Van Asperen de Boer, 1969) in developing a Vidicon IR camera for imaging underdrawings, it has been known that pigments are most transparent to IR radiation in the 1 μm to 2 μm range.

The physical magnitude involved is the *Diffuse Reflection Factor (R)*. It is described by the Kubelka–Munk (KM) theory (Kubelka & Munk, 1931) as the percentage ratio between the intensity of the incident light and the intensity of the light reflected from the surface in a non-specular way (Bertani, et al., 2007). The main assumptions of the KM theory are *i)* the paint layers or any turbid medium is homogeneous in the sense that the particle sizes are much smaller than the thickness of the layer; *ii)* the transverse extent of the layer is much greater than the thickness; *iii)* the illumination is diffuse and the light propagation in both directions are uniformly diffuse.

I indicates the incident radiation flux, while J the radiation flux backscattered towards the detector. K and S are respectively the absorption and diffusion coefficients of the radiation in the paint layer. Passing through the dx thickness, the intensity I varies due to the absorption and to the diffusion of a quantity dI, which also includes the J

contribution due to backscattering effect; making similar considerations for the J flux we obtained:

$$\begin{aligned} dI &= (K+S)I(x)dx - SJ(x)dx \\ dJ &= SI(x)dx - (K+S)J(x)dx \end{aligned} \tag{1}$$

then we can obtain the reflectance of each point inside the pictorial layer, i.e. the ratio:

$$R(x) = J(x)/I(x) \tag{2}$$

The MSI consists of covering with narrow bandpass interference filters the wider region of wavelengths λ as possible. With this technique each filter, centered on a different λ, with a bandwidth of a few tens of nm, produces an image in grays scale of the painting — called λ *channel*. At each point of the image (or CCD camera pixels) are associated reflected light intensity n values detected at that point (n number of filters).

These values set — containing the spectral information — and those with the pixels position — containing the spatial information — allow complex statistical analysis that can highlight some specificities of the painting not visible to the naked eye. Statistical methods for the visual analysis of the artworks will be discussed further in section 2.2.6.

2.2.4 False Color Imaging

Once obtained three high spectral resolved images and an IR reflectogram, it is possible to extend the deductible information using the False Color Imaging technique, also called *Infrared False Color* (IRFC). This method is based on the fact that two surfaces with similar hue but with strongly different spectra can appear identical under a given illuminant, e.g. under visible light, and completely different under another (*metamerism*). After an initial experimentation with a photographic film — the *Kodak Ektrachrome Infrared 2236* — and the later use of the Vidicon tube, nowadays the IRFC is mostly a computer-based technique as result of the use of the already mentioned CCD cameras or scanner devices (Cetica, et al., 2007).

IRFC techniques combines RGB color images and IR reflectograms to create a "pseudo-color" image where each pigment is represented by a specific false-color that depends on its type of interaction with the IR light. Only the Red and Green components of the color images are overlapped with the grey scale IR reflectogram. Usually the Red RGB component is substituted with the IR, the Green with the Red, and the Blue with the Green. An example of this procedure is shown in fig. 9, using a set of images acquired on a detail of the painting *The Crowning of the Virgin* by Ghirlandaio, preserved at the Palazzo Eroli Museum in Narni (TR). Resulted images present pseudo-colors closely related with the chemical composition of the pigments.

It should be noticed that the different degree of IR radiation reflected by each pigment might also depend on the specific painting technique used by the artist. Indeed, paintings are generally complex systems characterized by paint layers with different thickness, color, and composition. Especially in the case of transparent pigments or thin layers, the ground preparations can give a significant contribution to the false-color image. In this particular case, complementary information obtained with other chemical analysis should be obtained in order to improve the interpretation of false-color data (Mazzeo, et al., 2007).

Reproducibility of false-color is a key factor. Imaging modes need to be calibrated with standards of known reflectance in order to quantitatively compare images collected under different exposure conditions and employing different equipment. In this way it is possible to obtain an exact numerical estimation of the chromatic components that make the image ever reproducible and available to all the image post-processing procedures.

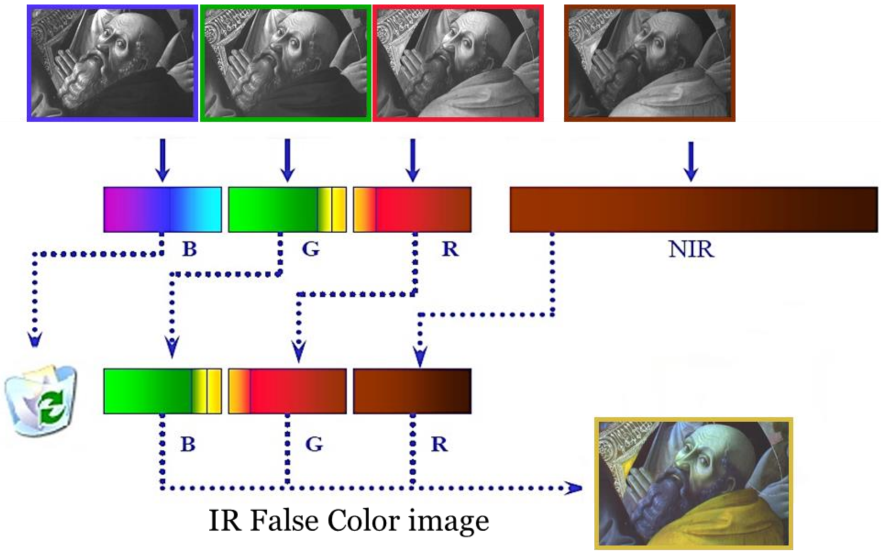

Fig. 9 Scheme of the formation of an IRFC image starting from four monochrome images related to R, G, B, IR bands.

2.2.5 UV induced Fluorescence Imaging

Ever since the 1920s, paintings have been investigated under a UV light source to reveal the visible fluorescence emission of the various materials present on their outer layers. Due to the relatively short UV radiation λ, and therefore to the limited capacity of this radiation to penetrate, fluorescence emission of artworks depends on the contribution external layers, namely on the (semi)transparent varnishes, on the painted layers, i.e. the coloring agent, or pigment, and the binding medium, and on their chemical interactions. The incident UV radiation is partly reflected and partly absorbed by them. Part of the absorbed energy is then re-emitted by fluorescence in the form of radiation whose λ is in the visible light spectrum (400-700 nm). The fluorescence image of the artwork can be photographically captured. However, this method only gives qualitative indications. It does not allow a spectral signature evaluation, nor a correct colorimetric measurement (Pelagotti, et al., 2006).

Generally a Wood lamp is used as UV source. It is a mercury vapor lamp filtered by a nickel oxide-based glass that blocks wavelengths in the visible and it is characterized by an emission in UV range (300-400 nm – UVA) with a central peak at 365 nm. The characteristic emission spectrum of a Wood lamp has a residual parasite emission in the blue-violet region of the spectrum that is reflected from the surface under investigation and it is added to the fluorescence signal. It is basically needed to subtract with a barrier filter the part of radiation that was not due to fluorescence emission but to the strays light reflection. Recently UV LEDs are replacing Wood lamps.

2.2.6 Multivariate Statistical Methods for Visual Analysis

In the last decades, several techniques have been proposed for extracting or evidencing hidden patterns through the elaboration of the digital images (Legnaioli, et al., 2013). Most of these methods can be applied using blind algorithms, which operates automatically without the intervention of an operator. Among these statistical methods my research group has used particularly the *Chromatic Derivative Imaging* (ChromaDI), *Blind Separation Methods* (BSM) and the Neural Networks Analysis (Salerno, et al., 2014).

ChromaDI Imaging and BSM, imply the application of linear transformations on the original multispectral images. These latter Blind Methods depend on the definition of a distance among (hyper)colors, that can be chosen to be Euclidean or being related to the angle between the (hyper)vectors representing the optical behavior of the materials under study. Finally, non-linear methods based on the use of Artificial Neural Networks can be applied to obtain a segmentation of the image according to the different pigments used.

More in detail, ChromaDI is a variant of IRFC which is obtained through the subtraction of consecutive couples of spectral images. The method creates a False Color image which takes into account the information from all the multispectral images acquired, without excluding *a priori* one of the four images in the multispectral set.

BSM are typically applied for the unsupervised separation of features in the MS images set that are not immediately apparent in the corresponding Color/False Color/ChromaDI images. A simple assumption is that the observed images result from the superposition of individual patterns that combine linearly to form the final appearance. If *x(i,j)* is an N-vector map representing the multispectral image and *s(i,j)* is an M-vector map representing the collection of the original patterns, we can assume that:

$$\boldsymbol{x}(\boldsymbol{i},\boldsymbol{j}) = \boldsymbol{As}(\boldsymbol{i},\boldsymbol{j}) \tag{3}$$

where:

- *(i,j)* are the pixel indices, and *A* is the N×M mixing matrix.

Blind Separation techniques consist in estimating s from the multispectral data *x*, making assumptions of statistical nature. For example, the elements of vector *s* can be considered as mutually independent, non-Gaussian random variables. This leads to the class of separation techniques denoted as *Independent Component Analysis* (ICA) (Tonazzini, et al., 2004 and 2010; Feng, et al., 2008). Alternatively, incorrelation rather than independence can be imposed (Cichocki & Amari, 2002). This leads to the *Principal Component Analysis* techniques (PCA) (Wold, et al., 1987; Baronti, et al.,1998), through which a set of N multispectral channels produces N images representing mutually uncorrelated patterns. The images sets *s(i,j)* produced by ICA or PCA are often much more readable than the original multispectral images. Each output image carries information from the entire multispectral set, and is likely to highlight patterns with peculiar spectral signatures that are not represented in the others. An example of application of the PCA analysis is what we carried on MS images of the mural painting of an Etruscan tomb in Chiusi (SI) (Legnaioli, et al., 2010).

The Artificial Neural Networks method (Haykin, 1999) is called Kohonen *Self-Organizing Map* (SOM) (Kohonen, 1990). The SOM Network is a self-organized Neural Network that consists of neurons representing a N-dimensional weight vector, where N is the dimension of the multispectral (hyper)vector. The pixels in the image are assigned to the node which is 'closer' to their (hyper)color. The different neurons adjust their weights (hypercolors) in order to get the largest possible number of pixels, in a competitive way. The SOM method is particularly suited for classification purposes (Villmann, et al., 2003; Kuncheva, 2004), since each neuron of the map is associated to samples that are in some way different from the ones associated to the other neurons. From a practical point of view, the number of neurons in the map is chosen in order to cover the chromatic variations in the image to be analyzed. The SOM approach can be used for identifying in the painting the zones corresponding to pigments which shows a similar optical behavior. The technique is fast and works in a fully automatic way.

2.3 Reality Based 3D surveying

2.3.1 General Considerations

Digitization of artifacts is the process of converting spatial and color information into digital formats. 3D digitization refers specifically to creating a digital representation of an object in three spatial dimensions, that is, Cartesian *x*, *y*, and *z* coordinates. During 3D digitization, depth, size, proportion, and textural information about the artifact are recorded and stored in electronic form.

There is a wide range of techniques available in the field of 3D digitization. The specific approach to digitization differs depending on the artifact and the final intended data application.

One of the most interesting properties of the *Reality-based 3D Modeling* is the possibility of replacing a real object with its digital copy, interacting with it and adapting the informative content level of the copy according to the different survey purposes.

In the surveying and in the Cultural Heritage (CH) modeling, realism — or better the photorealistic rendering in terms of appearance details, colorimetric, geometric, and radiometric accuracy — is a basic requirement. Virtual representation is closely related to the issue of the validity of information – commonly referred to as authenticity – and to the importance of the accuracy of this information (Roussou & Drettakis, 2003).

The accuracy required by restorers for a proper modeling of the process involved in painting maintenance is about 0.01-0.1 mm precision (that is typical of close-range metrology). High-level digitization is obtained when the sampling and quantization values are high and the "aliasing" value – that is the information loss – is minimal. Then, the digital model must be the combination of all the measures and interpretations necessary to the knowledge of the original.

Over the last twenty years, the progress of the various data capture methodologies has achieved results with a high degree of fidelity to the real investigated object, even if the computational effort for obtaining a realistically valid product is usually proportionate to the final goal. It is known that there is a difference between the modalities of virtual restitution required by the research field of art historians, museum professionals or diagnosticians, in comparison with the needs of presentation for educational purposes that have a wider audience as target. Here we are obviously interested to the first case.

2.3.2 Methodologies, techniques and tools

Going into the details, *Reality-based 3D* digitization is intended as the complex of all measurements necessary to the representation and to the metric rendering of an artwork at a certain time. The overall process of 3D digitization involves three broad steps: *i)* raw data acquisition, *ii)* data processing, and *iii)* modeling phases. From the technical point of view, the 3D data capture methodologies, which have these same operational phases in common, can be divided into two large families: *range-based,* and *image-based techniques*. Both of them use *non-contact* optical sensors (Marbs, et al., 2001) that are respectively *active* or *passive* systems. The choice or the integration of the two determines the 3D modeling approach to follow, that depends on object dimensions, location constraints, instrument's portability and usability, surface characteristics, project budget, and so on.

- *Active optical sensors* employ instruments that emit electro-magnetic signal (in the VIS, IR, X-Rays, etc.), which is then recorded, by the instrument itself in order to derive a measure of distance (*Range Based Method - RBM*). *Time-of-Fligh*t (ToF) or triangulation-based Laser scanners, Total stations, Radar, Structured Light systems are all range based instruments that produce quantitative 3D digital representations — dense point clouds or range maps — with an accurate high resolution (up to tens of microns). One of the main advantages of 3D scanning is therefore the quality of the representation obtained, where quality is meant as accuracy of the representation — shape + surface attributes — with respect to the original, even if the high quality of the shape representation is often coupled with a considerable complexity — due to high resolution sampling — of the model produced. However, there are some inherent disadvantages: extract the most significant geometric elements of the scene or create a polygonal geometric model require long editing time because of the high number of non-structured information. Cameras normally mounted on the active instruments are of low quality that usually results in a loss of good texture. Lastly, the costs are high and the portability of the equipment is not so practical.
- On the other hand, *passive sensors* (*Image-Based Method — IBM*) deliver direct data flow from digital cameras, which is then processed by the use of automatic recognition algorithms of homologous points in photographic image sequences of the same object (*Stereo/Multi-photo matching approach*). It is possible to infer 3D information from at least two 2D image acquisitions using perspective or projective geometry formulations (Yastikli, 2007; Remondino, 2011).

The main difference between the image-based systems — of which photogrammetry is part — and the range-based systems, consists in the fact that in the first one there is the need to switch from 2D acquisition data (two-dimensional images) to three-dimensional data for the model constitution. Indeed, photogrammetry transforms 2D data into 3D models by establishing a geometric relationship between the three-dimensional positions of points and those of their images on photographs. The theoretical basis on which photogrammetry is based are the epipolar geometry and equations of collinearity.

The tendency of many current projects reveals a gradual overcoming of the use of active sensors, privileging passive indirect techniques because they result to be far more versatile in terms of time, cost, and ease of use. *123D Catch (Autodesk), Visual SfM, PhotoScan (Agisoft), Apero/MicMac* are just some of the existing applications of automatic correlation of images — both commercial and open source — all of which offer accuracy and resolution comparable to laser scanning, as confirmed by specific literature. Anyway, the integration of multiple sensors or the modeling approach with differentiated resolution currently represents the state-of-art *(Integrated Multi-Source and Multi-Resolution Digital Survey)* (Remondino, 2011).

Furthermore, the idea of creating digital informative models — also defined "semantic description models" — intended as interfaces of preferential access to various kinds of CH data and metadata is advancing more and more. Indeed, on the models obtained, all analyzes, diagnosis, and informational enrichment can be carried out. To that effect, the digital models can become collectors of heterogeneous information – both quantitative and qualitative – related to the analyzed artifact (such as geometric 2D and 3D surveys, current and historical images, iconographic sources, restoration data, multispectral acquisitions, maps of chemical-physical analysis, etc.) and displayed within a unique integrated platform (De Luca, et al., 2011).

It is reasonable to think that the new perspective that will open in Digital Imaging will be to embed the knowledge resulting from different branches in a multi-dimensional digital object. To give a speculative and applicative contribution to the implementation of digital and three-dimensional acquisition technologies while getting a variety of structural and spectral information on a single model is at the core of my Ph.D project.

In order to experience the applicability of our method and in relation to the available equipment in our lab, we used passive sensors, therefore basically IBM techniques.

2.3.3 Photogrammetry

Photogrammetry is part of the IBM techniques. It is considered the best technique for the image data modeling, being able to deliver at any scale of application an accurate, metric, and detailed 3D information with estimates of precision and reliability of the known or unknown parameters from the measured image correspondences (tie points) (Remondino & El-Hakim, 2006).

According to Atkinson, «photogrammetry is the science, and art, of determining the size and the shape of objects as a consequence of analyzing images recorded on film or electronic media» (Atkinson, 1996). This definition, which is currently the most accepted, underlies the idea that photogrammetry is a critical tool for reading of reality itself because it is not only a method to accurately acquire objective measurements but also a tool to investigate and to know the reality in its most complex aspects of interrelation between the parts. Specifically to our purposes, it is a discipline that allows us to understand the artwork as a whole, capturing all values – from those dimensional to those constructive, from those formal to those cultural.

The photogrammetry field is constantly evolving because closely related to digital technology, which thrives on continuous and rapid updates. Over the decades, it changed from an *Analogic Photogrammetry*, to an *Analytical Photogrammetry* (numerical knowledge of the object detected), up to the *Digital* today. Between the last decade of the 20th century and the early years of the 21th, Digital Photogrammetry has acquired its own connotation thanks to the use of automatic techniques developed in the field of Computer Vision, the discipline that analyzes and reinterprets in computer-key projective geometry of vision.

As the photogrammetric survey is almost completely digital in all of its phases, in the literature it is often replaced directly by the term "digitization". Therefore, it is important that the digitization of CH includes both humanistic disciplines, and the *Information and Communications Technology* (ICT).

Technological developments seem to have pursued those features described in the *American Lessons* written by Italo Calvino in 1985 for the University of Harvard: *Lightness*, *Quickness*, *Exactitude*, *Visibility*, *Multiplicity*, *Consistency*. They are exactly the performance expected today by the new equipment and tools. They are the perspectives that the research pursues.

Photogrammetry can be categorized in many different ways:

- by camera position and object distance;
- by number of measurement images;
- by method or by recording and processing;
- by availability of measurement results;
- by application or specialist area.

Our application areas are highlighted in yellow, in the following table:

Tab. 1 Photogrammetry categories. Table credits: (Luhmann, et al., 2013).

By **camera position and object distance**	
▪ Satellite photogrammetry	Processing of remote sensing and satellite images, h > ca. 200 km
▪ Aerial photogrammetry	Processing of aerial photographs, h > ca. 300 m
▪ Terrestrial photogrammetry	Measurements from a fixed terrestrial location
▪ Close-range photogrammetry	Imaging distance d < ca. 300 m
▪ Macro photogrammetry	Image scale > 1 (microscope imaging)
▪ Mobile mapping	Data acquisition from moving vehicles, d < ca. 100 m
By **number of measurement images**	
▪ Single-image photogrammetry	Single-image processing, mono-plotting, rectification, orthophotos
▪ Stereo photogrammetry	Dual image processing, stereoscopic measurement
▪ Multi-image photogrammetry	n images where n >2, bundle triangulation
By **method of recording and processing**	
▪ Plane table photogrammetry	Graphical evaluation (until ca. 1930)
▪ Analogue photogrammetry	Analogue cameras, opto-mechanical measurement systems (unitl ca. 1980)
▪ Analytical photogrammetry	Analogue images, computer-controlled measurement
▪ Digital photogrammetry	Digital images, computer-controlled measurement
▪ Videogrammetry	Digital image acquisition and measurement
▪ Panorama photogrammetry	Panoramic imaging and processing
▪ Line photogrammetry	Analytical methods based on straight lines and polynomials
By **availability of measurement results**	
▪ Offline photogrammetry	Sequential, digital image recording, separated in time or location from measurement
▪ Online photogrammetry	Simultaneous, multiple, digital image recording, immediate measurement
▪ Real-time photogrammetry	Recording and measurement completed within a specified time period particular to the application
By **application or specialist area**	
▪ Architectural photogrammetry	Architecture, heritage conservation, archeology
▪ Engineering photogrammetry	General engineering (construction) applications
▪ Industrial photogrammetry	Industrial (manufacturing) applications
▪ Forensic photogrammetry	Application to diverse legal problems
▪ Biostereometrics	Medical applications
▪ Multi-media photogrammetry	Recording through media of different reflective indices
▪ Shape from stereo photogrammetry	Stereo image processing (computer vision)
▪ Structure from motion photogrammetry	Multi-image processing (computer vision)

As already mentioned, photogrammetry provides three-dimensional (3D) coordinates of an object from two dimensional (2D) digital images at least. It establishes a geometric relationship between photographs and the object scene at the shooting time using central projection imaging as its fundamental mathematical model.

Shape and position of an object are determined by reconstructing bundles of rays in which for each camera, each image point together with the corresponding perspective center defines the spatial direction of the rays to the corresponding object point. The parameters of interior orientation that describe the principal point location and calibrated focal length of the camera and focal plane have to be known. The exterior orientation parameters can be determined by collinearity equation (eq. 4, p. 50) (Elnima, 2015) that defines the relationship between object and image coordinates if at least three control points are available in the overlapping image area. So, perspective projection, collinearity equations, relative orientation of two images, bundle triangulation algorithm, and the *Direct Linear Transformation* (DLT) are involved in the photogrammetric process.

2.3.3.1 Perspective projection

An image of an object is a plane representation of a 3D object. The mathematical operation that relates the each point of a 3D object to its position on a plane is called a *projection*.

Standard photogrammetric routines are commonly based on the perspective projection algorithm. In these models the sensor is seen as a plane, i.e. the image plane, and a point, i.e. the perspective center. The general assumption adopted is that on the same straight line we have a point on the target in 3D space, its corresponding point on the image plane, and the perspective center. The principal distance is defined as the distance between the image plane and the perspective center. The image plane captures a mirror image of the target object. The focal axis is the normal of the image plane passing through the perspective center. The principal point of an image is instead defined as the point where the focal axis intersects the image.

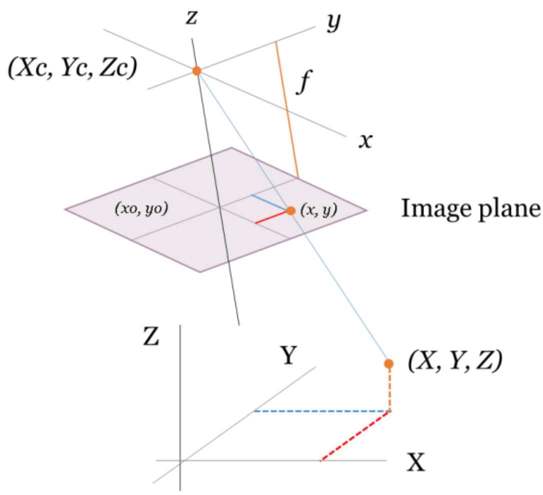

Fig. 10 3D depiction of the perspective projection.

In fig. 10 the straight line we referred to previously is depicted. In particular what is shown is that the target point in 3D space of coordinate (*X*, *Y*, *Z*), the same projected point on the image (*x*, *y*), and the perspective center (*Xc*, *Yc*, *Zc*) all lie on a straight line. The principal distance, *f*, while (*xo*, *yo*) is the principal point of the image. The *XYZ* coordinate system is the coordinate system of the lab, while with *xyz* we refer to as the coordinates of the image space; the *z*-axis is the focal axis. The image space — the coordinate system in which image coordinates are measured — has axes parallel to the *x*- and *y*-axes of the image coordinate system, and the focal axis passes through the image plane at the principal point (*xo*, *yo*). There is a rotation of the image coordinate system (*xyz*) with respect to the 3D coordinate system (*XYZ*). This rotations of the image coordinates with respect to the lab are described by three ordered rotations about the *X*-axis, *Y*-axis, and *Z*-axis, respectively, that in standard photogrammetry are respectively called ω, ϕ, κ. These rotations have a 3 x 3 matrix representation. Six parameters

(ω, ϕ, κ, Xc, Yc, Zc), the so called *Exterior Orientation Parameters* (EOP), describe the position and orientation of the camera in the lab space. The three parameters (f, xo, yo) are instead *Interior Orientation Parameters* (IOP) because they describe geometry within the image space.

2.3.3.2 Collinearity equations and the coplanarity equation

The collinearity equations (eq. 4) are the fundamental equations describing the perspective projection (Wolf & DeWitt, 2000). They express the 2D image projection (x, y) of a point with coordinates (X, Y, Z) as a function of the perspective center coordinates and three rotation angles (EOP) of an image:

$$
\begin{aligned}
x &= x_0 - f\left(\frac{m_{11}(X - Xc) + m_{12}(Y - Yc) + m_{13}(Z - Zc)}{m_{31}(X - Xc) + m_{32}(Y - Yc) + m_{33}(Z - Zc)}\right) \\
y &= y_0 - f\left(\frac{m_{21}(X - Xc) + m_{22}(Y - Yc) + m_{23}(Z - Zc)}{m_{31}(X - Xc) + m_{32}(Y - Yc) + m_{33}(Z - Zc)}\right)
\end{aligned}
\tag{4}
$$

where:

- (x_o, y_o) are the coordinates of the principal;
- f, is the the principal distance;
- m_{ij} terms are the elements of the rotation matrices;
- (Xc, Yc, Zc) are the coordinates of the perspective center;
- (X, Y, Z) are the coordinates of a point on the 3D object.

The collinearity equations are used extensively in photogrammetry and form the basis of the bundle triangulation algorithm.

The coplanarity equation (eq. 5) is derived as a generalization of the collinearity equations when two images are considered. The coplanarity condition states that for a given point in 3D space (*X*, *Y*, *Z*), the point lies on a common plane with the two perspective centers of the two images (Xc_1, Yc_1, Zc_1) and (Xc_2, Yc_2, Zc_2) and the two image points (x_1, y_1) and (x_2, y_2) (fig. 11).

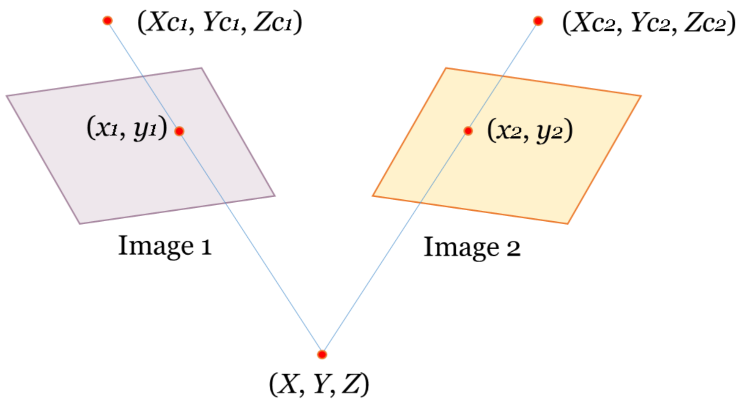

Fig. 11 The coplanarity condition.

The coplanarity equation is expressed as a triple vector product (Mikhail, Bethel, & McGlone, 2001). The three vectors are the baseline vectors: $\vec{\boldsymbol{b}}$ is the vector from one perspective center to the other, the other two, $\overrightarrow{\boldsymbol{uvw}}_1$ and $\overrightarrow{\boldsymbol{uvw}}_2$, point from the perspective center to the image point of each of the two images:

$$\vec{\boldsymbol{b}} = \begin{vmatrix} b_x \\ b_y \\ b_z \end{vmatrix} = \begin{vmatrix} Xc_2 - Xc_1 \\ Yc_2 - Yc_1 \\ Zc_2 - Zc_1 \end{vmatrix}$$

$$\overrightarrow{\boldsymbol{uvw}}_1 = \begin{vmatrix} u_1 \\ v_1 \\ w_1 \end{vmatrix} = M_1^T \begin{vmatrix} x_1 - x_0 \\ y_1 - y_0 \\ -f_1 \end{vmatrix}$$

$$\overrightarrow{\boldsymbol{uvw}}_2 = \begin{vmatrix} u_2 \\ v_2 \\ w_2 \end{vmatrix} = M_2^T \begin{vmatrix} x_2 - x_0 \\ y_2 - y_0 \\ -f_2 \end{vmatrix}$$

where:

- (x_1, y_1) and (x_2, y_2) are the image points of image 1 and 2 respectively;
- f_1 *and* f_2 are the principal distances of image 1 and 2 respectively;
- (x_o, y_o) is the principal point;
- M_1 and M_2 are the rotation matrices.

The three baseline vectors are linearly independent. Their triple vector product gives the coplanarity equation:

$$\vec{\boldsymbol{b}} \cdot (\overrightarrow{\boldsymbol{uvw}}_1 \times \overrightarrow{\boldsymbol{uvw}}_2) = det \begin{vmatrix} b_x & b_y & b_z \\ u_1 & v_1 & w_1 \\ u_2 & v_2 & w_2 \end{vmatrix} = 0 \tag{5}$$

That is:

$$b_x(v_1 w_2 - w_1 v_2) + b_y(u_1 w_2 - w_1 u_2) + b_z(u_1 v_2 - v_1 u_2) = 0 \tag{6}$$

where:

- b_x, b_y, b_z are the elements of vector $\vec{\boldsymbol{b}}$;
- u_1, v_1, w_1 are the elements of vector $\overrightarrow{\boldsymbol{uvw}}_1$ for image 1;
- u_2, v_2, w_2 are the elements of vector $\overrightarrow{\boldsymbol{uvw}}_2$ for image 2.

2.3.3.3 Bundle triangulation algorithm

The bundle triangulation algorithm — or multi-image triangulation — is a standard procedure in photogrammetry. It is the major algorithm in photogrammetry for 3D reconstruction. It is a robust algorithm capable of simultaneously solving for the EOP, the IOP, and the 3D coordinates of target points. It also provides statistical information regarding the precision of the calculated solution. The standard bundle triangulation algorithm is based on perspective projection, and is derived from the collinearity equations.

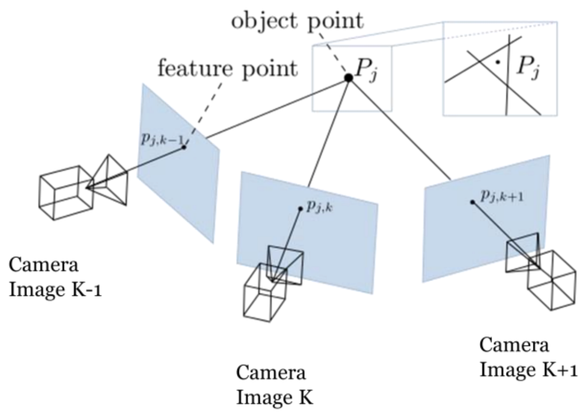

Fig. 12 Bundle triangulation.
Figure credits: (openMVG: "Open Multiple View Geometry".
<http://imagine.enpc.fr/~moulonp/openMVG/coreFeatures.html>).

As shown in fig. 12, the primary input for the bundle triangulation algorithm is a set of point correspondences across the images (camera images *K-1*, *K*, *K+1*) of the analyzed object. A point correspondence happens when a certain point on the target object in 3D space is localized in several images — i.e. the image coordinates across several images are recorded for a given point on the target. The bundle triangulation algorithm requires the collection of a set of points of correspondence.

The second major input for the bundle triangulation algorithm is a set of initial trial approximations of all unknowns to be as the starting point of the algorithmic iterative. The initial trial approximations should be fairly close to the correct values, in order to have a fast convergence to an accurate solution. Given a set of point correspondences and a set of satisfactory initial trial approximations, the bundle triangulation algorithm can solve for the EOP and the IOP of the images and the 3D geometry of the target points.

2.3.3.4 Direct Linear Transformation

The *Direct Linear Transformation* (DLT) (Abdel-Aziz & Karara, 1971) is a standard photogrammetry method to solve for the EOP and the IOP of a single image relative to a set of 3D coordinates. This method requires that the 3D coordinates of several points on the target are known and are visible in the image. The DLT can be derived from the collinearity equations. The EOP and the IOP of the camera are described by 11 *L*-terms. The *L*-terms can be solved for from a set of control points with known XYZ coordinates. The set-up is as follows:

$$\begin{bmatrix} x_1 \\ y_1 \\ x_2 \\ y_2 \\ \ldots \end{bmatrix} = \begin{bmatrix} X_1 & Y_1 & Z_1 & 1 & 0 & 0 & 0 & 0 & -x_1X_1 & -x_1Y_1 & -x_1Z_1 \\ 0 & 0 & 0 & 0 & X_1 & Y_1 & Z_1 & 1 & -y_1X_1 & -y_1Y_1 & -y_1Z_1 \\ X_2 & Y_2 & Z_2 & 1 & 0 & 0 & 0 & 0 & -x_2X_2 & -x_2Y_2 & -x_2Z_2 \\ 0 & 0 & 0 & 0 & X_2 & Y_2 & Z_2 & 1 & -y_2X_2 & -y_2Y_2 & -y_2Z_2 \\ \ldots & \ldots & \ldots & \ldots & \ldots & \ldots & \ldots & \ldots & \ldots & \ldots & \ldots \end{bmatrix} \begin{bmatrix} L_1 \\ L_2 \\ L_3 \\ L_4 \\ L_5 \\ L_6 \\ L_7 \\ L_8 \\ L_9 \\ L_{10} \\ L_{11} \end{bmatrix} \qquad (7)$$

In eq. *7* (x_1, y_1) represent the image coordinates of the target point (*X1*, *Y1*, *Z1*,) etc. The *L* terms can be solved by inversion of the matrix on the right hand side. Once the *L* terms have been derived from the control information, the EOP (*Xc*, *Yc*, *Zc*, ω, ϕ, κ) and IOP (*f*, *xo*, *yo*) can then be solved for from the *L* terms.

2.3.3.5 Camera calibration

One important step in most photogrammetry applications is the calibration of the camera and the optical lenses. This calibration gives the response function of the sensor over a set of predefined analytic blank images, so to adjust the bias over the principal distance, and the location of the principal point (the IOP) of the acquisition phase. However there are cases — such as ours — where one is forced to work with images captured with an unknown or uncalibrated sensor. The problem can be solved by the *self-calibration* method of the *Structure from Motion*, the technique object of the following paragraph.

2.3.4 Structure from Motion (SfM)

Among the IBM techniques, the one commonly called *Structure from Motion* (SfM) deserves a special focus.

While traditional photogrammetric approaches require a previous characterization of the cameras and a planned shooting strategy to be used for capturing the images, SfM is more spontaneous and does not need any sort of planning or cameras calibration. Knowing the position of camera is not necessary because SfM photogrammetry determines internal camera geometry, camera position and orientation automatically by means of robust computer vision algorithms that automatically detect matching features in the images (Lowe, 2004; Furukawa & Ponce, 2010;

Westoby, et al., 2012). For this reason, SfM frequently appears in association with the field of Computational Vision. It is even possible to use images taken with different cameras at different points in time. However, it is ever necessary to locate overlapping areas or areas in the objects that are included in different images. The need for a high degree of overlap to cover the full geometry of the object or scene of interest, gives rise to the name: structure derived from a sensor moving among a range of different positions (James & Robson, 2012; Micheletti, Chandler, & Lane, 2015).

Nowadays, speaking of SfM and photogrammetry separately is therefore complex and confusing (Mundy & Zisserman, 1994), as the majority of photogrammetry tools frequently end up incorporating SfM processes in order to automate certain procedures, being able to utilize large amounts of images to describe, in as much detail as possible, the geometry of scenes and objects.

Automatic photogrammetric techniques are able to provide metric and accurate products, testifying the great potentiality of the method to derive 3D information (point clouds) at different scales, comparable to those obtained with active optical sensors (Pierrot-Deseilligny, et al., 2011; Remondino, 2011). The level of detail is solely conditioned by the resolution and number of images to be used.

Basically, the SfM has become a powerful and an increasingly used tool for the construction of three-dimensional models for two reasons: the development of extraction and triangulation algorithms from images have led to an increase in the quality of data obtainable from a pair of stereo images; the low cost and the quality improving of digital cameras and of their calibration methods have led to the use of photogrammetric modeling by a wider audience (Remondino & Menna, 2008; Westoby, et al. 2012).

2.3.4.1 Methodology

As already mentioned, SfM automatically generates a dense point cloud of the documented object orientating a set of images.
Initially, the *Scale Invariant Feature Transform* (SIFT) (Lowe, 2004) identifies common feature points across the images set, sufficient to establish the spatial relationships between the original image locations in an arbitrary 3D coordinate system.

The sparse bundle adjustment (Brown, 1958; Triggs et al, 1999; Snavely, et al., 2008; McGlone, 2013) transforms measured image coordinates into 3D points covering the area of interest. The result is three-dimensional locations of the feature points in the form of a sparse point cloud in the same local 3D coordinate system.

Discrete point cloud thus generated can vary in density depending on the connections detected among the images. In the traditional processes of manual adjustment of common points among images, these clouds were not especially populous; with SfM, however, these clouds can end up having thousands of points.

The sparse point cloud is then intensified using *Multi-View Stereo* (MVS) techniques (Furukawa & Ponce, 2010; Rothermel, et al. 2012). These techniques are able to generate very high resolution datasets, isolating and removing gross errors.
The process continues with the creation of a structured geometric polygon model (mesh) and ends with its texturization.

2.4 X-Rays induced Fluorescence

Starting from the first issue in 2000 of *X-Rays Spectrometry Journal* — which was entirely dedicated as a special edition to the applications of X spectroscopy of CH — the wide specific literature shows that the application of *X-Rays induced Fluorescence* (XRF) analysis for the study of polychrome surfaces and artworks' constituent materials is now strongly consolidated. From the first attempts of the late sixties to date, huge strides have been made (Seccaroni & Moioli, 2004).

XRF is an elemental technique that provides accurate, punctual and qualitative results. The complex stratigraphy of the paintings and the common mixing of pigments, prevent in fact to obtain quantitative concentrations of the different elements in the analyzed point. The intensity of fluorescence spectral lines depends on the concentration of a given element, but on the other hand it depends also on the overall composition of the spot measured, and therefore by the presence of other species such as binders, varnishes and generally of all those low weight elements that X-rays cannot reveal. Despite this premise, some efforts have been made to give a quantitative valence to the XRF measurements (Milazzo, 2007).

One of the limits of the technique is that it is able to return information relating to only the most superficial paint layers, without getting deep. Furthermore, it only detects elements related to pigments of mineral origin with the exception of almost all organic pigments. Pigments consisting of low atomic number elements, such as those that constitute the Ultramarine Blue, are not detected because of the chemical-physical principles discussed later.

Being a micro-analytical technique that does not require sampling, it is possible to carry on unlimited spot analysis in order to obtain the elemental distribution map referring to the pigments used in the artist's palette. In addition to commercial portable instruments for the essential *in situ* survey, several research groups have also set some Mobile XRF scanning devices. These recent advances allow obtaining a chemical-elemental imaging of the entire painting's surface area, instead of the more usual sparse elemental mapping (Matthias, et al., 2013; Romano, et al., 2014 and 2016).

In addition XRF enables scholars to date artworks. Because some materials were available in particular regions and periods, the retrieval of pigments with a well-known date of invention allows art historians to date artifacts *post quem*. Other pigments may be known to have disappeared from the artists' palette, so their presence permits experts to date artifacts *ante quem*.

Spectroscopy is also extremely useful to recognize forgery. Fake artworks can be spotted when anachronisms arise in the materials, and the materials do not align with those used in known works by the same artist. Finally, XRF qualifies and distinguishes the elements belonging to the original pigments from those of restoration.

2.4.1 Underlying physics

XRF is the emission of characteristic "secondary" X-rays from a material that has been excited by ionizing high-energy radiation. When a sample is exposed to primary radiation source of short-wavelength, the ionization of the component atoms of its materials, the so-called *photoelectric effect*, may occur whether an atom is exposed to a radiation with energy greater than its ionization potential:

$$E = h\,\nu = h\,\frac{c}{\lambda}$$

where:
- h is the Planck constant;
- ν is the frequency of the incident photon;
- λ is the wavelength of the incident photon;
- c is the speed of light.

In other words the electron can be expelled only if the incident photon energy is at least equal to the electron binding energy:

$$h\nu \geq W_{e.}$$

where;

- (W_e) is the extraction work

The removal of an electron makes the atom unstable and it induces temporary modifications of its electronic structure due to orbital population rearrangements. The vacancy generated in an inner orbital, of energy *En*, is then filled with electrons of an outer orbital, with energy *Em*, along transition L→K (K_α), M→K (K_β), M→L (L_α)...

The energy of the photons released is equals to the difference in energy between *Em* and *En:*

$$hV = Em - En.$$

The energy of these secondary X-rays is a specific characteristic of the atoms present.

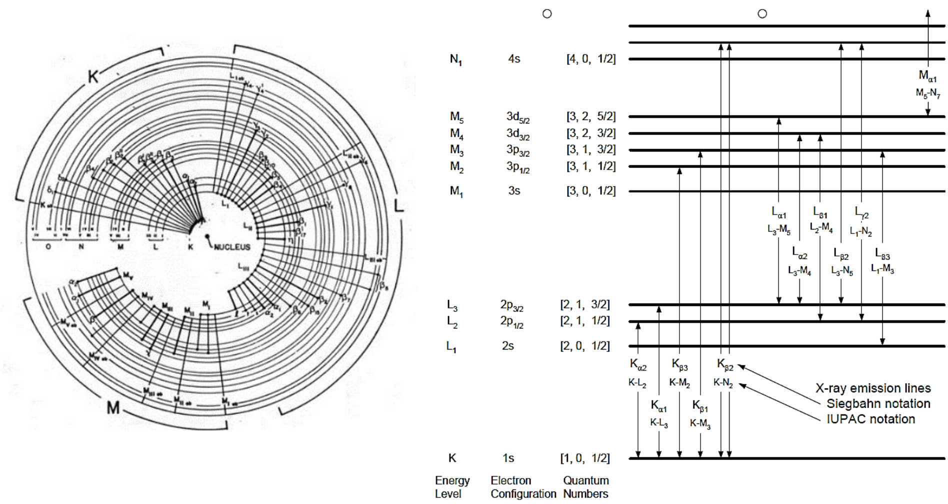

a) *b)*

Figg. 13 a), b) Atomic models, showing electron transitions that may follow electron vacancies. Transitions are labeled with conventional notation for associated emission lines.

The term *fluorescence* is applied to phenomena in which the absorption of radiation of a specific energy results in the re-emission of radiation of a different energy — generally weaker. The wavelength of this fluorescent radiation can be calculated from Planck's Law:

$$\lambda = \frac{hc}{E}$$

Instead of emitting an X-Rays photon, the excited atom might recombine by transferring its excess energy to another electron (*Auger effect*), which will then be ejected from the atom.

In the analysis of the re-emitted X-rays radiation some issues must be considered:

- The energy of the re-emitted X-rays radiation decreases with the decreasing of the atomic number. Consequently, the X-rays fluorescence of elements such as *C*, *N* and *O* cannot be revealed with spectrometers operating in free air because the fluorescence photons cannot reach the detector.

- Some matrix effects occur. The combination of all components of the sample other than the analyte influences the measurement of the quantity of the analyte. The two main matrix effects are: *i)* the attenuation of characteristic peak intensity due to inelastic scattering of photons, emitted by atoms of one chemical element, on atoms and electrons of other components; *ii)* the enhancement of characteristic peak intensity due to additional excitation of atoms of one element by photons, emitted by other components.
- The intensity of the emitted radiation will be as more attenuated as greater is the mass absorption coefficient (μ_i) of the material absorber *i*, (when density (ρ_i), and thickness (x_i) to pass through remain constant):

$$I(\lambda) = I_o \exp[-(\mu_i \rho_i x_i)]$$

There are two main methodological techniques for revealing fluorescent X-rays emitted: *Wavelength Dispersive Analysis* (WD-XRF) and *Energy Dispersive Analysis* (ED-XRF). The first method is basically performed with laboratory instrumentation: the fluorescent X-rays emitted by the material sample are directed into a diffraction grating monochromator. By varying the angle of incidence and take-off on the monochromator, a single X-rays wavelength can be selected.

The wavelength obtained follows the *Bragg's law*:

$$n \cdot \lambda = 2d \cdot \sin(\theta)$$

where:

- n is a positive integer;
- λ is the wavelength of the incident wave;
- d is the spacing of atomic layers parallel to the crystal surface;
- θ is the scattering angle

The path difference between two waves undergoing interference is given by $2d\cdot sin(\theta)$, and constructive interference occurs when this length is equal to an integer multiple of the wavelength of the radiation.

The portable XRF instrumentation – the most utilized in CH – uses solid-state detectors that operate with the EDX method. Solid-state detectors, such as PIN diode, Si(Li), Ge(Li), *Silicon Drift Detector* (SDD), produce a "continuous" distribution of pulses with voltages proportional to the incoming photon energies. The electric signals are then processed by a *Multi-Channel Analyser* (MCA), which produces an accumulating digital spectrum from which analytical data can be extracted. Despite their widespread use in portable devices, the solid-state detectors restrict the ability to discriminate light elements such as *Na* and *Mg* due to absorption of the thin *Be* foil placed for the protection of the detector.

In the fifth chapter we will describe in more detail the portable device that we used that has a SDD sensor and operates with the EDX method.

3

Integration of 3D and Multispectral data for Cultural Heritage applications.

The state of the art

3.1 Quality and Quantity. The measure of the spatial and spectral properties of the works of art.

The 2D multispectral digitization and the 3D modeling of easel paintings are common non-contact acquisition techniques that collect complementary information (spectral and spatial), such as: pigment identification, precise color measurement, highly detailed recording and visualization, as well as for the measurement of the shape of the (wooden) support or the paint-layer roughness (Lahanier, et al., 2005).

More in detail, the knowledge of the shape of an art object — being an archeological find, a monument, a painting or a fresco — is an important element for its study and for its preservation. The data obtained from a measurement of shape significantly enriches the documentation of the work of art. By measuring the shape of an object repeated at successive times it is possible to get quantitative information on eventual deformations, splits, cracks, or cupping of the paint layer derived from mechanical stress, microclimatic variations or from modifications introduced by restoration operations. Indeed, the characterization of the shape contributes to the determination of the state of conservation of the artifact and to the predisposition of an eventual monitoring project (Fontana, et al., 2007).

The accuracy required by restorers in the evaluation processes concerning the painting maintenance is typically that one of a close-range metrology (0.01-0.1 mm precision). The surveying techniques, which could fulfil these requirements, are photogrammetry and short-range active sensors (Remondino, et al., 2011).

Active sensors, in particular interferometric techniques (e.g. micro-profilometer based on conoscopic homography) (Fontana, et al., 2005), short-range laser scanners (Blais, et al., 2007) and stripe projection systems (Akca, et al., 2007), are all good methods for the 3D surveying and deformation monitoring of paintings. Range sensors are indeed able to survey large surfaces in detail and deliver dense 3D data useful for:

- 3D reconstruction of the surface details at very high geometric resolution (Blais, et al., 2005);
- instant evaluations of the entire shape of the painting;
- multi-temporal analysis and measurement of the movement of the (wooden) shape of the support.

For large paintings (some meters), *Time of Flight* (ToF) sensors could be employed to determine the gross shape of the painting and check its deviation from a theoretical planarity. Triangulation-based sensors or conoscopic micro-profilometer are instead more suited to study the small features of the surface, to analyse *craquelure* patterns, to highlight and document colour raisings, detachments or engraving as well as deliver high-resolution 3D models.

On the other hand — as described in the previous chapter — the acquisition of MS images of painted surfaces allows the detection of a variety of information as: purely qualitative observations (i.e. RGB images in Color Imaging), the discrimination of pigments used (IRFC, Visible UV Induced Fluorescence), the highlighting of the artist's underdrawings or *pentimenti* (IR Reflectography), the alteration of chromatic relationships due to the aging of varnishes, etc. Furthermore, MSI techniques let to analyze an object through individual spectral bands within the wavelength region from UV up to NIR, for then statistically treat the acquired images (Cetica, et al., 2007).

Nevertheless, it should be noted that the most widespread tendency — especially among photogrammetrists — is to consider the paintings as two-dimensional objects on which apply all the different imaging techniques ignoring the depth information. Just apparently, the planar nature of a painting justifies this approach. Indeed, the reverse side of the paintings can be highly informative for conservators, diagnosticians and restorers. An approach tailored to the photogrammetric survey of both sides of a painting has been followed recently by Abate (Abate, et al., 2014). Patches, stitching, wooden dowels, wedgelike insertions, dovetails, crossbars, signs that recall linings or mending, all testify the «emergence of the physical structure of the work of art» and its conservative history. Not surprisingly, the iconography set of Cesare Brandi's *Teoria del Restauro* (Brandi, 1963) just began with the image of the back side of the *Ecce Homo* by Antonello da Messina preserved in Spinola Palace in Genoa, in order to point out the identity of the artwork related to its physical consistency.

From these assumptions emerges the need to integrate the analysis of radiometric contents using 2D multispectral images and the 3D surveying of a painting for its geometric deformation analysis along time, to create a complete package of information about an opera and for increase its understanding (Fontana, et al., 2005). For the sake of art diagnostics and visual CH, it is often needed to compare different sets of information, coming from different sources and stored in different datasets. For instance, such need is highlighted in a study of Lahanier (Lahanier, et al., 2005) where the author successively perform MS acquisitions of the oil painting on wood *La dame en prière* and two 3D digitizations of its surface but they rely on independent viewers to explore each dataset. Clearly, the instrumental and analytical integration in a single coordinate system can enhance the potential insights into data analysis. Therefore, conservators, diagnosticians and art historians can use the "augmented" models for both virtual reality applications but even more as improvement of 3D models for analysis and study of works of art.

Historically, the restorer Vermehren performed one of the earlier attempt to simultaneously synthesize spatial and spectral information in the 1950s, developing a prototype of a stereo-strati-radiographic system (Vermehren, 1952). Since that time, the interest in combining MS and morphometric data sets in order to create 3D models with MS texture has continuously grown.

3.2 Data Registration strategies

Many recent surveying and documentation projects (El-Hakim, et al., 2008; Guidi, et al., 2010; Fassi, et al., 2011) evidence that the best 3D modelling results are achieved by integrating different surveying techniques. However, in most works that have incorporated MS data into 3D models, the 3D shapes are generated by range devices rather than from MS images directly. This means that the current imaging systems (such as

MS cameras and imaging scanners) and 3D sensing devices are practically used independently. Over the years, the research groups that have tried to develop MS 3D digitization systems mostly have proposed to register the independent data sets, i.e. mapping the spectral information to the 3D shape, via post-processing.

Create MS 3D models is not an easy task because imaging systems and 3D sensing systems are generally based on different physical principles and built on different concepts. Therefore, when separate devices are used, a registration procedure — i.e. «the determination of a geometrical transformation that aligns points in one view of an object with corresponding points in another view of that or another object» (Sonka & Fitzpatrick, 2000) — is required. More in detail, data registration is necessary as the information might come from:

• Different imaging sensors (*multi-modal data*): where data related to the same object or scene are acquired by different sensors e.g. working in different parts of the light spectrum (*multispectral data*). The data collected need to be aligned afterwards and overlapped for information fusion, multi-spectral analysis or other diagnostic applications.

• Different viewpoints (*multi-view data*): data of the same object or scene are acquired from different standpoints for 3D reconstruction purposes or to generate high-resolution views or panoramas.

• Different acquisition times (*multi-temporal data*): data of the same object or scene are acquired at different times e.g. to evaluate changes or movements.

Furthermore, registration can be performed between 2D-2D data (e.g. images), 2D-3D data (e.g. an image mapped onto a 3D model applying *the Direct Linear Transformation* DLT registration method, referred to the Tsai method) or 3D-3D (e.g. range maps). Data registration is often performed manually, iteratively setting the parameters of the geometrical transformation or interactively seeking the corresponding features. As it is evident, this is not a trivial approach: usually it is time consuming and it can give subjective results.

For the reasons given above, most of the combined systems already used to acquire data related to the same object or scene by different sensors or in different modes (*multimodal*), lacks flexibility. With the advent of the new 3D Data capture image-based methodologies, new scenarios that avoid the hardworking phase of registration are opening up.

It should be noted that increasing the amount of acquired data also increases the need for new data analysis techniques for their interpretation. Henceforth, image segmentation, recognition and classification algorithms (Szeliski, 2010), will have to be based on the whole integrated dataset, and no more on a single aspect (3D or MS). New visualization and interaction methods must be developed so that specialists and non-specialists can interact intuitively with these augmented models.

What follows is an overview of selected recent advances and on some data integration practices proposed by several research groups. They are mostly related to active sensors, i.e. to the range based methods. In this regard, the very useful article of Chane (Chane, et al., 2013) has been used as resource survey. Afterwards, I will present the field related works carried out by my research group.

3.3 Overview on recent advances in data integration practices

There are several integrated acquisition systems that combine color and single sensor/multiple sensors 3D acquisition devices or that combine MS - 3D acquisition devices. As already said, in the case of multiple sensors, it is necessary to resort to 2D-3D registration algorithms; on the contrary when using a single sensor, shape and texture are automatically registered.

To avoid the difficult task of identifying homologous points between the 2D and 3D data - much more complex than "image to image" or "geometry to geometry" registration – Pelagotti (Pelagotti, et al., 2009) proposed an automatic texturing of the 3D model with multispectral/multimodal images, achieved as a result of a 2D to 2D image registration. The method relies on the extraction from the model geometry of a depth map, in form of an image, whose pixels maintain a correspondence with vertices of the 3D model. The subsequent registration step is carried out by means a robust custom registration algorithm, based on *Maximixation of Mutual Information* (MMI) (Viola & Wells, 1997).

Prominent examples of integration between color / 3D acquisition devices with a single sensor are the work carried out by the National Research Council of Canada that has developed an RGB laser scanner, also used to analyze the *Mona Lisa* (Beraldin, et al., 2000; Bernardini, et al., 2001; Taylor, et al., 2003; Blais, et al., 2005; Blais & Beraldin, 2006).

When different sensors are attached to one another, a simple calibration procedure can determine the internal parameters and the fixed relative position and orientation of the sensors. A few sensors based on this setup are those presented by Levoy, Ikeuchi and Blais (Levoy, et al., 2000; Blais, et al., 2007; Ikeuchi, et al., 2007).

A few integrated 3D/MS acquisition systems have been developed over the fifteen years but not all are dedicated exclusively to CH. For instance, Manabe presented an interesting approach to represent spectral information as 3D model (Manabe, et al., 2000). They first constructed 3D model using two different hardware and then mapped the spectral information to the 3D model. This method, however, did not explore relationship between spectra and structure. Kim introduced a system for capturing spectral data on 3D objects (Kim, et al., 2012). A hyperspectral imager was used to acquire high spatial resolution band images from Near-UV to Near-IR range. This imager was then integrated into a 3D scanning system to capture the spectral reflectance and fluorescence of objects. Similarly, Nieto developed a hyperspectral 3D modelling system for the mining industry. 3D model was generated based on depth data captured by a laser scanner, with hyperspectral image mapped to this 3D model (Nieto, et al., 2010). Mansouri and Sitnik have both developed an integrated acquisition system based on an interference filter-wheel, a projector and a single sensor to acquire either 3D and MS data (Mansouri, et al., 2007; Sitnik, et al., 2010). The system developed by Tonsho also acquires a combination of MS, 3D and gonio-photometric data using a triangulation laser scanner, a MS camera and a tungsten lamp in seven successive positions together with a turntable for surveying the full object (Tonsho, et al., 2001).

With regard to the field of CH, Brusco has developed an integrated 3D/MS acquisition system aimed to digitizing frescoes — that are large and planar objects — to be used *in situ*. It is based on a commercial spectrophotometer and a ToF laser scanner. A rotating mirror and a rotating stage are used to scan the surroundings respectively vertically and horizontally. The calibration parameters are calculated using the correspondence between projected spots from the laser scanner and their image in MS datasets (Brusco, et al., 2006). Liang set up an additional spectral imaging system that allows an automatic, *in situ*, remote imaging of wall paintings providing both spectral reflectance information per pixel both the 3D position and distance measurements. This system called PRISMS (*Portable Remote Imaging System for Multispectral Scanning*) consists of modular components: a telescope (for imaging at distances >3-4 m), lenses (for close range imaging at distances <3-4 m), interference filters with CCD detectors (for imaging in the range VIS/NIR) and an imaging AOTF spectrograph and an InGaAs detector (for imaging in the SWIR) (Liang, et al., 2014).

Among the few existing integrated systems, special mention goes to the *Multi-Vis-Nir Scanning* Device (SMIRR technique) developed by CNR-INO's Cultural Heritage Group (Daffara, et al., 2010; Fontana, et al., 2011; Daffara & Fontana, 2011; Fontana, et al., 2015). This is one of the most advanced tool of the field, which has been part of the mobile instrumentation of the CHARISMA project (2009-2013). This contactless optical scanner operates in the VIS (380-750 nm) and in the NIR (750-2500 nm) regions of the electromagnetic spectrum. In a single measurement session, it simultaneously provides two types of information: *i)* a single-point information, in the form of spectral data, and *ii)* an areal information of the surface. The autofocus system maintains the optimal target-lens distance during the entire scanning, providing a set of 32 perfectly overlapping monochromatic images, free of any aberration (16 VIS - 16 NIR images; spatial sampling 250 μm; spectral sampling 20-30 nm in the Vis, and 50-100 nm in the NIR), that can be analyzed as a spectral cube. Indeed, the reflected light from a single point is collected and distributed using a fibre bundle to a series of detectors with different interference filters. The multi-NIR scanner overcomes the limitations of most of the systems currently used for MS imaging. Point-by-point sampling solves the problems related to the use of extended detectors and filter tuning and provides precise information in the spatial and spectral domain, namely, a metrically and optically correct set of images that are mutually registered. This system's inherent characteristic avoids the post-processing phase and it restricts the introduction of any errors. The spectral sensitivity of the detection system (increased up to 2500 nm), the quality of focusing and uniformity of the acquired images, and the possibility for selective imaging in NIR bands in a registered dataset, amplify the NIR analysis potential, specially because many pigments show relevant transparency precisely in this spectral range. Furthermore this system is optimized for *in situ* measurements and it allows to visualize each of the spectral bands image in real-time. Finally, being essentially a range based device, the instrument also indirectly provides three-dimensional and profilometric information of the investigated surface area.

3.4 The SUMUS project. A Multispectral 3D integrated system proposed by ICCOM ALSLab

In 2011, the CNR-ICCOM ALSLab – the research group where I carried out my Ph.D. – participated at the SUMUS project (*SUperfici MUltiSpettrali*) together with Menci Software s.r.l., Art-Test s.a.s., and CNR-ICVBC. The project aimed at the development of a portable prototype for extending the information gained through the multispectral analysis of CH along the third dimension. In particular the design of the tools developed by SUMUS had the target of surface profiles reconstruction of paintings, frescoes, etc. and at the same time a colorimetric and NIR information "mapping" on them, using proprietary algorithms developed by the proposing companies.

The prototype was tested during some targeted measurement campaigns: *i)* the frescoes of the Monumental Cemetery of Pisa, *ii)* the mural paintings of the *Tomb of the Monkey* in Chiusi (SI), *iii)* the panel painting depicting the *Annunciation* by Benozzo Gozzoli in Narni (TR), *iv)* the *Altarpiece of St. Catherine from Alessandria* by Simone Martini at the National Museum of San Matteo in Pisa, and *v)* the *Deposition from the Cross* by Beato Angelico in the National Museum of San Marco in Florence (FI).

Fig. 14 SUMUS System with the DTA Chroma4-DSP C250.

The system devised by the project was based on the classical photogrammetry principles, i.e. using a properly calibrated digital camera, it generates a RGB point cloud simply by acquiring three images of the same portion of the object (called "triplet"), taken from different angles.

The size of the investigated area ranged from 2 to 20 cm^2 according to the shooting distance. The system consisted of a 260 mm long motorized bar, along which flowed both a digital SLR Canon EOS 400D equipped with a macro lens Canon EFS 60 mm, and a MS camera DTA Chroma4-DSP C250 (fig. 14).

The micro-photogrammetric system was completed by a set of three dedicated software that allowed the acquisition of the area of interest (*ZScan Micro*®), the generation of the point cloud (*ZScan*®), and the processing of models (*Z-Map*®). *ZScan Micro*® software managed remotely the system (camera position along the motorized bar and acquisition control); once identified the area of investigation, the software proceeded in an automatic evaluation of the distance between the camera sensor and the area to be scanned, suggesting the better acquisition distance. During the acquisition phase the software required a 50% of overlap between two consecutive shots.

After the generation of the point cloud, once the model has been built using a specific algorithm, a texture has been applied with a precision of about ± 20 µm along the x and y directions, and of about ± 50 µm along the z direction. The use of different focal length lenses, such as a 28 mm lens,

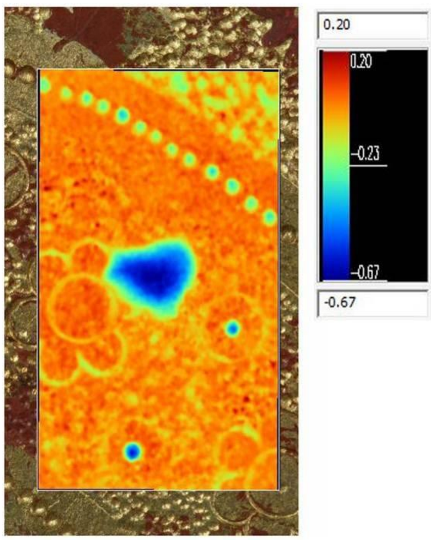

Fig. 15 DEM of a detail of the punching on a golden area of the Altarpiece of St. Catherine from Alessandria by Simone Martini'.

allowed the reconstruction of larger areas, which can in turn be stitched within a single model.

Once a reference plane was identified (*User Coordinate System* UCS), the *Z-Map®* software was also able to generate the DEM (*Digital Elevation Model*) or the color-altimetric raster representation of the distribution of the heights of a surface (fig. 15). The software automatically provided the value of the maximum and minimum coordinates of the surface pattern, represented in a chromatic scale, respectively from the red to the blue color. Furthermore, specific software functions allowed the overlapping of the areas acquired even with different focal length lenses.

The same overlapping function has been used to acquire areas at different times, such as before and after a cleaning treatment. In this case, it was possible to keep on a comparative analysis of the two surfaces, providing the DEM of the individual models, the histogram of the surface heights, the DEM of difference between the two models, and the differences of the frequencies between the two shots. Choosing a direction on the investigated area, surface sections could be generated and the details of these profiles easily exported into a spreadsheet software for a matter of further analysis (fig. 16).

Even in this case, as for the other systems above mentioned, the most critical point of the whole system was just the registration of MS images on the model photogrammetrically obtained in RGB.

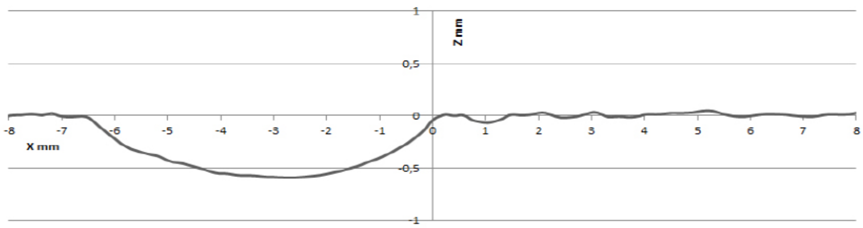

Fig. 16 Profile of a section of the surface. The graph shows the trend of a lack in the paint film deep about 0.6 mm and wide about 6.5 mm.

Moreover, the presence of different spectral filters interposed between the sensor and the optics mounted on the DTA C4-C250 DSP required further complex mathematical methods and computational tools for the calibration. The interposition of the filters, with different optical / physical / geometric characteristics, had a considerable effect in the optical path of the recovery. The geometric implications of this configuration were understood, studying the physical model.

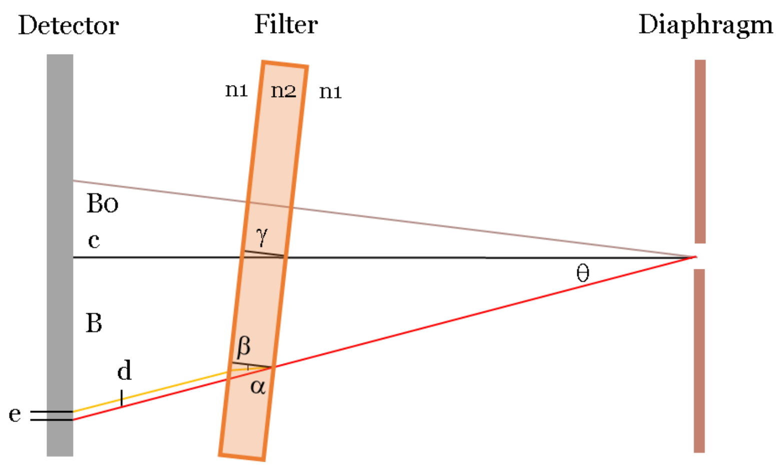

Fig. 17 Sketch of the geometrical model with the interposition of a filter.

In which:

• Focal *b*

• Filter thickness *d*

• Filter Refractive Index $n2$
• Refractive deviation α
• Deviation to the sensor e
• Filter Misalignment γ

By varying a filter, α and γ parameters vary too, producing interference fringes. Since the thickness of the filter, its refractive index, and the misalignment angle caused distortions in the generation of images (in particular deformations with transversal stretching), than an acceptable albeit not resolutive approach required a subsequent registration using area-based, feature-based algorithms, or Fourier Filters. Furthermore, the fact that the position of the filters was not adequately orthogonal to the optical axis has been verified. The angle θ was variable from filter to filter, consequently a distinct geometrical calibration was required for each of them we mounted on the DSP DTA C4-C250 camera. Whenever large calibrations are involved, it will always results in higher costs in both economic and temporal terms. For these reasons, the system was not considered particularly flexible so that the software *ZScan®* is currently out of production.

Nevertheless, within the project some of the experiments produced good – even if partial – results. For example, in the case of the panel painting depicting the *Annunciation* by Benozzo Gozzoli, the MS images (Visible UV Induced Fluorescence, NIR) were successfully projected on 3D surface reconstructed with the Menci's software suite, getting the full model of the painting front, also viewable in anaglyph mode (i.e. the stereoscopic 3D effect achieved by means of encoding each eye's image using filters of chromatically opposite colors, typically red and cyan) (figg. 18-20).

Fig. 18 3D RGB image (left); 3D RGB image - Anaglyph mode (right)

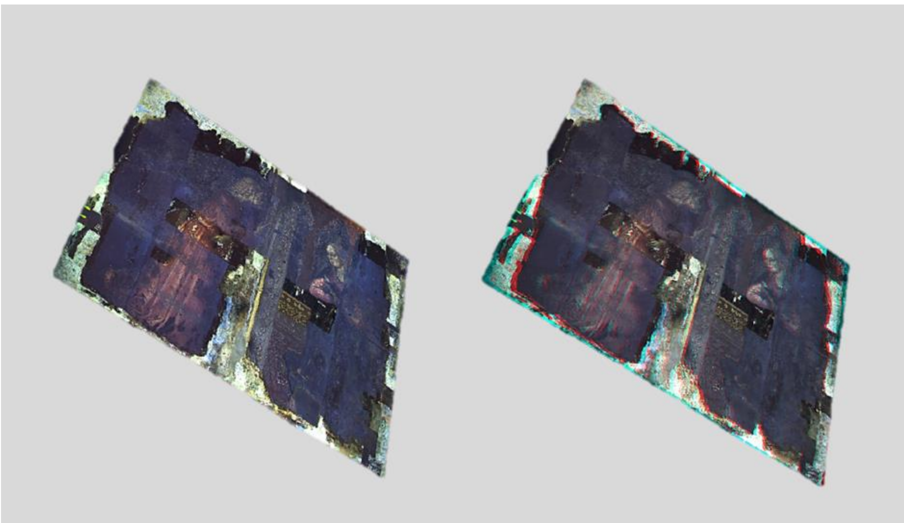

Fig. 19 3D UV image (left); 3D UV image - Anaglyph mode (right)

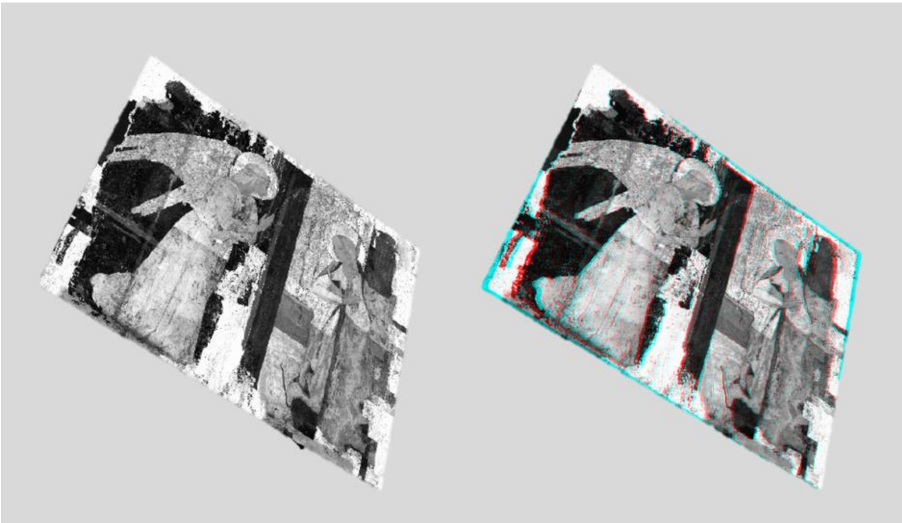

Fig. 20 3D IR image (left); 3D IR image - Anaglyph mode (right)

In the case of the *Altarpiece of St. Catherine from Alessandria* realized by Simone Martini, the experimentation was focused on selected areas of interest because of the large dimensions of the artwork, in particular on the panels depicting St. Philip and Mary Magdalene. As shown in fig. 21 the first selected area was acquired with 400nm, 500nm, 650nm and 750nm filters, in order to create their respective 3D models.

Later the further model obtained with the RGB micro-photogrammetric method was superimposed over them (fig. 22a). Having identified on each model the same reference plane (UCS), individual DEM were generated. On these, the surface roughness profiles of both models were obtained.

As it was expected, the analysis of the color-altimetric scale of the two DEM pointed out the smaller definition of the details relating to the DEM of MS model (fig. 22b, 22c).

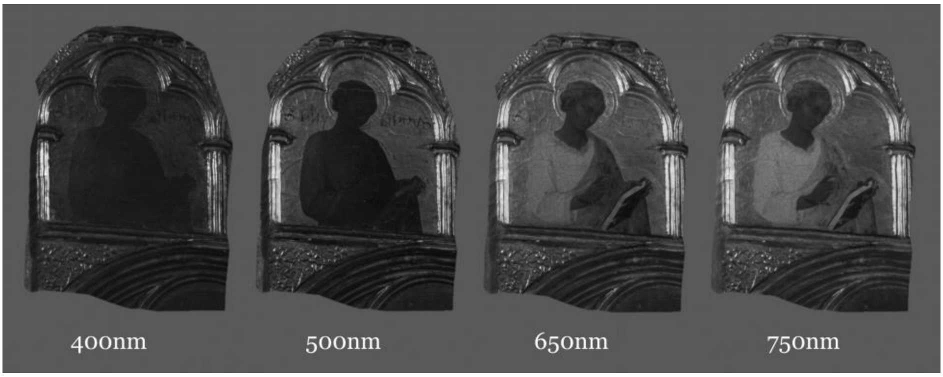

Fig. 21 3D models of the panels depicting St. Philip, respectively acquired in 400nm, 500nm, 650nm and 750nm bands.

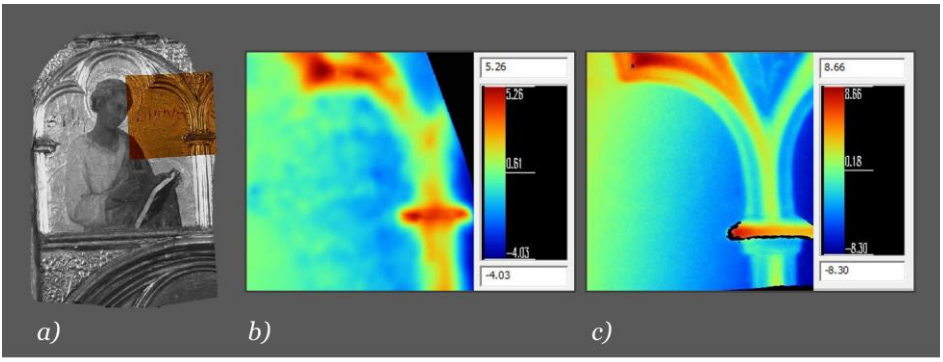

Fig. 22 a) Superimposition of the RGB micro-photogrammetric model; b) and c) the two DEMs generated on both the 3D models.

The graphs of roughness profiles for the two DEM (in red those of the 3D MS model, in blue those of the 3D RGB model) showed a similar trend, but with loss of details for those obtained with the MS system (fig. 23).

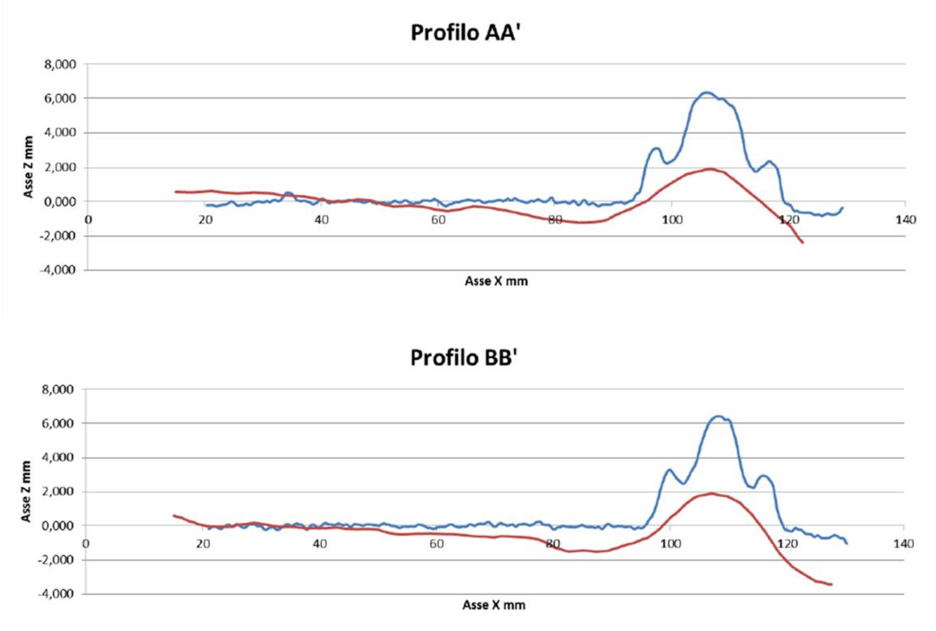

Fig. 23 Graphs of roughness profiles for the two DEM (in red those of the 3D multispectral model, in blue those of the 3D RGB model).

For the acquisition of the second selected area, we used two lenses: a 28 mm lens for the model of the entire panel, and a 60 mm lens for focusing on the details of the vertical crack presented in the pictorial layer. To correctly visualize the criticalities of such vertical crack 12 small models (64 x 68 mm each) have been generated. Stitching together the single acquisitions resulted in the model of the entire area of the crack (size c.a. 251 x 63 mm). The 3D model was generated with *ZScan®* with a resolution of 5 pixels (1 three-dimensional point every 5 pixel of the photographic image). The subsequent analysis of the models (DEM generation and surface profiles) was performed with *Z-Map®* software (figg. 24, 25). The measurement was effective because it enabled the calculation of the size of the crack (between 0.20 to 0.60 mm in the *xy* plane).

Fig. 24 On the left the RGB 3D model of the entire panel depicting Mary Magdalene; in the centre the reference plane (UCS) chosen for the DEM generation of the area with the crack and a geographically representation of the same DEM; on the right the DEM of with its reference scale.

As it is clear from the above-mentioned study cases, the SUMUS system has resulted in quite good results, though not entirely satisfactory. The described limitations have indeed reduced the initial enthusiasm in its systematic and continual use, despite the fact that it was an averagely flexible system.

Consequently, the focus of our research group over the past three years has been oriented towards the experimentation of a more versatile and practical alternative technique, while maintaining the characteristics of sub-millimeter accuracy required by the 3D modeling survey of easel artworks. As it will be described in the next chapter, the 3D modeling procedure directly based on MS images that we are now proposing is a good compromise in terms of flexibility, portability, cost, and precision.

The conceptual assumption is that the Multispectral Imaging is an extension of Color Imaging. Thus, taking advantage from the SfM techniques for the rendering of the different spectral bands without any need of neither to proceed to the registration, nor to necessarily know the calibration parameters of the devices used, it results in an increased flexibility and ease of use. As demonstrated later, with this practice it is possible to get as output a single 3D model while starting from a variety of input data such as: color images, IR Reflectography data, UV Induced Fluorescence images, Thermal images, etc. The precondition is that the input raw data can be preliminarily processed to be included in the dedicated 3D modeling software as .jpeg or .tiff format.

The portable system that we propose provides contactless capture mode that can be used directly in museums, monuments or any other non-laboratory site, even if it does not provide real-time calculations because of the medium-long computational time required.

We believe that this is an avant-garde and promising method from which we expect great developments and a future widespread use. The fact that this is effectively a method to be looked with interest has been proved by Zia's latest work (Zia, et al., 2015). In their paper the authors present a method similar to our own to reconstruct a 3D model from hyperspectral images. It first generates 3D point sets from images at each wavelength using the typical SfM approach, and then a structural descriptor characterizes the spatial relationship between the points, allowing robust point matching between two 3D models at different wavelength. Lastly, a 3D registration method is introduced to combine all band-level models into a single and complete hyperspectral 3D model.

The authors also claim that, to the best of their knowledge, their attempt is the first one in reconstructing a complete 3D model from hyperspectral images. We may therefore say that ours is the first attempt to reconstruct a complete 3D model from MS images about works of art.

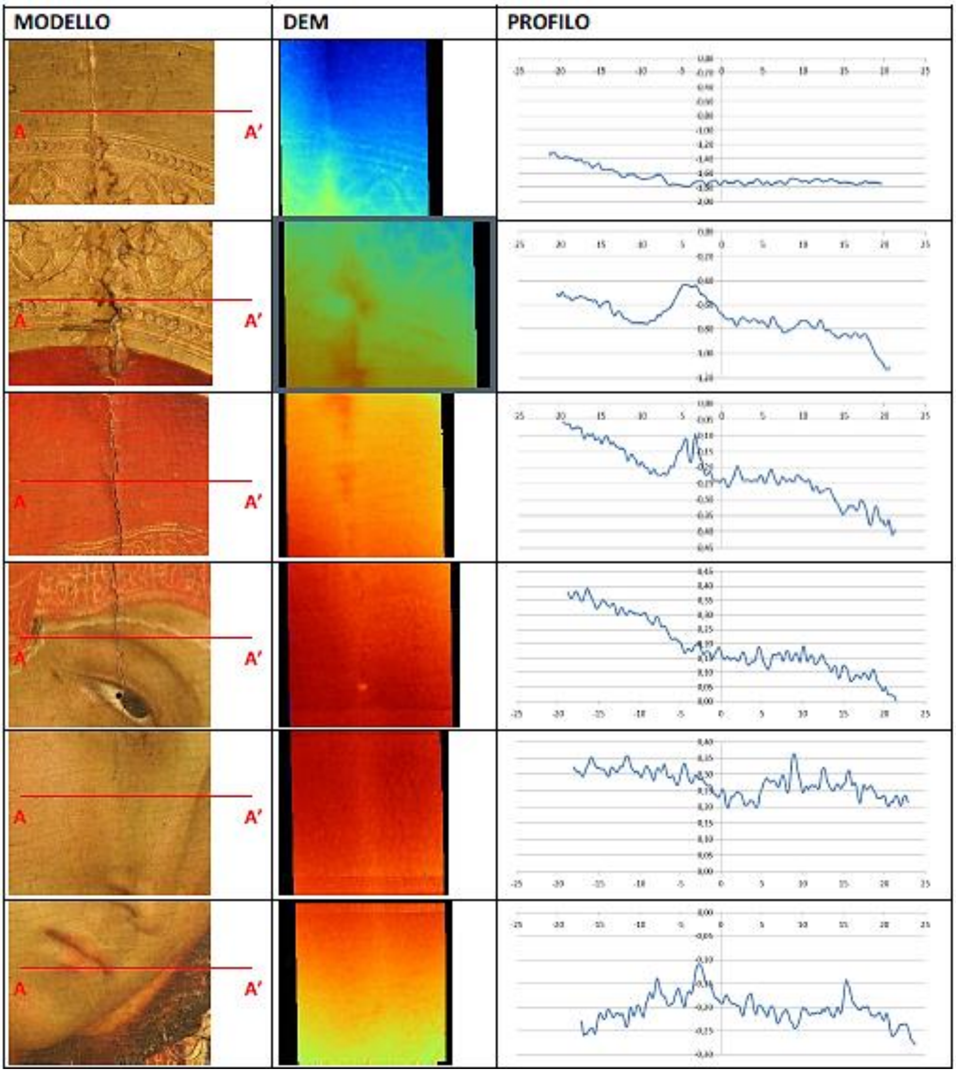

Fig. 25 Single models of the crack, DEMs and surface roughness graphs.

4

Photogrammetric and Multispectral procedural Modeling

In this chapter I will give a detailed description of how we obtained the 3D models of the panel painting depicting the *Madonna and the Child* by Barnaba da Modena, both in RGB and in the IR bands, with a high level of morphological and radiometric detail.

The study highlights the critical issues encountered, due to the specificities of the subject and of the inedited method tested on a work of art tending to the two-dimensionality.

The entire procedure has been replicated on the second case study, previously introduced: the Sicilian panel painting titled *Madonna and the Child, and the Pentecost* in order to verify the repeatability of the MS photogrammetric approach and to confirm the results obtained with the first case study. Lastly, the relative accuracies of the models in revealing deformations at sub-millimetric level without using any special network design concept are here evaluated.

4.1 Case Studies

We chose to launch our study starting from panel paintings since this type of artifacts is known to be well suited to the MS sequence. Indeed, their executive techniques usually include a preparatory underdrawing realized with carbon derivatives — graphite and charcoal — opaque in the NIR spectral region, the use of some pigments transparent to NIR light, the presence of an easily recognizable varnish by the UV fluorescence, and so on. Moreover, the three-dimensional restitution of their carpentry can enhance the evidence of all those structural or restoration elements - as dowels, wedges, crossbars, etc., that further enrich the knowledge of the work of art in its entirety.

The first selected artwork (fig. 26) is a traditional religious painting, technically realized with egg tempera on poplar panels and executed with exceptional mastery. It is dated at the second half of the 14^{th} century and it is currently preserved at the National Museum of San Matteo in Pisa.

The inscription beneath the Madonna tells us that Barnaba da Modena (Agocchiari) painted it: BARNABAS DE MUTINA PINXIT.

This painter was particularly active in Genoa and Pisa. In the latter city there are several of his works which suggest a solid reputation, especially among collective commitments and merchants. Examples of the Sienese and Venetian paintings — with their previous Byzantine characters — contribute towards forming his style, subtly decorative and still dependable to archaic motifs.

The iconographic theme of the *Madonna Lactans* is often replicated by Barnaba da Modena, with minor variations, in multiple works (figg. 27b, 27c).

Fig. 26 Barnaba da Modena, Nursing Madonna, 82 × 61 cm, 1370 c.a, National museum of San Matteo, Pisa.

These paintings show an accentuated derivation from the *Nursing Madonna* of Ambrogio Lorenzetti (fig. 27a) who had the merit to renovate the figure of the Virgin through a composition no longer referring to the hieratic immobility of Byzantine icons, but in an intimate maternal relationship with the child. In the painting preserved in Pisa, the Virgin is indeed depicted in the loving gesture to breastfeed the infant. Her cloak is decorated with golden highlights and on the background a precious fabric with the motive of the pine cone is held up by four angels. There is a molded and polylobate emerging frame. In the top corners, inside the medallions, two miniatures depict the *Annunciation*.

The state of preservation is good. Previously to our measurements, the painting has been subjected to a woodworm treatment and to a retouching.

Fig. 27 a) Ambrogio Lorenzetti, Nursing Madonna, 90 x 45 cm, 1335, Museo Diocesano di Arte Sacra, Siena. b) Barnaba da Modena, Madonna and Child, 117.8 × 86.2 cm, 1367, Stadel Museum, Frankfurt. c) Barnaba da Modena, Nursing Madonna, 109 × 72 cm, 1370 c.a, Louvre Museum, Paris.

Fig. 28 Unknown, Madonna and Child. Pentecost (in pinnacle), 67 × 36 cm, 15th Century, Bellomo Museum, Syracuse.

The second painting[1] (fig. 28) is also realized with egg tempera on wood. It dates back to the 15th and it is preserved in the Regional Gallery of Palazzo Bellomo in Syracuse. The panel size is 67 × 36 cm and the support, constituted by two boards, ends with a cusp. The author is unknown, but the painting is attributable to the more general Sicilian school. The figurative characters are quite archaic and provincial. It is probable that this object was made for a devotional use.

On the bottom, the painting shows a significant loss of the paint film and of the preparatory layers that leave visible and uncovered the wooden support. In this area two passing through holes are evident, successively compensated with circular wooden inserts. These holes can be traced back to the presence of two parallel nodes in the boards or more likely they may be two housing holes for crossbars for using the painting as a processional banner. The state of conservation is good, thanks to a recent restoration.

[1] The painting has been investigated during the high training course promoted within the IPERIONCH.it project, in collaboration with Opificio delle Pietre Dure, CNR, INFN, ENEA, INSTM, MIUR and the Bellomo museum.

4.2 Methodologies, software and tools

As known, SfM is composed of a matching, scene reconstruction, and point cloud generation functions. In general, precision and accuracy are used to evaluate 3D measurement from the photogrammetric viewpoint. In this light, several field studies (e.g. Schoning & Heidemann, 2015, Yanagi & Chikatsu, 2016) have evaluated performance of some photogrammetry software packages, as *PhotoScan* and *PhotoModeler* (commercial low cost software), *Autodesk 123D Catch*, *Photosynth*, *Bundler*, *SfMToolkit*, *Smart3DCapture* (freely downloadable software), and so on. However we must admit that there is no a standardized procedure or a fixed method but instead there is an adjustment from time to time to the specific goals, requirements and restrictions of the survey.

In relation to our needs, we chose to combine *Photoscan Pro 1.2*, *CloudCompare*, *Meshmixer* and *Meshlab* software, as it will be described later in a detailed way.

The general workflow has comprised two separate pipelines, one for the building of the RGB 3D model (RGB-M) and one for the building of the IR 3D model (IR-M), as shown in fig. 29. Regardless of the different acquisition sessions — necessarily due to the different equipment — we tried to keep the same procedural steps to obtain comparable results at a later time.

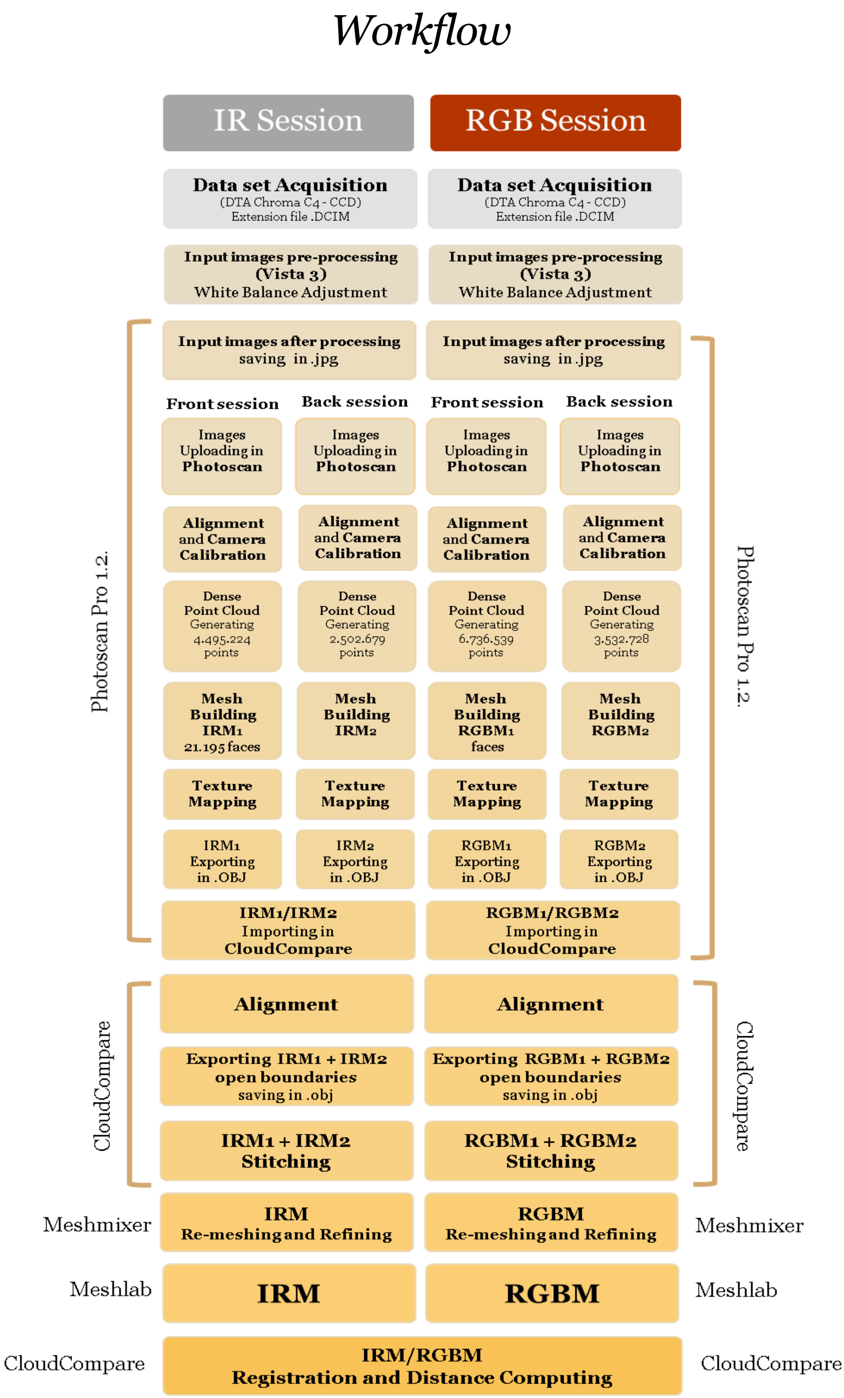

Fig. 29 General workflow of the MS procedural modeling

4.2.1 Cameras

- The RGB imagery has been collected using the semiprofessional Nikon D7000. This is a *Digital Single-Lens Reflex* camera (DSLR) that employs the Nikon DX-format CMOS sensor (23.6 × 15.6 mm; 4.78 µm pixel size), with a maximum resolution of 16.2 effective Mpixels (4928 × 3264). This camera produces great image quality and feels very responsive in most shooting situations. In order to avoid camera micro-shake effects and to produce better quality photos, the camera has been always mounted on a tripod. For all photo-editing operations, we used the full-features imaging software *CaptureNX2* produced by Nikon.
  The table below shows some basic specifications:

Tab. 2 Nikon D7000 Technical Specifications.

Technical Specifications

Image Sensor

Sensor Type:	CMOS
Sensor Manufacturer:	Sony
Effective Megapixels:	16.2
Sensor Format:	APS-C
Sensor size (Aspect ratio):	368.16 mm² (23.60 x 15.60 mm) 3:2
Approximate Pixel Pitch:	4.78 µm
Focal Length Multiplier:	1.5x
Color Filter Type:	RGBG

Image Capture

Image Resolution:	4928 x 3264 (16.1 MP, Other),
Image File Format:	JPEG (EXIF 2.3), NEF (RAW) 12 or 14-bits, RAW+JPEG

- The IR imagery has been collected using the multispectral camera ChromaC4-DSP, C250ME model, produced by DTA srl. This camera is equipped with a Kodak KAF-8300ME[2] full-frame *Charge-Coupled Device* (CCD) sensor which is a 22.5mm diagonal (Four Thirds Format) with an active area of 242 mm^2; it has a resolution of approximate 8 Mpixel effectives, with 16-bits grayscale dynamic range and it is cooled (40°C ΔT) for reducing the electronic noise during the acquisition. The spectral resolution is obtained through the use of an internal integrated 8position filter-wheel for interferential filters with ± 25 nm pass bands around the central wavelengths (fig. 30a). For the analysis, images in the IR spectral band (1050 nm) were acquired and processed. The central wavelength of the IR band was chosen taking into account the spectral sensitivity of the CCD sensor (*Quantum Efficiency* - QE) (fig. 30b), which drops dramatically around 1100 nm. For all photo-editing operations, we used the in-house imaging software *Vista3*. The table below shows some basic specifications:

Tab. 3 ChromaC4 C250ME Technical Specifications.

Technical Specifications

Image Sensor

Sensor Type:	CCD
Sensor Manufacturer:	Kodak
Total Number of Pixels:	3448 x 2574
Number of Active Pixels	3366 x 2544
Effective Mpixels:	approx. 8
Sensor Format:	4:3
Sensor size(Aspect ratio):	242 mm^2 (17.96 x 13.52 mm) 22.5 mm (diagonal)
Approximate Pixel Pitch:	5.4 μm^2
Focal Length Multiplier:	2x
Quantum Efficieny (QE) (450, 550, 650 nm):	45%, 57%, 48%

2 http://www.kodak.com/ek/uploadedFiles/Content/Small_Business/Images_Sensor_Solutions/Datasheets(pdfs)/KAF-8300LongSpec.pdf

a)

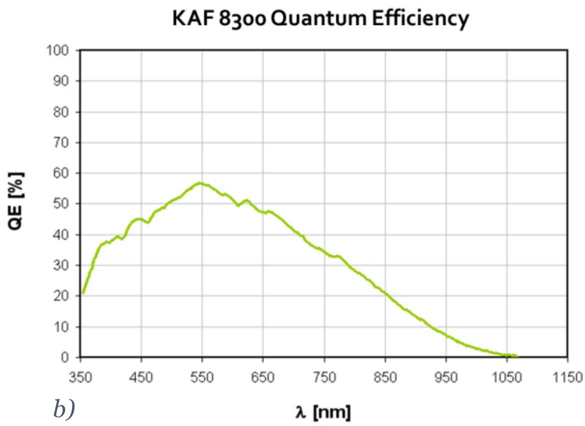

b)

Fig. 30 a) Internal integrated 8position filter-wheel;
b) KAF-8300 Quantum Efficiency.

4.2.2 Software Packages

- *PhotoScan Pro* 1.2[3] is a low-cost commercial software produced by the Russian-based company AgiSoft LLC. As they advertise, the software is «an advanced image-based solution for creating professional quality three-dimensional (3D) content from still images» (AgiSoft LLC, 2010a). Built to operate on Windows systems (from XP onwards), *PhotoScan* uses a multitude of .jpeg, .tiff, .png, .bmp or .mpo files to generate three-dimensional meshes and accompanying mesh textures in an automatic way. Even though the user can set a large number of input parameters, the reconstruction itself is an easy three-step process. At any stage, it is possible to intervene and disable/enable individual photographs, mask parts of the images or import textures and meshes created in other applications. Its excellent performance has been validated in previous studies (Verhoeven, 2011; Eltner & Schneider, 2015) and it has also been confirmed by our own.

[3] http://www.agisoft.com.

- *Meshlab*[4] is an advanced 3D mesh processing software system that is oriented to the management and processing of unstructured large meshes that arise in the 3D scanning pipeline. MeshLab is free and open-source software, developed by the ISTI CNR research center (Cignoni, et al., 2008). It provides a set of tools for editing, cleaning, healing, inspecting, rendering, and converting 3D complex meshes. For example, the automatic mesh cleaning filters includes removal of duplicated, unreferenced vertices, non-manifold edges, vertices, and null faces. Remeshing tools support high quality simplification based on quadric error measure, various kinds of subdivision surfaces, and two surface reconstruction algorithms from point clouds based on the ball-pivoting technique and on the Poisson surface reconstruction approach. For the removal of noise, usually present in acquired surfaces, MeshLab supports various kinds of smoothing filters and tools for curvature analysis and visualization.
- *Meshmixer*[5] (Autodesk) is a free program developed by Ryan Schmidt (Schmidt & Singh, 2010) that includes a suite of manipulation and repairing tools for smoothly blending different meshes, deforming meshes with control points, as well as deleting or filling unwanted holes.
- *CloudCompare*[6] (Girardeau-Montaut) project began in 2003 with the initial purpose to quickly detect changes in 3D high density point clouds acquired with laser scanners in industrial facilities or building sites. Afterwards it evolved towards a more general and advanced 3D data processing software. It is now an independent open source project and a free software. It is very powerful in

[4] <http://meshlab.sourceforge.net>.
[5] <http://www.meshmixer.com>.
[6] <http://www.danielgm.net/cc>.

comparing dense point cloud data, visualizing data and data analysis. *CloudCompare* provides both a set of basic tools for manually editing and rendering 3D points clouds and triangular meshes (even thought for the software these last are primarily point clouds, i.e. sets of vertices that have particular structures in addition to numerous other structures: octree, kd-tree, colors, normal, scalar fields, calibrated photos) both various advanced processing algorithms, among which methods for performing:

- projections
- registration
- distance computation
- statistics computation
- segmentation
- geometric features estimation

Moreover *CloudCompare* can handle unlimited scalar fields per point cloud on which various dedicated algorithms can be applied (smoothing, gradient evaluation, statistics, etc.). A dynamic color rendering system allows to visualize per-point scalar fields in an efficient way.

4.3 General workflow

4.3.1 Shooting conditions:

The painting has been constrained to a painter's easel. As a matter of precaution, it couldn't be left standing by itself. There was no possibility of freely move around it, therefore it was impossible to perform a shot-campaign with a 360 deg. of sweep. As a result, the tripod and the lights have been arranged in a static location and the acquisition flow of the photos-set was not carried out in continuous among the two faces. We used two different sessions: the first one to scan the front, while the second one to scan the back of the painting from which two different 3D models have been produced. This is clearly not a by-the-book procedure. Measurement condition in real life scenarios needs a certain amount of compromises. This was the reason why the correct aligning and merging of the two models has been a challenging, as shown in the following pages. To overcome this difficulty, an experimental implementation could be obtained introducing some external constrain as a temporary adaptable frame, capable of supporting the subject and that could also be scanned as a reference of the scene.

The subject was uniformly illuminated in order to keep harsh shadows to a minimum and to properly render the extremely reflective golden areas of both painting and frame that otherwise would have caused any problems or irregularities in the succeeding post-processing phase. The spotlights with the same intensity for both RGB and IR acquisitions have been placed at 45 deg. from the painting on either side and they have been equipped with two umbrella diffusers to soften and to better homogenize the light. Following the *International Commission on Illumination* (CIE) recommendations[7], we used a standard illuminant A as light source, in particular two lamps Philips HalogenA 100W with aluminum reflector. Their *Color Rendering Index* (CRI or R_a) is equal to or greater than 90%. Their relative *Spectral Power Distribution* (SPD) is that of a Planckian radiator at a temperature of approximately 2856 K and it covers part of the NIR band, as shown in fig. 31.

[7] ISO 11664-2:2007(E)/CIES014-2/E:2006.

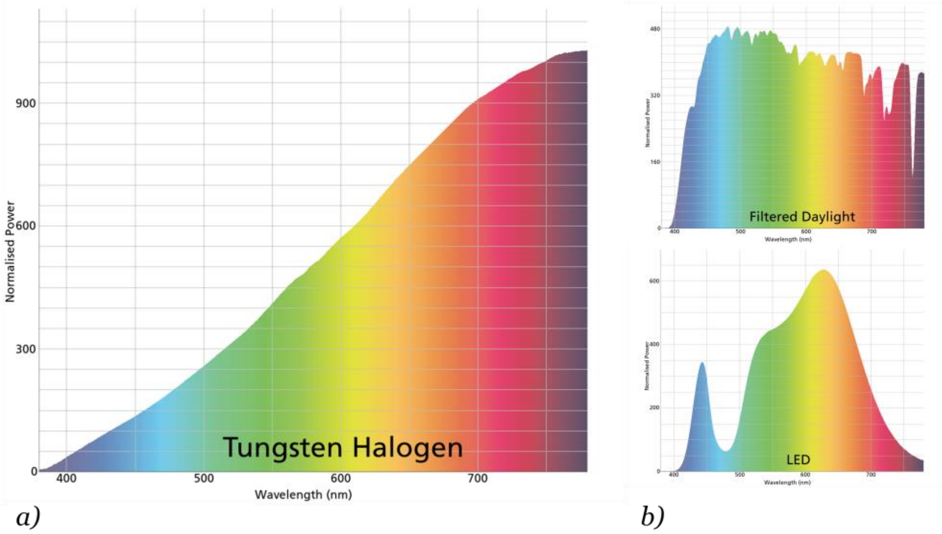

Fig. 31 Example Spectral Power Distribution (SPD) curves. a) Standard tungsten curve (as Philips HalogenA). b) On the top, filtered daylight curve; on the bottom a LED based source.
Figure credits: (The National Gallery. http://research.ng-london.org.uk/scientific/spd/?page=home)

4.3.2 Cameras positioning and Imaging Settings

Generally, during the photographic session there may be some photogrammetric error sources that can consequently lead negative impacts on modeling and surveying, including camera internal parameters (i.e., type, principal point, principal distance, and camera lens distortion coefficients), and imaging settings (i.e., shooting distances, baselines, percentage of photo overlaps, number of overlapping photos, camera intersection angles, and angles of incidence). The existing literature based on the experimental results concludes that also the manufacturing quality of the camera models, the camera calibration, the changes of focal length, the image scale, and the shooting distance can all influence the accuracy of the measurement (Hu, et al., 2011).

In summary, the measurement errors associated with photogrammetry can be attributed to two large categories: *i)* the systematic error due to camera factors, and *ii)* the systematic error due to poor planning of camera network geometry, as shown by the table provided by Dai (Dai, et al., 2014):

Factor	***Behavior***
Distance	Farther distance, lower accuracy (40 m: 6 ~ 10 cm)
Number of overlapping photos	The larger number of overlapping photos, the better accuracy
Intersection angle	The closer to 90°, the better accuracy
Angle of incidence	The closer to 0°, the better quality of images, so the better accuracy
Camera model	Higher end, higher accuracy
Resolution	Strong correlation with accuracy (raise by 1.6% per 1 MB increase)
Features (texture)	More features, higher accuracy; higher accuracy by colorful texture than grey/plain texture
Focal length	Longer focal length, higher accuracy; set to obtain optimum coverage
Camera lens	Less distortion, higher accuracy

Tab. 4 Behavior of photogrammetric modeling in Dai, et al., Photogrammetric error sources and impacts on modeling and surveying in construction engineering applications, 2014.

Taking into account what has been previously said, first of all it has been important to plan the camera network geometry to overcome the practical shooting constraints imposed by the mounting of the target subject. Therefore, we tried to capture a photo with a spatial sweep of roughly 10-15 deg. — both horizontally and vertically — ever maintaining a 60-70% overlap between consecutive photos. Indeed, the relationship between overlap criterion and accuracy level of 3D model rendered is verified: the achievable accuracy tendentially increases with increasing the overlap ratio. With this overlap percentage, it has been sufficient acquiring 20-30 continuous photo — only relating to the front of the painting — to get a good 3D model. Moreover, existing a strong correlation of the measurement error with the shooting distance (Dai, et al., 2013), we placed at close distance to the object, about 1.5 meters.

To obviate the problem of focal distortion, we used the same lens by mounting it on both cameras. We chose an Auto-Focus Nikkor 35mm f/2D that is a fixed focal length bright lens with reduced distortion and vignetting effects. However, it should be considered that it works differently once it is fitted on the respective cameras due both to the different size of the sensor that to the different *Flange Focal Length* (FFL). In addition, the latter is furtherly different between the two digital devices. The FFL is in fact dependent on both the focal point position of each camera, and the presence of an external adapter ring placed on the mounting flange of the MS camera. The *Back Focus Distance* (BFD) is affected by the previously mentioned reasons.

As already specified, Nikon D7000 is equipped with RGB CMOS sensor with 16.2 Mpixels, having a size of 23.6 mm x 15.6 mm and with a crop factor (FOV crop) of 1.5. Chroma C4 instead has a full frame sensor with 8 Mpixel monochrome CCD, having a size of 17.96 x 13.52 mm and with a FOV crop equals to about 2 (fig. 32). Therefore, the *Equivalent Focal Length* (EFL) that results from the fitting of the 35 mm lens on the APS-C camera is 50 mm, while the EFL on the Chroma C4 is more than 70 mm, better not calculable because of the adapter ring thickness. It is clear that the shooting distance and the resulting image scales have been strongly influenced by these intrinsic conditions.

Furthermore, using the MS camera we set a long exposure times to get maximum depth of field.

To ensure that the image area would cover better all the smaller size of the MS camera sensor, the painting has been placed horizontally.

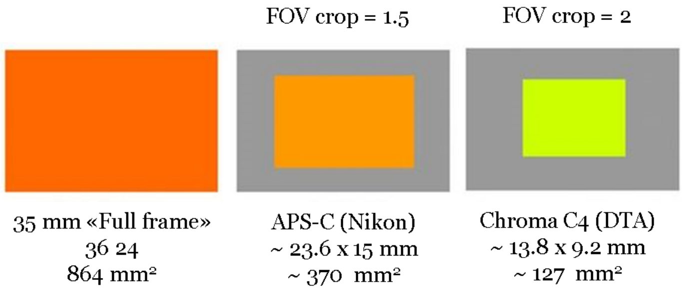

Fig. 32 Size of the sensors of used digital devices relative to a standard 35 mm frame.

4.3.3 Input images pre-processing

The RGB images have been acquired in 14-bit RAW format by setting the Auto White Balance mode directly from the camera. Medium-low ISO values have been used to prevent the sensor luminance noise, maintaining the exposure under the clipping limit value. At first, a test picture has been captured by inserting the image quality target *Kodak Color Control Patches Q14* directly in the frame. After that, it has been possible to proceed with the color correction by the black/white control point's tool on the *Capture NX* editor, as shown by the following images (fig. 33).

IR images have been acquired in the Chroma C4 proprietary file format. Usually, it is important to do first a dark frame with the same exposure length, ISO and ambient temperature as the light (normal) frames, because an IR image requires longer exposure time than a RGB one. Dark frame is automatically subtracted from the photos for long exposure noise reduction. Before saving every single file, we proceeded with a manual stretch control of the relative histogram in *Vista 3* software.

Any blurry or unfocused shots have been removed during the selection phase, and at the end all the selected images have been saved in .jpg format through batch processing.

Fig. 33 a) Before and b) after the Color correction in Capture NX editor.

4.3.4 Images uploading and Camera calibration

RGB and IR images sets have been imported into four different Photoscan project files: RGB-M_1 (Front), RGB-M_2 (Back), IR-M_1 (Front), IR-M_2 (Back).

As known, camera calibration is one of the fundamental component needed in the photogrammetric measurement. Nowadays, auto-calibration has become an integral and routine operation applied in photogrammetric triangulation, especially in high-precision close range measurement (Remondino & Fraser, 2006). Unfortunately, the instrumental adaptations previously described have resulted in wrong automatic detection of the MS camera EXIF data by the software. Moreover, it has been necessary to preliminarily adjust the format size of images using a scale factor in order to obtain final comparable results. In any case, the relative sets of images with a good texture have been sufficient for the extraction of natural corresponding image points (Barazzetti, et al., 2011). These have been automatically matched with feature-based approaches and robust estimation techniques: the auto-calibration procedure of *PhotoScan Pro* software has compensated the required values adjustment with an 8-terms physical mathematical model to optimize the photos alignment, determining the camera's internal parameters as: principal distance, format size, principal point offset, and lens distortion coefficients (Tab. 5).

This kind of target-based camera calibration assumes the central projection camera model, which exploits the now well-known self-calibrating *Bundle adjustment* approach.

Tab. 5	**Chroma C4 (DTA) Camera Calibration**		**Nikon D7000 Camera Calibration**
	Initial	Adjusted	Initial
Pixel size (mm):	Unknown Unknown	1536 1024	3264 4928
Focal Length (mm):	Unknown	Unknown	35
Fx:	2133.33	4082.12	7104.03
Fy	2133.33	4082.12	7104.03
Cx	768	707.676	1632
Cy	512	494.426	2464
K1	-	-0.103891	-
K2	-	0.224469	-
K3	-	-1.32246	-
K4	-	0	-
P1	-	-0.000258695	-
P2		-0.000585238	-

fx, fy: Focal length in x- and y-dimensions measured in pixels;

cx, cy: Principal point coordinates, i.e. coordinates of lens optical axis interception with sensor plane;

k1, k2, k3, k4 Radial distortion coefficient;

p1, p2, p3, p4 Tangential distortion coefficients.

4.3.5 Alignment, camera positions estimating and Feature matching

Once the align command is launched (*Workflow> Align Photos*), *PhotoScan* calculates the positions of each photo station/placement and its external orientation from which a sparse point cloud and camera positions are obtained.

Furthermore, in this first stage the SfM algorithms in *PhotoScan* detect image feature points in the source photos which are stable under viewpoint and lighting variations — i.e. various geometrical similarities such as object edges or other specific details — and it generates a descriptor for each point based on its local neighborhood. This descriptor is later used to detect correspondences, monitoring the movement of those points throughout the sequence of multiple images. Using this information as input, the locations of those feature points can be estimated and rendered as a sparse three-dimensional point cloud. It should be recorded that before alignment, masks have been applied to all the selected images. Consequently, in photo alignment procedure it has been chosen to constrain features by mask with the highest accuracy. With this option, masked areas have been excluded during both the feature point detection and the processing. Points excluded were not taken into account so that it has reduced the complexity of the resulting dense cloud.

In this mode, the program calculates depth information for each camera to be combined into a single dense point cloud which is defined by a collection of vertices having color information, normal vector and texture coordinates but no connectivity information. At each stage, the same parameters have been used for each project.

4.3.6 Dense Cloud Generating

The resulting RGB and IR dense clouds consist in the following number of points:

	FRONT	BACK
RGB	6.736.539	3.532.728
IR	4.495.224	2.502.679

Tab. 6 Total points number of the resulting RGB and IR dense clouds.

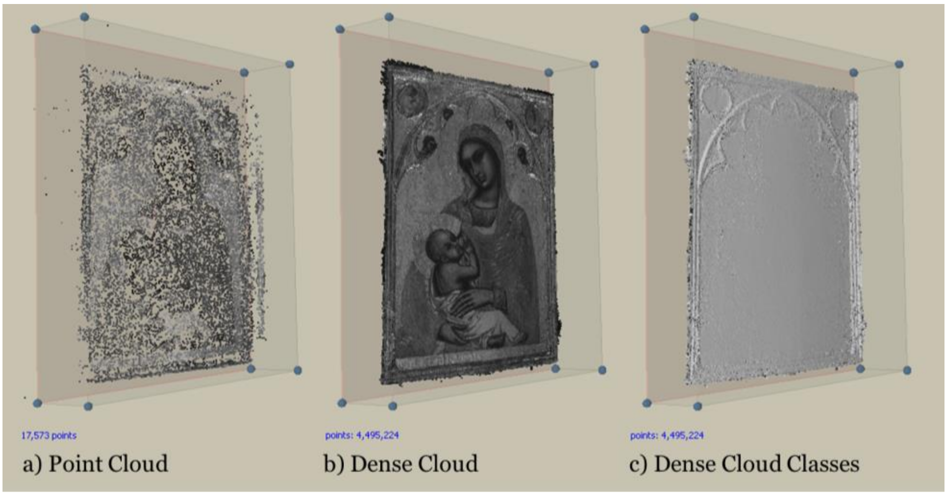

Fig. 34 3D modeling Process: from the sparse point cloud (a) to the dense point cloud (b). On the right, points classes viewing mode (c).

The recognition of object surfaces in point clouds is often the first step to extract evidences from a not manipulated native format output. Indeed, dense clouds provide explicit morphometric information on the geometry, the shape (Blomley, et al., 2014) and the structure of time-varying surfaces (Schnabel, et al., 2007) that, properly treated, can provide guidelines to diagnostic investigations. So, many recent studies have focused the attention on the analysis of objects dense clouds: the extraction of semantic content from 3D point clouds is an important topic for a wide field of applications.

To enhance this information level, many different approaches and relative algorithms including the one called “segmentation” — which is a process that decomposes 3D model into cluster points with similar characteristics into homogeneous regions for classification and feature extraction – have been introduced (Nguyen & Le, 2013). This is potentially very useful for mapping all those morphological discontinuity as decorative details in relief, gaps in the paint layer or in the underlying layers, cracks, insert of restoration, etc. directly on the 3D model.

Surely, even the simple dense point cloud non-containing the texture information can be a very valuable tool for time-space recording. For instance — in the specific case of our target subject — it gives us information about structural features, the support deformations (warping) and it allows us to verify future possible dimensional variations.

4.3.7 Mesh Building

A 3D mesh represents a 3D surface using sets of mesh elements, i.e. vertices, edges, and polygons (faces) along with incidence and/or adjacency relations (fig. 35). The mesh vertices are 3D points. Each edge, is defined by two distinct vertices. While each face is defined by three or more edges such that each pair of edges share a vertex. In the case of a triangular mesh — which is the most widely used type of mesh due its relative simplicity — the face is exactly defined by three edges or by three distinct vertices. There are different types of mesh representations, depending on how the data of the mesh are stored and organized in data structures.

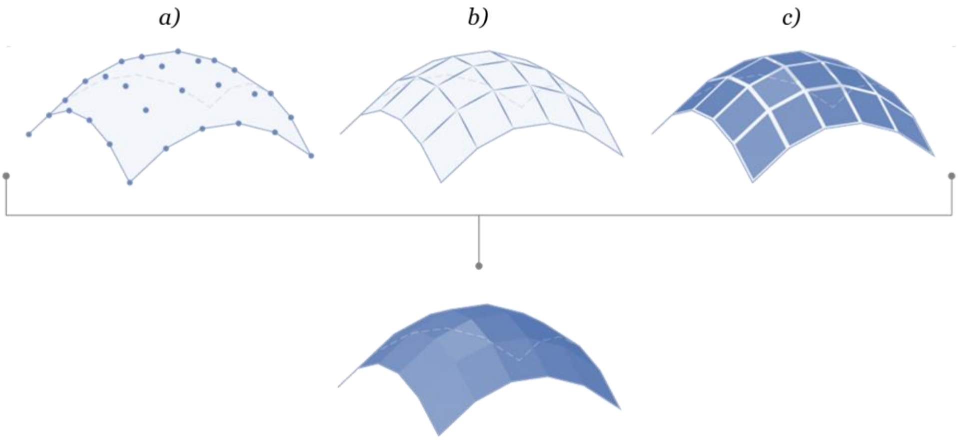

Fig. 35 Basic Anatomy of a Mesh.
a) Mesh vertices; b) Mesh edges; c) Mesh faces.
Figure credits: (https:// http://grasshopperprimer.com/en/1-foundations/1-6/1_What%20is%20a%20Mesh.html)

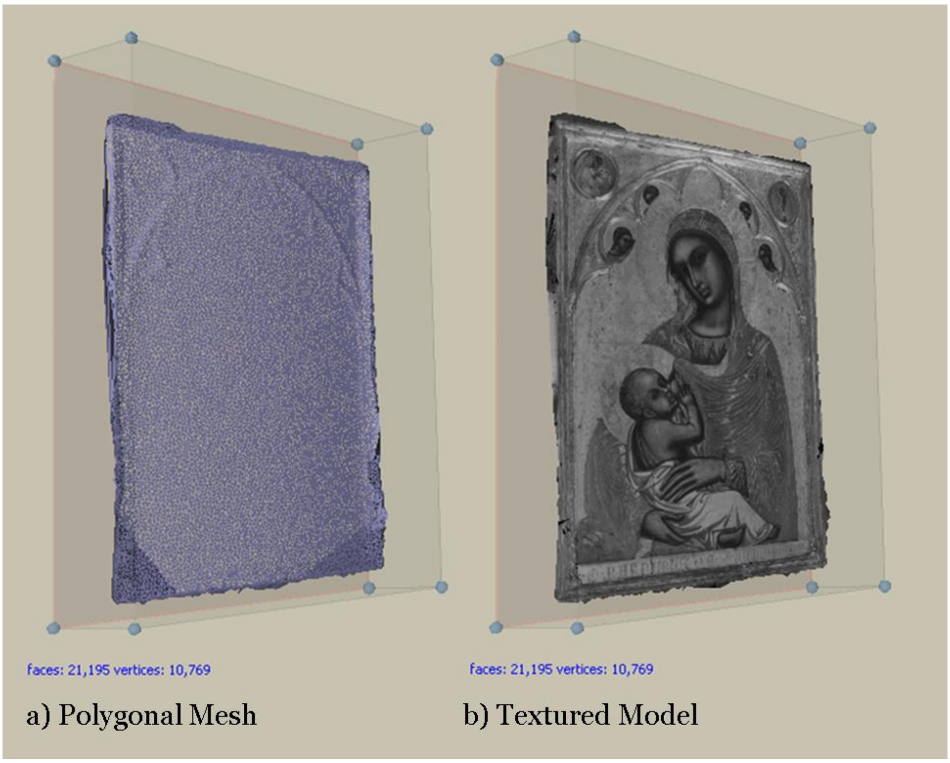

Fig. 36 3D modeling process: from the polygonal mesh (a) to the textured model (b).

Using *PhotoScan*, the majority of geometric scene details are built by applying a dense, multi-view stereo-reconstruction on the aligned image set. Whereas SfM algorithms operate on a sparse set of feature points extracted from the source photographs, these dense reconstruction algorithms operate on the pixel values (Scharstein & Szeliski, 2002; Seitz et al., 2006). As all pixels are utilized, this reconstruction step enables proper handling of fine details present in the scenes and represents them as a mesh. So, we proceeded with the mesh building starting from the given data set, by setting Height field Surface type, Dense Cloud Source data, and High Polygon count parameters (fig. 36a).

Height field surface type is based on pair-wise depth map computation and it is typically used for modeling of almost planar surfaces; its only drawback is the computation time penalty. Using dense cloud as source data has allowed us to obtain a greater quality output. It was also considered that 90,000 polygons maximum were an optimal number for a mesh of good level of detail, with a high geometry resolution.

4.3.8 Texture mapping

Texture mapping onto the wireframe model greatly enhances the realism of the models (fig. 36b). At this stage *PhotoScan* parametrizes a surface possibly cutting it in smaller pieces, and then blends source photos to form a texture atlas (fig. 37). This latter is a bitmap image/rendering resource containing a collection, or “atlas”, of sub-images, each of which is indexed by UV mapping for 3D rendering — the letters “U” and “V” denote the axes of the 2D texture because “X”, “Y” and “Z” are already used to denote the axes of the 3D object in model space. The most important option to be found here is the mapping mode. By default, the generic mapping mode is selected as the texture atlas for arbitrary geometry can be parameterized, i.e. the process of calculating the necessary parameters for a specification of a geometric object. No assumptions are made regarding the geometry and the method generates textures as uniformly as possible. For our purposes, we set the average blending mode, that uses the weighted average value of all pixels from individual photos, and we enabled the color correction too.

Fig. 37 IR-M_1 and IR-M_2 Texture atlas

4.3.9 M_1/M_2 Exporting and Alignment

In order to combine the meshes of the two opposite sides of the painting in a single continuous surface it has been necessary to first export the respective project files in external software. To do that, we decided to save each project in .obj format which is a simple data-format that represents 3D geometry alone — namely, the position of each vertex, the UV position of each texture coordinate vertex, vertex normals, and the faces that make each polygon defined as a list of vertices, and texture vertices. It also saves the texture atlas in a separate file.

The corresponding M_1/M_2, both RGB and IR, were imported in *CloudCompare* in order to be aligned (fig. 38). Each pair of meshes was already scaled, so we moved on to the next step, carrying out a manual registration of the two entities, interactively rotating and translating them. This first rough recording was fixed with the *Point pair based* alignment tool, used directly on meshes. As regards IR-M_1 and IR-M_2, the common points along the edges of the two separate meshes were quite a few although we provided at least a good acquisition which spanned over both sides of the corner below the painting. This is surely due to the lack of photos related to the thickness of the painting and therefore and to the photo-shooting strategy not sufficiently appropriate. This has resulted in the creation of a non-manifold geometry which obviously is not acceptable in a rigorous survey.

Fig. 38 M_1/M_2 Alignment.

4.3.10 M_1/M_2 Stitching

The major difficulty encountered in our process has been the combination of the aligned meshes, i.e. integrating multiple views in a single model. The goal of integration was to arrive at a seamless blending of the elements for describing the overall topology of the painting.

This is a crucial issue in the context of the mesh manipulation. Indeed, a certain number of works have addressed the problem of "mixing" a set of independent models, taking into account the user's need to be extremely careful to avoid artifacts in the resulting mesh. Turk & Levoy (1994) is one of the first successful approach for stitching multiple range images into a single consistent mesh. Sharf et al. (2006) allow meshes to be cut, composed with snapping using a variant of *Iterative Closest Point* (ICP) (Chen & Medioni, 1992; Rusinkiewicz & Levoy, 2001) and stitched together. Schmidt (2010) describes a Part-based representation for 3D models, including tools for stitching parts together, which is the basis for the *Autodesk Meshmixer* software. Recently, Huang et al. (2007) proposed a volumetric field for parts of meshes which can be used to interpolate and stitch together the mesh parts.

In this thesis, the full topology of the surface has been realized by zippering and bridging the two complementary photo scans into one continuous surface (fig. 39). In acceptable overlapping areas — respectively the top and bottom edge of each model — it has been used the above mentioned method proposed by Turk & Levoy (1994), later implemented by Marras (2010) by introducing quality criteria in the selection of redundant data. Generally, this algorithm first step aligns meshes by means ICP algorithm. The second step removes overlapping regions between two adjacent meshes, by deleting triangles and leaving only those that do not overlap or that overlap only partially. The final step stitches meshes by the points where the partially overlapped triangles intersect. The stitching procedure adds vertices at the intersection and new triangles are built on top of the original ones. When there is no overlap, meshes cannot be aligned using ICP and the stitching cannot be built on top of existing triangles. For practically doing that, we used the *ZipperEdge Brush* function available in *Meshmixer* in terms of a geometry repairing tool (fig. 40). However, the algorithm proposed by Turk assumes that meshes have initially surfaces in common. When the overlap is not possible because of the acquisition or application constraints, it is necessary to proceed differently. Trying to solve this issue, some authors as Brandao, et al. (2012), proposed the JASNOM algorithm that aligns meshes with no overlap and connects the meshes without using existing triangles. As claimed by the authors, it is ideal for the construction of object models from meshes captured from sensors in diametrically opposite positions with respect to the object.

For sewing areas with little or no overlap, we used the *Bridge* feature — also available in *Meshmixer*. This tool first constructs a minimal triangulation that crosses the gap, and then uses re-meshing to produce a high-quality triangulation. Moreover, it does not require the same number of boundary edges on either side of the gap: it easily handles large differences in the number of boundary edges on either side.

However, after this mesh manipulation we must conclude that the final result is only partially acceptable because it involves radiometric and colorimetric artifacts although it provides a reasonable performance in global geometry and shape rendering. Accordingly, the documentation and the interpretation of the painting's edges data for conservation purposes can be only fictitious.

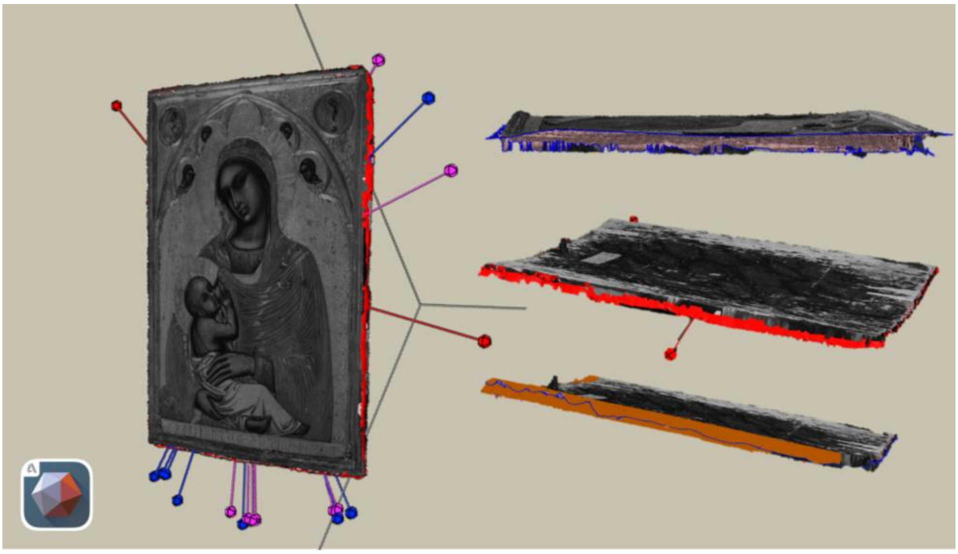

Fig. 39 Integration of the multiple views in a single model.

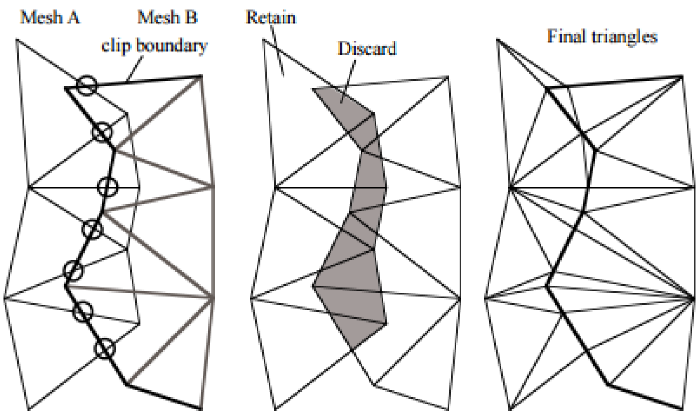

Fig.40 Representation of the zippering algorithm.
Figure credits: (Turk & Levoy, 1994).

4.3.11 Re-meshing and Model Refinement

Complete models thus obtained, IR-M and RGB-M respectively, were imported at two separate times in *MeshLab* in order to improve the quality of the meshes, in terms of vertex sampling, regularity (Alliez, et al., 2002; Alliez, et al., 2003; Botsch & Kobbelt, 2004) and triangle quality. This improvement process is called *Re-meshing*. There is no precise definition of re-meshing, since it often varies according to the targeted goal or application. Nonetheless, one possible definition could be: «Given a 3D mesh, compute another mesh, whose elements satisfy some quality requirements, while approximating well the input» (Alliez, et al., 2008). "Quality" has several meanings. It can be related to the sampling, grading, regularity, size and shape of elements. Often a combination of these criteria is desired in real applications (Amenta, et al., 1999). In brief, we can say that high-quality re-meshing means to generate a new discretization of the original geometry with a mesh that exhibits following the three properties: well-shaped elements, uniform or isotropic sampling and smooth gradation sampling.

From this premise it is clear that, first of all, the input mesh has to be a valid mesh because it will affect the whole process. This usually means that it should be a simple manifold and also closed. Therefore, the quality of mesh elements is crucial for robustness and numerical stability, required for numerical simulation as well as for geometry processing. Numerical computations, such as finite element analysis, require fairly regular meshes, both in terms of geometry and connectivity. Another important issue that occurs during the re-meshing process is the fidelity between previous and newly generated meshes. This latter has to best approximate the original shape geometry, preserving the features and keeping the mesh complexity below a given budget. This involves choosing an error metric, as well as to decide between interpolation and approximation.

Lastly, for an efficient object rendering is required a continuous *Levels-of-Detail* (*i.e.*, continuous-resolution representations). Some studies (Sharma, 2014; Maiti & Chak, 2016) have analyzed in particular the performance of two algorithms among the most applied in the re-meshing operation: *Poisson reconstruction* (Kazhdan, et al., 2006; Li, et al., 2010; Kazhdan & Hoppe, 2013) and *Ball Pivoting* (Bernardini, et al., 1999). In order to obtain a new mesh with all the features mentioned above we considered more appropriate to use the Poisson approach. This algorithm aims at creating a 3D mesh by minimizing the difference between the surface normal (n_x, n_y, n_z) directions of the reconstructed surface and the 3D points in the point cloud. So, achieving for first oriented normals is a necessary task for this kind of point-set procedure (Yu, et al., 2015). This is commonly divided into two steps: normal estimation and orientation. Normal estimation gains unoriented normals out of the point cloud (fig. 41). *Principal Component analysis* (PCA), is what Hoppe et al. (1992) put forward and seems to be the most favorite approach by now. It optimizes a tangent plane formed by *k*-nearest neighbors at each point and it uses the normal of the plane to estimate the normal of the point (figg. 42a, 42b). So, we practically compute vertex normal going to *Filters->Normals, Curvatures and Orientation->Compute Normals for point sets*, using default *Meshlab* parameters.

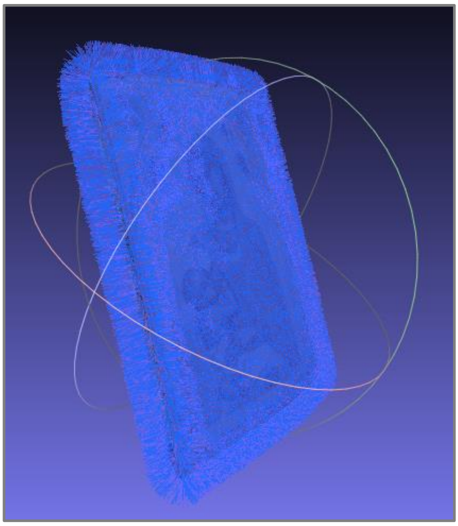

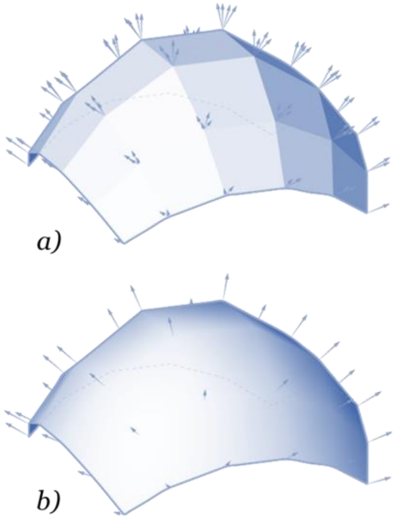

Fig. 41 Normal estimation and orientation in Meshlab.

Fig. 42 a) Normals set according to the face normal results in discrete polygonal shading; b) Adjancent face normals are averaged together to create vertex normals, resulting in smooth shading across faces.

Figure credits: (http://grasshopperprimer.com/en/1-foundations/1-6/1_What%20is%20a%20Mesh.html)

After that, we applied Poisson Reconstruction going to: *Filters->Remeshing, Simplification and Reconstruction-> Surface Reconstruction: Poisson*. There are several parameters available that affect the result of Poisson reconstruction in terms of reconstruction quality and computation time:

a. *Octree depth:* the octree is a structure designed to speed up the processing of spatial data. It is a recursive and hierarchical slicing of space (decomposing the space into cubes) (fig. 43). From a general point of view, the octree is defined by its subdivision level: the first level (level 0) is the smallest cube that entirely contains the point cloud. At level N+1, the octree is built by dividing each of the cubes in level N into 8 sub-cubes of the same size. Therefore, an octree of depth D produces a three dimensional mesh of resolution $2^D \times 2^D \times 2^D$. As the octree depth increases, mesh resolution increases. So, the memory consumption is also increased drastically. The default value of octree depth used in Poisson reconstruction is eight, we set nine.

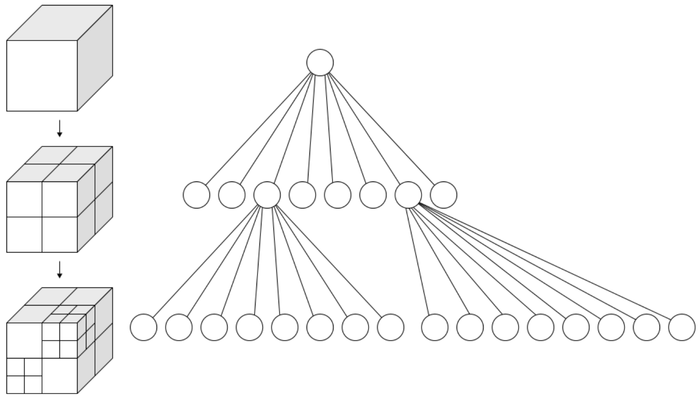

Fig. 43 Octree depth structure. Left: Recursive subdivision of a cube into octants. Right: The corresponding octree.
Figure credits: (https://en.wikipedia.org/wiki/Octree)

b. *Solver divide:* Solver divide specifies the depth up to which a conjugate gradient solver is used to solve the Poisson equation. If the solver divide is increased, computation time decreases as at greater value. We maintained default *Meshlab* parameters.

c. *Samples per node:* Samples per node (SN) indicates the minimum number of points that is assigned at each octree leaf node by the marching cube algorithm. Increasing the value of SN improves the overall quality of the reconstructed surface. However, 3D surfaces that are generated using higher values of SN, have some surface-smoothing effects. Also, finer details of the surfaces are lost for very high values of SN. We maintained default *Meshlab* parameters.

d. *Surface offsetting:* This parameter indicates a threshold correction value for the reconstructed surface. Value of 1 indicates no correction, <1 is used for internal offsetting and value of >1 is used for external offsetting. We maintained default *Meshlab* parameters.

The regularization effect due to the re-meshing process is graphically summarized in the image below (fig. 44).
Also this step has been replicated for both IR-M that for RGB-M.

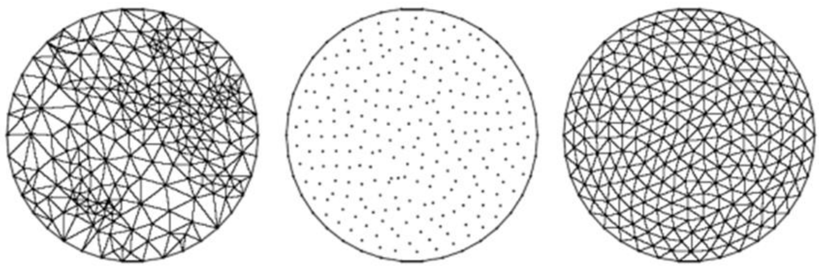

Fig. 44 Regularization effect due to the re-meshing process.

4.3.12 RGB/IR-Point Clouds Comparison

Quantitative Evaluation Approach

To verify that the two 3D clouds obtained with the different survey techniques were comparable and equivalent, we quantitatively and qualitatively evaluated their difference through the *Hausdorff distance*.

The algorithm related to the *Hausdorff distance* was implemented in 2002 in the *Metro tool* software, displaying the errors numerical values and their distribution as a histogram and also a visualization of errors at a local level, by using a color palette (Cignoni, et al., 1998), in the *MeshDev* software (Roy, et al., 2002) and in the *CloudCompare* software (CloudCompare, 2012). For our purposes, we chose the latter.

In detail, the *Hausdorff distance* — named after Felix Hausdorff — is the most famous metric for comparing two point clouds or mesh surfaces, providing a global comparison. It measures the extent to which each point of a reference model-set lies near some point of a similar model-set and *vice versa* (fig. 45). Thus, the distance can be used to determine the degree of resemblance between two objects that are superimposed (Huttenlocher, et al., 1993; Aspert, et al., 2002).

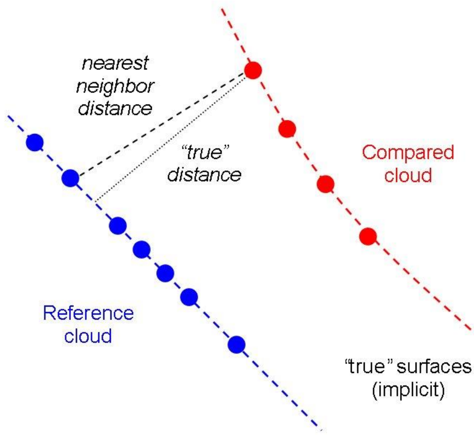

Fig. 45 Nearest neighbor distance.

Considering two surfaces *S* and *S'*, the distance between *S* and *S'* can be defined as:

$$d_s(S, S') = \max\,[d(p, S')], \forall p \in S$$

where $d(p, S') = \min[d(p, p')], \forall p' \in S'$ and *d(p, p')* is the *nearest neighbor distance* (Euclidean) between two points in $\mathbb{R}^3$. Distance d_s is not symmetric, i.e. $d(S, S') \neq d(S', S)$. The $d(S, S')$ distance is called the *forward distance*, while $d(S', S)$ is the *backward distance*. The Hausdorff symmetric distance $d_H(S, S')$ is defined as:

$$d_H(S, S') = max\,[d(S, S'), d(S', S)].$$

The symmetrical distance offers a more accurate measurement of the differences between two surfaces, because the one-side distance can lead to an underestimation of the distance values between the two surfaces, (Oniga & Chirilă, 2003). However, *Cloud to Cloud distance computation* tool as implemented in *CloudCompare* calculates the *nearest neighbor distance*, i.e. for each point of the compared cloud, the software looks for the nearest point in the reference cloud and then computes their distance. If the reference cloud is dense enough, then the *nearest neighbor distance* will be (almost) as accurate as the *true distance* to the underlying surface.

4.3.12.1 IR/RGB Point Clouds Registration

Prior to calculation of the distance, the two raw point clouds acquired by the two different sensors have been aligned and registered to the same coordinate system (fig. 46). As it has been done in the previous phase for the M_1/M_2 alignment, even in this step we carried out a previous manual registration of the two entities, interactively rotating and translating them. This first rough recording was then fixed with the *Point pair based* alignment tool, used directly on meshes. At the end, we used the registration automatic method to finely register the two datasets by ICP algorithm. The quality of the alignment obtained by this algorithm depends heavily on choosing good pairs of corresponding points in the two datasets. If too many points are chosen from featureless regions of the data, the algorithm converges slowly, finds the wrong pose, or even diverges, especially in the presence of noise or uncalibrated input data. Although collinear or co-planar points might lead to a poor alignment, we have obtained a fairly satisfactory result.

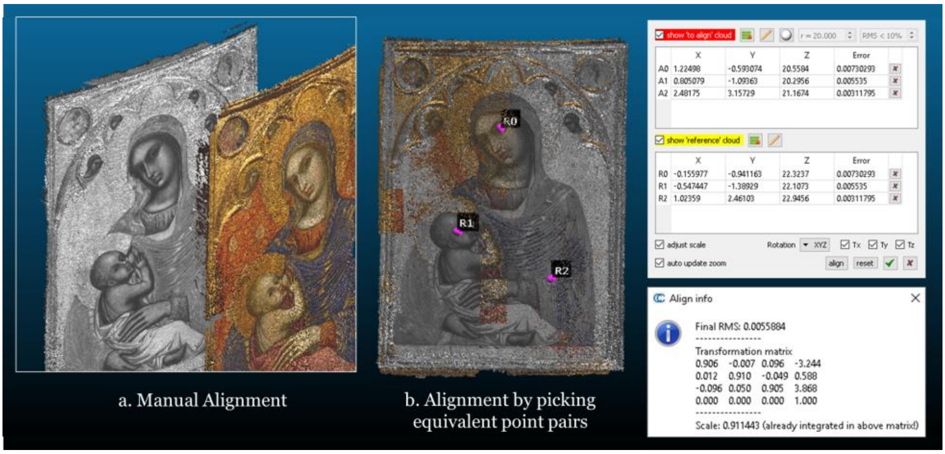

Fig. 46 RGB M1 / IR M1 alignment in CloudCompare.

Alignment method	Final RMS
Equivalent Point pairs Alignment	0.0055884 cm

The parameters of the alignment process were previously optimized by means of two identical point clouds. The optimization consisted of various attempts to contain the ICP alignment error of the two identical point clouds, then the parameters have been set to the optimal value and used in what follows:

a. *Number of iterations*: ICP is an iterative algorithm. During the process, the registration error (slowly) decreases, while increasing the number of iterations. We used the default value (20).
b. *RMS difference*: threshold used was 10^{-5}.
c. *Random sampling limit:* it consists in a random sub-sampling of the *data* cloud at each iteration. This parameter is the number of sub-sampled points. The default value (50.000) is generally a good

guess and its incidence on the result is not perceivable. However, to refine the registration even more, we set 500.000.

4.3.12.2RGB/IR Point Clouds Distance Computing

Once registered, we chose the clouds roles in order to start the distance calculation. We set the IR Cloud as the *compared* cloud, on which distances have been computed and where the generated scalar field has been hosted, while the RGB Cloud as *reference*.

The analysis has been carried out on a portion of both dense clouds (fig. 47). This has been done because to analyze high density clouds a huge computational power is needed, so we limited the data-set to a maximum of 8 millions of points. The selected area focuses on the faces of the two figures, their halos, part of the blue cloak of the Virgin and the polylobate frame.

Furthermore, the global coordinate system has been scaled on centimeters so that all the calculated distances were then expressed in the same units of the dense cloud coordinates.

Fig. 47 Selected area on which the distance has been calculated.

The main parameters for the computation are:

a. *Octree level*: this is the level of subdivision of the octrees at which the distance computation will be performed. The higher the subdivision level is, the smaller the octree cells are. Therefore the less points will lie in each cell and the less computations will have to be done to find the nearest ones. We set the maximum level (10), 2^{30} cubes.
b. *Max. distance*: to limit the search below a reasonable value to shorten the computation time, we set 1.90 so that all points farther than this distance didn't have their true distance computed - the threshold value it has been used.
c. *Split X, Y and Z components*: three more scalar fields corresponding to the (absolute) distance between each *compared* point and its nearest *reference* point along each dimensions (i.e. this corresponds to the three components of the deviation vector) have been generated.

A first approximate distance calculation between the clouds has been automatically performed by means *chamfer* distance, calculated via octree. Then a more accurate calculation was performed with the *Hausdorff* distance.

The point distance in the 3D models is ~0 cm with very few outlier at max distance of 0,99 cm. The 98,43% of point distances is between 0 and 1 mm, while 91,01% are between 0 and 0,7 mm.
More precisely:

- For qualitative results, the computed distances have been highlighted by setting the "*Blue>Green>Red*" palette from the software menu from which result that the entire area is colored in blue (fig. 48b).

- For quantitative results, all computed data distances have been exported and graphically presented by the following histograms (fig. 49).

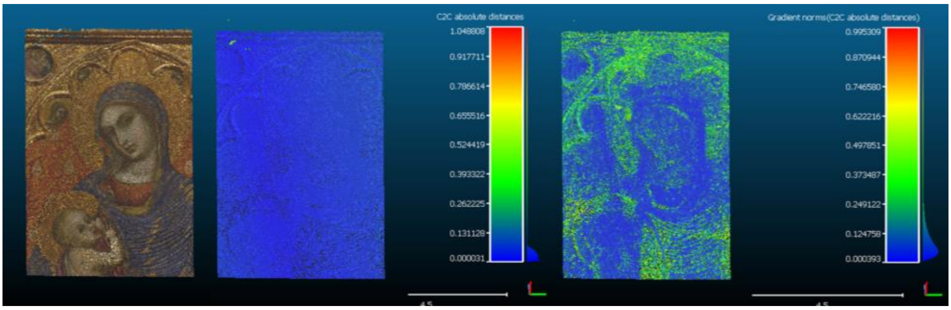

a) b) c)

Fig. 48 a) Point clouds aligned; b) Distances computed between the two point clouds; c) Gradients on the calculated distance distribution.

Tot. number points	7.678.348
mean value (μ)	0,041408 cm
standard deviation (σ)	0,055899 cm

Tab. 7 Total number of points considered; mean value and standard deviation value.

N° Points	***Percentage***	***C2C_ Absolute Distances [cm]***
4.479.905	58,34%	0 ÷ 0.0371
2508372	32,67%	0,0371 ÷ 0,0740
421896	5,49%	0,0371 ÷ 0,1110
148338	1,93%	0,1110 ÷ 0,1480
59734	0,78%	0,1480 ÷ 0,1849
28801	0,38%	0,1849 ÷ 0,2219
14278	0,19%	0,2219 ÷ 0,2588
7635	0,10%	0,2588 ÷ 0,2958
4461	0,06%	0,2958 ÷ 0,3327
2254	0,03%	0,3327 ÷ 0,3697
928	0,01%	0,3697 ÷ 0,4066

Tab. 8 Absolute Distances [cm] between the two point clouds.

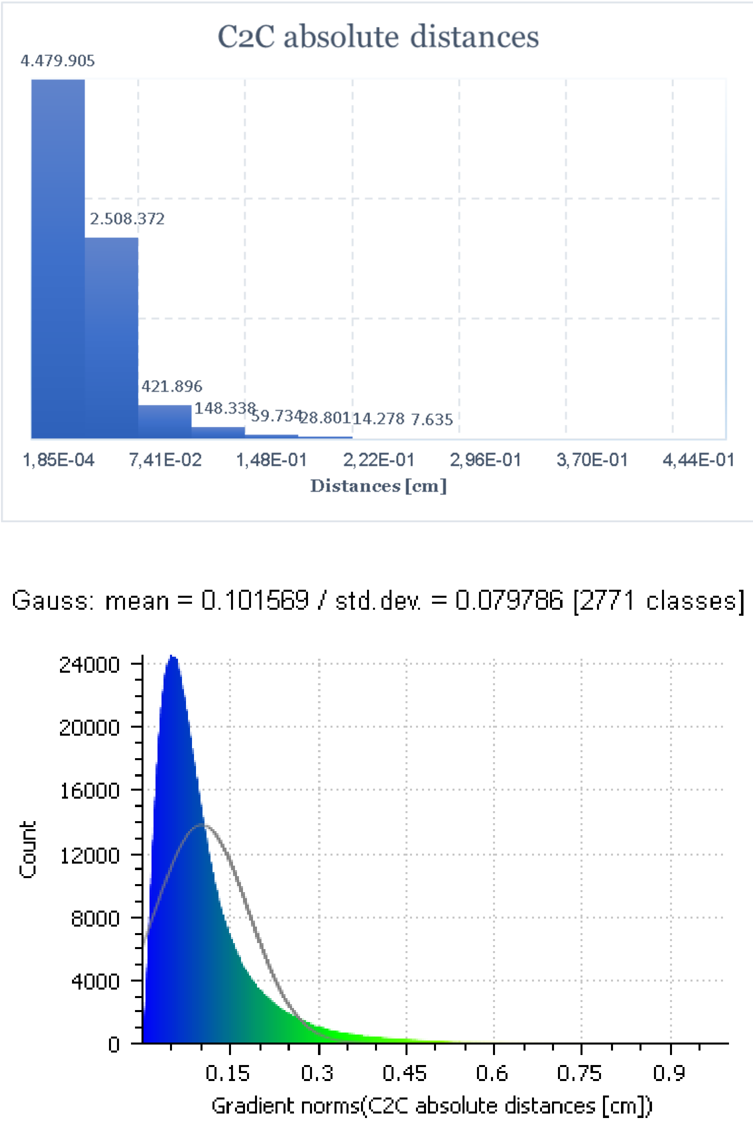

Fig. 49 Histograms of computed data distances and gradients.

Further, the gradient has been calculated. The gradient $\vec{\nabla \mathrm{d}}$ is defined as:

$$\vec{\nabla \mathrm{d}} = \left(\frac{\vec{\partial d}}{\partial x}\right)\hat{x} + \left(\frac{\vec{\partial d}}{\partial y}\right)\hat{y} + \left(\frac{\vec{\partial d}}{\partial z}\right)\hat{z}$$

Fig. 48c shows $|\vec{\nabla \mathrm{d}}|$ on the calculated distance distribution, highlighting zones of strong variation. Generally it is very sensitive to noise, especially when the two points are very close from each others. With euclidean distances we can cap that noise effect by applying a *Gaussian filter* to the calculated data, as we know that the gradient cannot be greater than 1. "*Blue>Green>Red*" palette has been chosen to visualize the results.

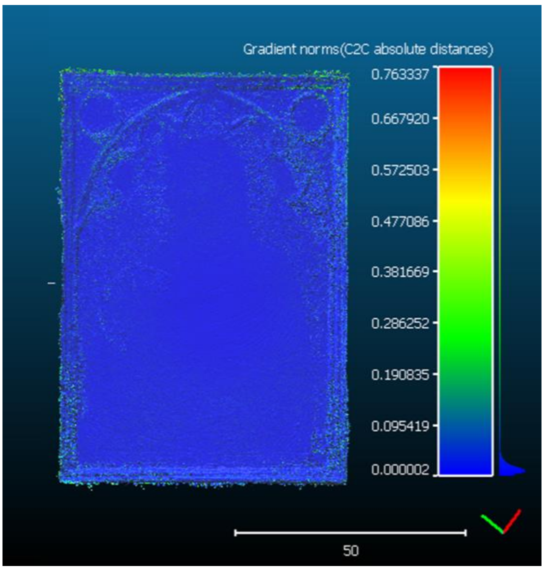

The same procedure were previously applied to two identical IR clouds to verify if the gradient were informative or not about the highlights of the (inexistent) differences. As expected, in this case the gradient is equal to 0 (fig. 50).

Fig. 50 Gradient of the two identical IR clouds.

Qualitative and quantitative results clearly show that the two models are morphometrically comparable. The green color corresponds to the golden areas, that is, to the frame and to the halos that are exactly the areas that generally are causing the most noise to the model due to the scattering of light by the gold leaf.

However, the entity of the distances between the points (mean value = 0.041408 cm) is about 5 orders of magnitude higher than the spectral distances between RGB and IR. Consequently, this type of analysis — at this level of detail— is not able to make dimensional differences of the single spectral bands appreciable.

To confirm the reliability and reproducibility of results, the analysis by *CloudCompare* software was also carried out on the 3D models in RGB, UV and IR bands referred to the Sicilian painting (fig. 51).

The same procedure as described above was applied. We compared before RGB/IR clouds (fig. 52); then RGB/UV clouds (fig. 55), always keeping the RGB cloud as reference.

As shown in the following histograms (figg. 53, 54) the 92% of the points (2.515.706) has a difference between the RGB/IR clouds which ranges from 0 to 0,08 cm, while the 80% of the points (2.178.342) has a difference that varies from 0 to 0,02 cm.

The 94.20% of the points (1,568,444) has a difference between the RGB /UV clouds that varies from 0 to 0,08 cm. The 64, 57% (1,074,899) has a distance that varies from 0,01 to 0,02 cm (fig. 56, 57).

The scalar fields of these models show a local trend to green in that areas with the greater variation which coincide to the peripheral edges of the painting and to the textural irregularities due to the discontinuity of the paint layer. This is probably due to some aberrations that may occur during the model building phase.

	Tot. Points	***Mean Distance (μ)***	***St. Dev. (σ)***	***Gradient***
RGB/IR Distance [cm]	2.734.240	0,0442	0,0925	0,0579
RGB/UV Distance [cm]	1.664.572	0,0336	0,0535	0,0567

Fig. 51 a) Sicilian panel painting. a) 3D RGB model; b) 3D UV model; c) 3D IR model.

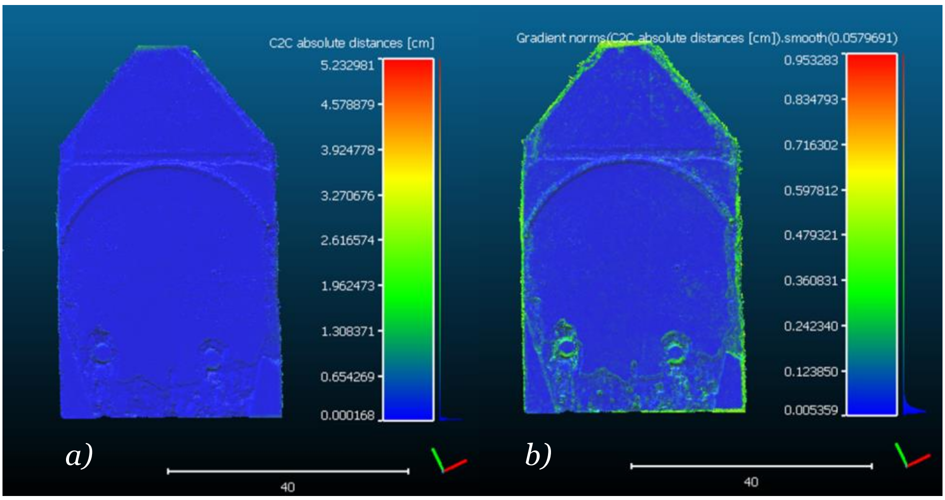

Fig. 52 a) RGB-IR models Absolute Distance in CloudCompare; b) RGB-IR models Gradient Absolute Distance in CloudCompare.

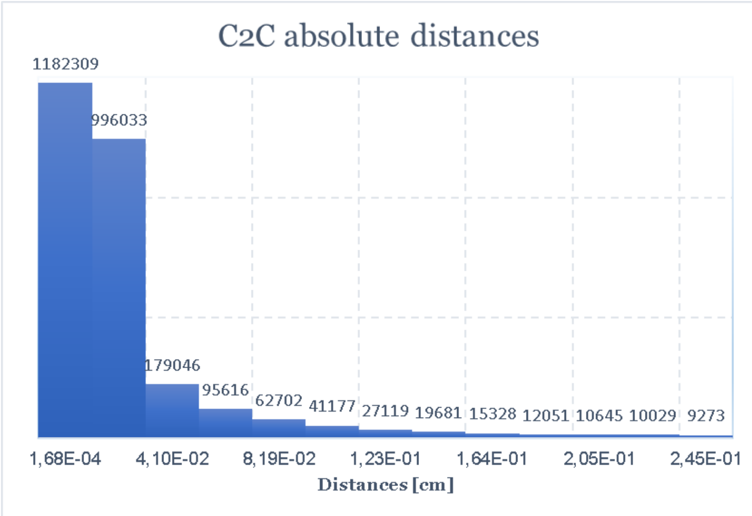

Fig. 53 Histogram of computed data distances between RGB-IR models of the Sicilian painting.

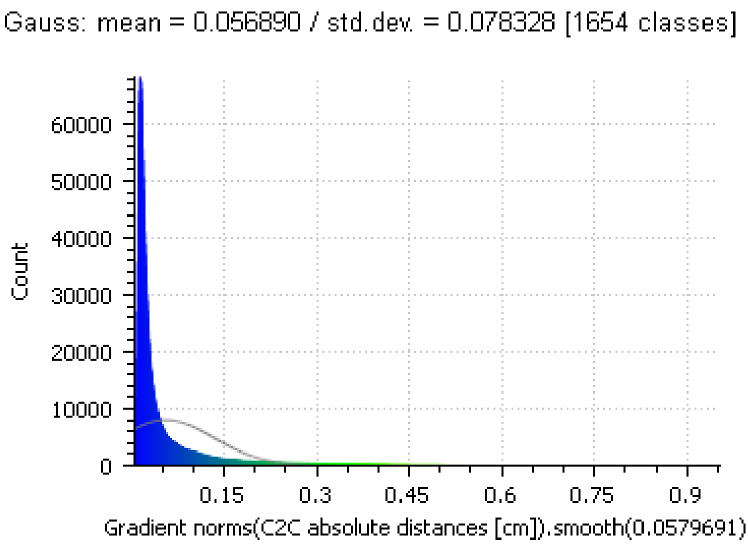

Fig. 54 Histograms of computed data gradients between RGB-IR models of the Sicilian painting.

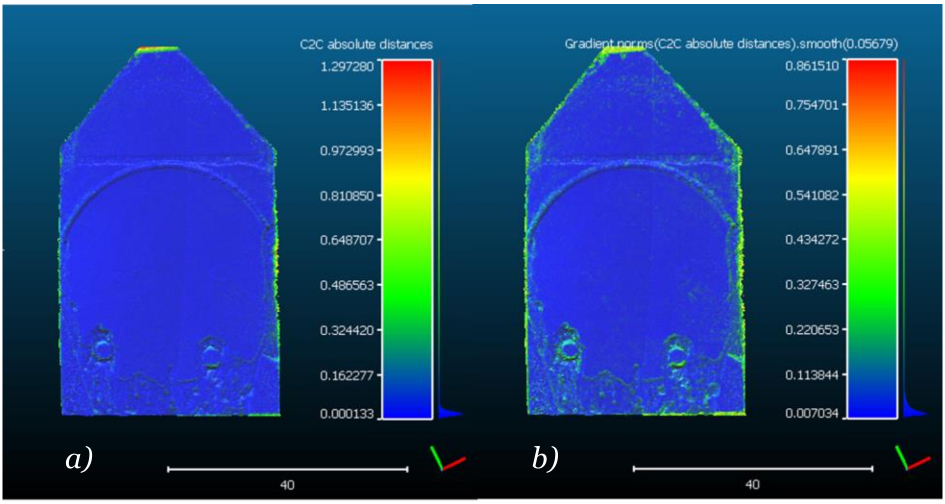

Fig. 55 a) RGB-UV models Absolute Distance in CloudCompare; b) RGB-UV models Gradient Absolute Distance in CloudCompare.

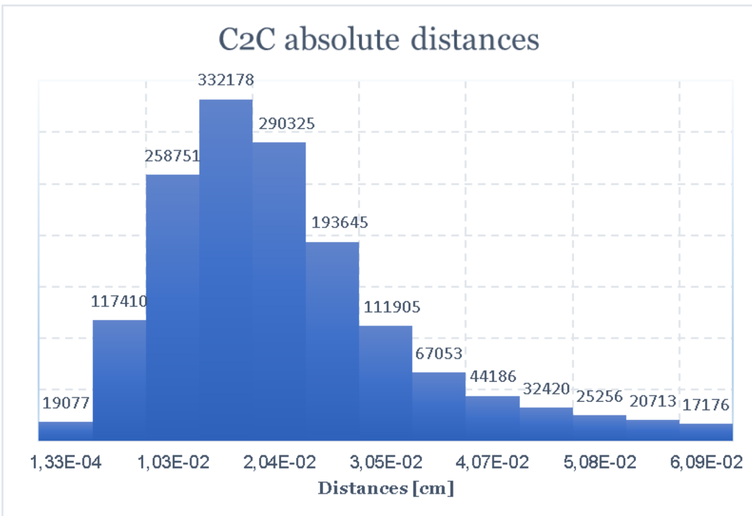

Fig. 56 Histogram of computed data distances between RGB-UV models of the Sicilian painting.

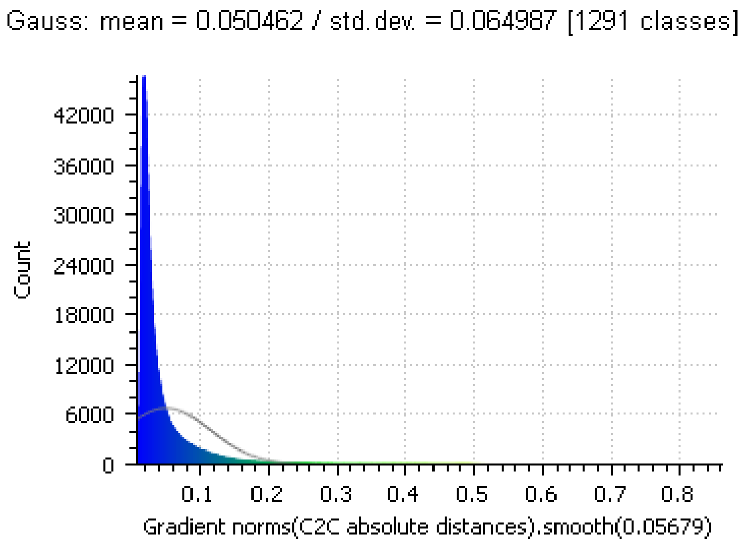

Fig. 57 Histogram of computed data gradients between RGB-UV models of the Sicilian painting.

5

XRF Survey

5.1 Set-up, data acquisition and interpretation

XRF measurements on the panel painting depicting the Nursing Madonna by Barnaba da Modena were carried out by means of the novel compact, portable and high performances XRF spectrometer ELIO produced by XGLab srl[1].

The instrument consists of an ultra-fast system with an active area of 25 mm² and a resolution of 135 eV to the K_α line of Mn, covered with a thin Beryllium window and cooled by a Peltier system. Its excitation source is a transmission X-Ray generator, 5-200 μA, 10-40 kV, Rh anode, therefore Elio is able to detect elements heavier than Al. The beam is collimated to a spot diameter on the sample surface of about 1.3 mm. ELIO has two pointing lasers (axial and focal), a microscope integrated permitting on field adjustments on analysis region as well as an external video camera. A great advantage of this instrument is its compactness; the detection head (2 kg) is mounted on any light-weight tripod, and it works in contactless mode. Elio Software 1.5.7.7 provides complete control of the measurement

[1] http://www.xglab.it/compact-portable-xrf-spectrometer-elio.shtml.

and of all the information, such as the elemental concentrations, the spectra and the images taken by the integrated microscope camera and the external video camera.

XRF measurements have been carried out by fixing the tube voltage at 40 kV, tube current at 20 μA, and the acquisition time at 60 seconds.

Fig. 58 Map of the points analyzed in XRF.

As shown in the fig. 58, 21 points of analysis were collected, choosing from the most representative color areas of the whole painting.

As expected, the measurement survey detected a ubiquitous presence of Pb, Ca ($CaSO_4$) impurities of Sr ($SrSO_4$) and Fe, which are all elements related to the impurities of the gypsum mixed with the animal glue for the preparatory ground.

With regard to the identification of the blue pigment used for both the mantle of the Virgin and for the background of the medallion on the right representing the Virgin Announced (P2, P4 and P21), Cu (Lα 8.04 keV) and Fe (Kα 6.40 keV, Kβ 7.06 keV) are present just in traces (fig. 59, 60). Consequently, we can indirectly infer the presence of the ultramarine pigment ($Na_{6\text{-}10}Al_6Si_6O_{24}S_{2\text{-}4}$) even if the air-path XRF spectrometer used is not able to detect all its constituent elements because of their low-Z. In the two points related to the mantle the presence of Pb, probably due to the adding of white lead in the mixture, it is noted.

Points sampled on the red garments and on the lips of the Virgin (P5, P18) show the key element (Hg) of the cinnabar that is a red-colored mercuric sulphide (Lα 9.95 keV, Lβ 11.87 keV) (figg. 61, 62), while the flesh tones contain Fe and Pb, and thus they are probably realized with an earth pigment (Fe_2O_3) mixed with lead white ($2PbCO_3$).

Regarding the golden background (P13), there is no doubt that the artist has used gold leaf (Lα 9.67 keV, Lβ 11.51 keV) (fig. 63). The Fe presence is due to the use of the red bole for the adhesion of the metallic foil. This element is no longer observable in the point on highlights of the blue mantle of the Virgin where gold mission was used (P3) (fig. 64). Around 10.50 and 12.60 keV we note the Pb peaks – respectively the Lα and the Lβ – due to the presence of some additive in the oleoresinous mixtion.

The results obtained are not surprising, because the detected elements refer to the most widespread pigments in the fourteenth century artist's palettes. Anyway, they highlight the richness of the pictorial materials.

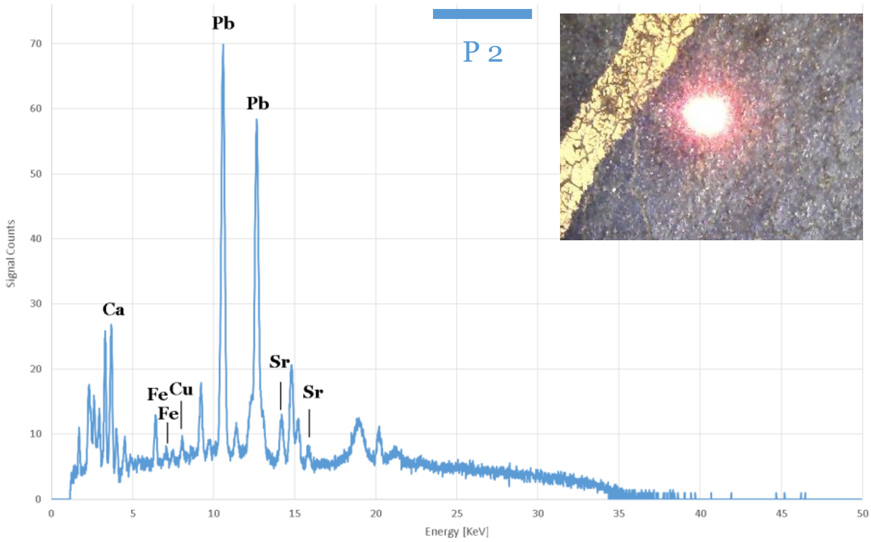

Fig. 59 Point 2 XRF spectrum.

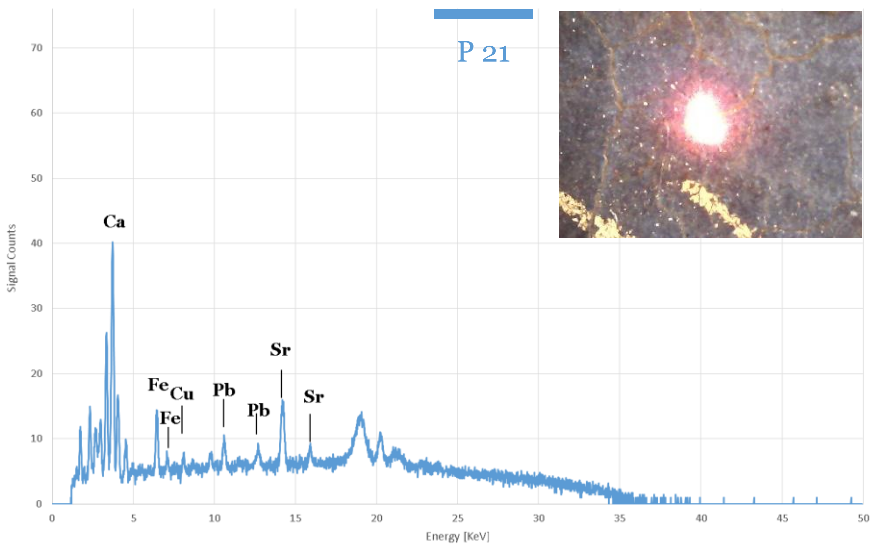

Fig. 60 Point 21 XRF spectrum.

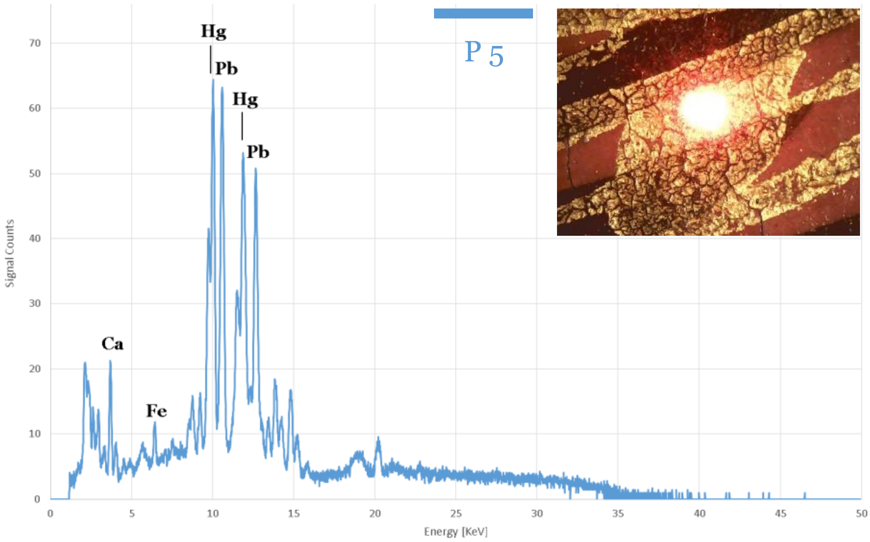

Fig. 61 Point 5 XRF spectrum.

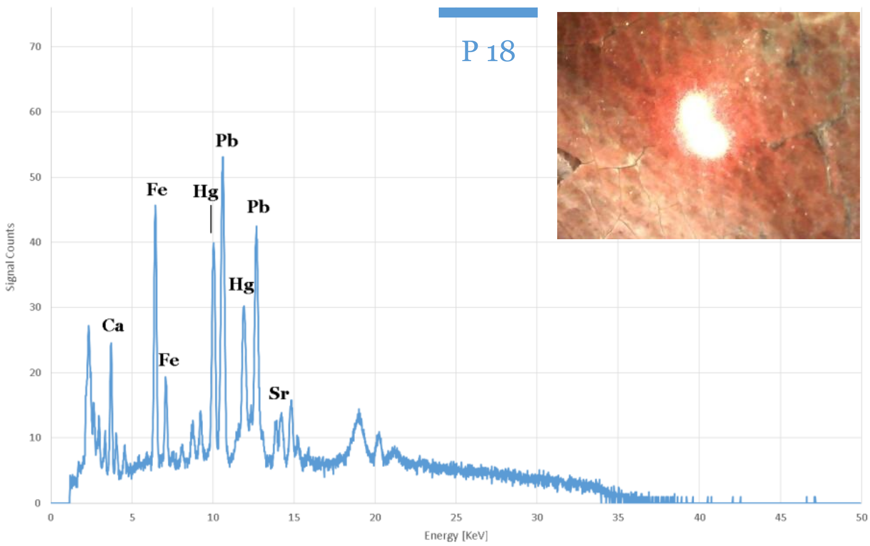

Fig. 62 Point 18 XRF spectrum.

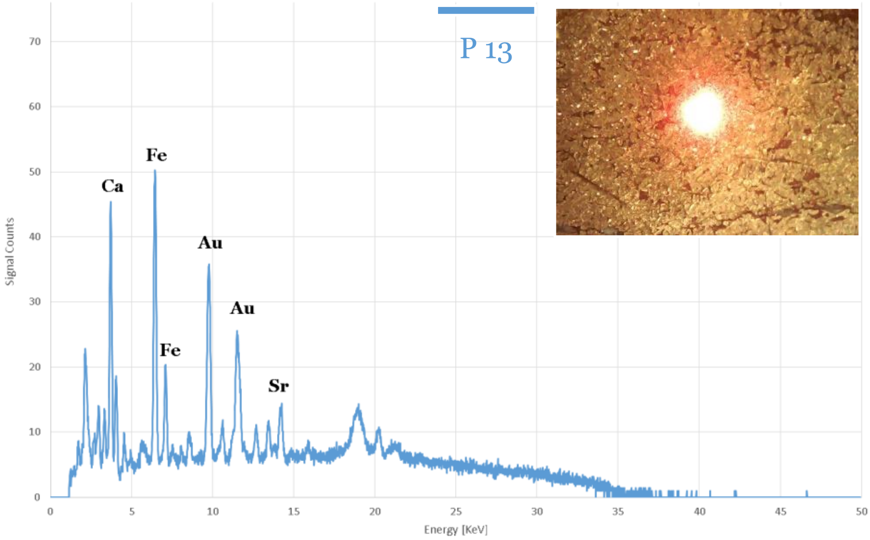

Fig. 63 Point 13 XRF spectrum.

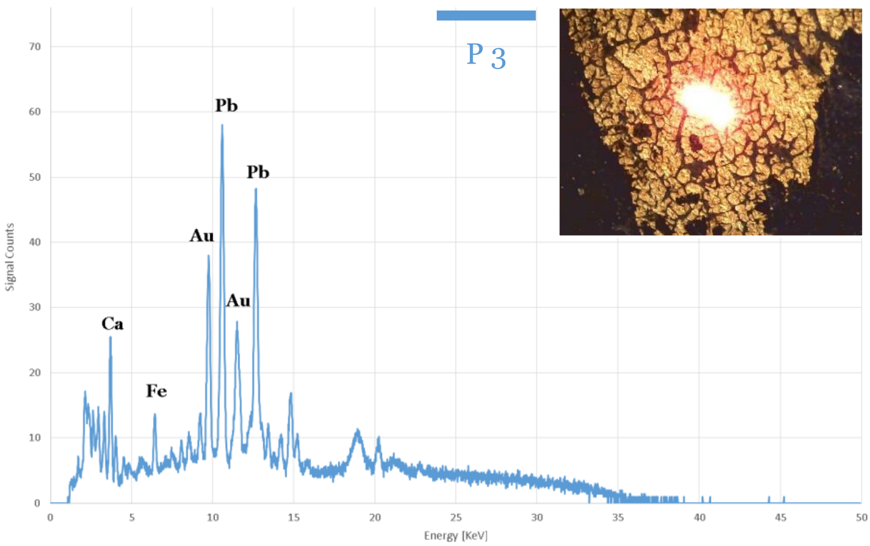

Fig. 64 Point 3 XRF spectrum.

The following table summarizes the presence of the major elements identified in each point analyzed.

Points	*Color*	*Pb*	*Au*	*Fe*	*Cu*	*P*	*S*	*Si*	*K*	*Ba*	*Hg*	*Ca*	*Sr*
P1	Gold (highligt)	●	●	●	○	●	●	●	●	●		●	●
P2	Blue	●		○	○		●	?	●	●		●	●
P3	Gold (highlight)	●	●	●	○	●	●	●	●	●		●	●
P4	Blue	●		○	○		●	?	●	●		●	●
P5	Gold (highlight)	●	●	●		●	●		○	○	●	●	●
P6	Ligh○ Red	●		○			●			○	●	●	○
P7	Dark Red	●		●			●		●		●	●	
P8	Red	○	●	●		○	●		●	●	●	●	●
P9	Gold	○	●	●		○	●		●	●	●	●	●
P10	Red	●		●		○	●		●	●	●	●	●
P11	Pink	●		●	○		●	○			?	●	●
P12	White	●		●	○		●	○			?	●	●
P13	Gold	○	●	●	○	●		○	●	○		●	●
P14	Gold	○	●	●		●		○	●	○		●	●
P15	Red	○	●	●	○		●		●	○	●	●	○
P16	Orange	●		●			●	○	●	●		●	●
P17	Pink	●		○			●			○	○	○	○
P18	Red	●		●			●		○		●	●	○
P19	Pink	●		○			●			○	○	○	○
P20	Brown	●		●			●	○	○	○	?	○	○
P21	Blue	○	?	○	○		●	●	●	●		●	●

○ Traces

Conclusions

and future perspectives

The idea behind this Ph.D project, i.e. to use a specific variant of 3D Reality Based Modeling integrated with the Multispectral Imaging technique, has proved to be strictly up to date.

The project has been in fact designed simultaneously to the launch of the EU Framework Program for Research and Innovation *Horizon 2020* where the digitization of Cultural Heritage is one of the pillars. The specific call titled "Advanced 3D modelling for accessing and understanding European cultural assets" recognized the key role that the digital models are now playing in the representation, reconstruction, preservation, and conservation of heritage. The EU program encouraged the development of new methods and tools for automated 3D modelling and analysis of physical cultural resources. At the same time it detected the analytic potential beyond the current levels of visual depictions in high-fidelity models of objects with particularly challenging features as regards surface, transparency, dimensions, materials degradation, etc. All this considered we feel satisfied in having been able to intercept the most cutting-edge trends in the field of the e-documentation and e-preservation.

The many case studies proposed by different research groups show that the computational approach is a well-established practice to obtain valid 3D models of artworks for documentary purposes, but on the diagnostic-purpose side the development of an integrated 3D Multispectral system is still in its experimental phase. We propose a *data fusion* method combining two techniques – now widely affordable for everyone – as a single solution able to provide digital products characterized by high level of spectral and morphometric detail. Considering that the information gathered in a single coordinate system obviously enhance the potential insights into data analysis of a specific art object, what we obtain at the end is a digital model collector of heterogeneous information — both quantitative and qualitative — for a multi-temporal evaluation process.

Assuming that the best 3D modeling results are achieved by integrating different surveying techniques, it has been noted as in most works that have incorporated MS data into 3D models, the 3D shapes are generated by range devices rather than from MS images directly. The originality of this Ph.D. project consists in a proposal of a method that avoids the complex registration procedures that is typical of acquisition set-ups composed of separate devices each based on different physical principles. Applying the Structure from Motion technique, the problems related to a rigid geometric strategy of shooting were avoided, favoring a more spontaneous configuration where neither post-processing step for mapping the spectral information to a 3D shape nor previous knowledge of the calibration parameters of the devices used are anymore necessary requirements. Furthermore, having used a bundle of open source software together with an inexpensive commercial Multispectral digital camera we tried to speed up MS Photogrammetric 3D reconstruction techniques towards a cost-effective solution. Since passive sensors are more versatile in terms of cost, time and ease of use, we imagined that this could be the nearest operating mode to that used by end-users, e.g. restorers and conservators. We believe in fact that once comfortable with this technique, the specialized operators will have no difficulty to switch to it as a routine operation.

As it is vastly confirmed by specific literature, photogrammetry allows reaching comparable results in terms of accuracy and precision in the representation of the morphological details to those provided by the surveying techniques based on range methods.

By performing a quantitative comparison of the respective point clouds, we obtain results where both RGB and IR digital models maintain a sub-millimeter accuracy; the one typically required by restorers in the evaluation processes concerning the painting maintenance. Considering in fact that the photogrammetry has a theoretical precision of 0.7 mm, 91% of the analyzed points were found to be in an acceptable range. The points with high discrepancies are mainly located along the peripheral edges of the painting. As it is well known in the literature, this is probably due to some aberrations that may occur during the model-generating phase.

Taking into account the use of two different digital cameras, the different spectral bands involved, the separate acquisition sessions — necessarily due to the different equipment — and the strong environmental constraints in the shooting conditions, the aforementioned result is not a foregone conclusion. Despite the procedure that is not exactly “by the book”, plus the systematic errors due to camera factors (different sensor size, different Flange Focal Length, etc.), qualitative and quantitative results clearly show that the two compared models are morphometrically comparable. However, the study also highlighted the critical issues encountered, mainly due to: *i)* the specificities of the subject, and *ii)* a not trivial inedited method tested on a work of art tending to the two-dimensionality.

Assuming that digital technologies are the visual and cultural interfaces currently available to study the Cultural Heritage, the aim of this thesis is to demonstrate the feasibility of obtaining a well detailed 3D IR model for broadening the range of deductive inquiries in a very affordable way.

It is reasonable to think that the new perspective opened in Digital Imaging will be to embed the information resulting from different branches in a multi-dimensional digital object. Therefore, the approach here proposed is definitely a starting point to be further refined, because it is opened to many possible future developments, e.g. the adaptability of the method using other types of input source images specifically related to the Digital Imaging (e.g. IR False Color images, Thermal images, etc.).

The greater challenge will be to get as much 3D digital models of the same subject as there are the major spectral bands in the VIS and in the NIR regions of the electromagnetic spectrum. This would make possible to check whether the calculated distance between the respective aligned point clouds are appreciable in the nanoscale. If appropriate software will be available in the future, the simultaneous display of these point clouds in a single IT platform will allow to appreciate a 4D spatio-spectral model where the fourth dimensions will be precisely the spectral one.

In addition, it should be noted that there is an increasing interest in semantically annotated 3D models. Among all the challenges more strongly encouraged in the computer vision domain, the major role is represented by the semantic segmentation of 3D models consisting in the recognition of sub-components that are generally characterized by uniform properties (Manferdini & Remondino, 2012). We envision useful applications of 3D model segmentation inside searchable databases in knowledge ontology contexts. The ontology defines machine-readable terms that are useful for semantic annotations to 3D Cultural Heritage artefacts. The incremented adoption of Semantic Web technologies into mainstream applications is leading to a range of projects that use ontologies and reasoning to annotate and infer new knowledge about 3D surrogates (Yu & Hunter, 2013).

Combine the semantic segmentation technologies to our 3D multispectral approach would be the *non plus ultra*.

Bibliography

Abate, D., Menna, F., Remondino, F., & Gattari, M. (2014). 3D painting documentation: evaluation of conservation conditions with 3D imaging and ranging techniques. *ISPRS Technical Commission V Symposium "Close-range imaging, ranging and applications", XL-5*, pp. 1-8. Riva del Garda, Italy.

Abdel-Aziz, Y., & Karara, H. (1971). Direct linear transformation from comparator coordinates into object space coordinates in close-range photogrammetry. Falls Church, VA: America. *Proceedings of the Symposium on Close-Range Photogrammetry*, pp. 1-18. Falls Church, VA: American Society of Photogrammetry.

Akca, D., Gruen, A., Breukmann, B., & Lahanier, C. (2007). High definition 3D-scanning of art objects and painting. *Proceedings Optical 3D Measurement Techniques Conference, 2*, pp. 50-58.

Alliez, P., Meyer, M., & Desbrun, M. (2002). Interactive geometry remeshing. *ACM Trans. Graph, 21*(3), pp. 347-354.

Alliez, P., Ucelli, G., Gotsman, C., & Attene, M. (2008). Recent Advances in Remeshing of Surfaces. In L. D. Floriani, & M. Spagnuolo, *Shape Analysis and Structuring*, pp. 53-82. Berlin, Germany: Springer.

Alliez, P., Verdière, E., Devillers, O., & Isenburg, M. (2003). Isotropic surface remeshing. *In SMI '03: Proceedings of the Shape Modeling International 2003*, p. 43. Washington, DC, USA: IEEE Computer Society.

Amenta, N., Bern, M., & Eppstein, D. (1999). Optimal point placement for mesh smoothing. *J. Algorithms, 30*(2), pp. 302-322.

Amenta, N., Bern, M., & Kamvysselis, M. (1998). *Proceedings of ACM SIGGRAPH*, pp. 415-422.

Amenta, N., Choi, S., & Kolluri, R. (2001). The power crust. *ACM solid modelling*, pp. 213-222.

Amenta, N., Choi, S., Dey, T., & Leekha, N. (2000). A simple algorithm for homeomorphic surface reconstruction. *In: Computational geometry*, pp. 213-222.

Aspert, N., Santa Cruz, D., & Ebrahimi, T. (2002). MESH: measuring errors between surfaces using the Hausdorff distance. *ICME*, pp. 705-708.

Atkinson, K. B. (1996). *Close Range Photogrammetry and Machine Vision*. Caithness: Whittles Publishing.

Barazzetti, L., Mussio, L., Remondino, F., & Scaioni, M. (2011). Targetless camera calibration. *International Archives of the Photogrammetry, Remote Sensing and Spatial Information Sciences, XXXVIII-5/W16*, pp. 335-342.

Barni, M., Pelagotti, A., & Piva, A. (2005). Image processing for the analysis and conservation of paintings: Opportunities and challenges. *IEEE Signal Processing Magazine, 22*(5), pp. 141-144.

Baronti, S., Casini, A., Lotti, F., & Porcinai, S. (1998). Multispectral imaging system for the mapping of pigments in works of art by use of principal component analysis. *Applied Optics, 37*(8), pp. 1299-1309.

Battro, A. M. (2010). From Malraux's Imaginary Museum to the Virtual Museum. In R. Parry, *Museums in a digital age*, pp. 136-147. London and New York: Routledge.

Benjamin, W. (2011). *L'opera d'arte nell'epoca della sua riproducibilità tecnica*. Torino: Einaudi.

Beraldin, J., Blais, F., Boulanger, P., Cournoye, L., Domey, J., El-Hakim, S., Taylor, J. (2000). Real world modelling through high resolution digital 3D imaging of objects and structures 55. *ISPRS J. Photogramm. Remote Sensing, 55*, pp. 230–250.

Bernardini, F., Martin, I., & Rushmeier, H. (2001). High-quality texture reconstruction from multiple scans. *IEEE Trans. Vis. Comput. Graph, 7*, pp. 318-332.

Bernardini, F., Mittleman, J., Rushmeier, H., Silva, C., & Taubin, G. (1999). The Ball-pivoting algorithm for surface reconstruction. *IEEE*, pp. 349-359.

Berns, R. (2001). The science of digitizing paintings for color-accurate image archives: a review. *J. Imaging Sci. Technol., 45*, pp. 305-325.

Berns, R., Taplin, L., Nezamabadi, M., Mohammadi, M., & Zhao, Y. (2005). Spectral imaging using a commercial color-filter array digital camera. *Proceedings of the 14th Triennial ICOM-CC Meeting*, *2*, pp. 743-750.

Bertani, D., Consolandi, L., & Bellaria, M. (2007). La riflettografia infrarossa. In M. Martini, A. Castellano, & E. Sibilia, *Elementi di Archeometria. Metodi fisici per i beni culturali*, pp. 253-276. Milano: Egea.

Blais, F., & Beraldin, J. (2006). Recent developments in 3D multi-modal laser imaging applied to cultural heritage. *Mach. Vis. Appl., 17*, pp. 395-409.

Blais, F., Taylor, J., Beraldin, J., Godin, G., Cournoyer, I., Picard, M., Aitken, G. (2005). Ultra-High Resolution Imaging at 50µm using a Portable XYZ-RGB Color Laser Scanner. *International Workshop on Recording, Modeling and Visualization of Cultural Heritage*, pp. 101-114. Ascona, Switzerland.

Blais, F., Taylor, J., Godin, G., Cournoyer, L., Beraldin, J., Picard, M., Lahanier, C. (2007). Ultra High-Resolution 3D Laser Color Imaging of Paintings: The Mona Lisa by Leonardo Da Vinci. *7th International Conference on Lasers in the conservation of Artworks*, pp. 435-440. Madrid, Spain.

Blomley, R., Weinmann , M., J. Leitloff, & Jutzi , B. (2014). Shape distribution features for point cloud analysis. *ISPRS Annals of the Photogrammetry, Remote Sensing and Spatial Information Sciences, II-3*, pp. 9-16. Zurich, Switzerland.

Boissonnat, J. (1984). Geometric structures for three dimensional shape representation. *ACM Trans Graph, 3*, pp. 266–268.

Bokova, I. (2016, June 13). *Lecture by Irina Bokova, Cultural heritage at risk: protecting cultural heritage in times of conflict*. June 20, 2006.
Retrieved from:
http://www.europelecture.com/id/vk4xd7fq2etf/lecture_by_irina_bokova#p2.

Botsch, M., & Kobbelt, L. (2004). A remeshing approach to multiresolution modeling. *In SGP'04: Proceedings of the 2004 Eurographics/ACM SIGGRAPH symposium on Geometry processing*, pp. 185-192. USA: ACM.

Brandao, S., Costeira, J., & Veloso, M. (2012). Joint Alignment and Stitching of Non Overlapping Meshes. *Proceedings of IROS - IEEE/RSJ International Conference on Intelligent Robots and Systems*. VilaMoura, Portugal. Retrieved from: http://www.cs.cmu.edu/~mmv/papers/12irosw-BrandaoCosteiraVeloso.pdf

Brandi, C. (1963). *Teoria del restauro*. Roma: Einaudi.

Brown, D. (1958). *A solution to the general problem of multiple station analytical stereotriangulation*. Tech. Rep. RCA-MTP Data Reduction Technical Report, Patrick Airforce Base.

Bruschi, A. (1978). Indicazioni metodologiche per lo studio storico dell'architettura. In A.A.V.V., *Lineamenti di storia dell'architettura*, pp. 13-29. Assisi-Roma: Carucci.

Brusco, N., Cortelazzo, G., Capeleto, S., Fedel, M., Paviotti, A., Poletto, L., & Tondello, G. (2006). A system for 3D modeling frescoed historical buildings with multispectral texture information. *Mach. Vis. Appl., 17*, pp. 373-393.

Burmester, A., Cupitt, J., Derrien, H., & Dessipris, N. (1993). The examination of paintings by digital image analysis. *3rd International Conference on Non Destructive Testing, Microanalytical Methods and Environmental Evaluation for Study and Conservation of Works of Art*, pp. 210-214. Rome (IT).

Cameron, F., & Kenderdine, S. (2007). *Theorizing digital cultural heritage: A critical discourse*. Boston: MIT Press.

Cardinali, M. (2002). Le radici teoriche della diagnostica artistica. In M. Cardinali, M. B. De Ruggeri, & C. Falcucci, *Diagnostica artistica. Tracce materiali per la storia dell'arte e per la conservazione*, pp. 13-29. Roma: Palombi Editore.

Cardinali, M. & De Ruggeri, M. (2013). La nascita della diagnostica artistica attraverso le prime riviste tecniche. Un percorso internazionale. In N. Barrella, & R. Cioffi, *La consistenza dell'effimero. Riviste d'arte tra Ottocento e Novecento*, vol. 5, pp. 317-330. Napoli: Luciano Editore.

Casini, A., Lotti, F., Picollo, M., Stefani, L., & Buzzegoli, E. (1999). Image spectroscopy mapping technique for noninvasive analysis of paintings. *Stud. Conserv., 44*, pp. 39-48.

Cetica, M., Marras, L., Materazzi, M., & Poggi, P. (2007). Tecniche di Imaging multispettrale. In M. Martini, A. Castellano, & E. Sibilia, *Elementi di archeometria. Metodi fisici per i beni culturali*, pp. 231-252. Milano: Egea.

Chane, C., Mansouri, A., Marzani, F., & Boochs, F. (2013). Integration of 3D and multispectral data for cultural heritage applications: Survey and perspectives. *Image and Vision Computing, 31*, pp. 91-102.

Chen, Y., & Medioni, G. (1992). Object modelling by registration of multiple range images. *Image and Vision Computing, 10*(3).

Cichocki, A., & Amari, S. (2002). *Adaptive blind signal and image processing*. New York: Wiley.

Cignoni, P., Callieri, M., Corsini, M., Dellepiane, M., Ganovelli, F., & Ranzuglia, G. (2008). Meshlab: an open-source mesh processing tool. *Eurographics Italian Chapter Conference*, pp. 129-136.

Cignoni, P., Rocchini, C., & Scopigno, R. (1998). Metro: Measuring error on simplified surfaces. *Computer Graphics Forum, 17*(2), pp. 167-174.

CloudCompare – CloudCompere User's Manual for version 2.1, 2012.

Costantini, P. (1986). Pietro Selvatico: fotografia e cultura artistica alla metà dell'Ottocento. *Fotologia*(4), pp. 54-67.

Costantini, P. (1986). Ruskin e il dagherrotipo. In P. Costantini, & I. Zannier, *I dagherrotipi della collezione Ruskin*. Firenze-Venezia: Alinari-Arsenale.

Cucci, C., Casini, A., Picollo, M., & Stefani, L. (2013). Extending hyperspectral imaging from Vis to NIR spectral regions: a novel scanner for the in-depth analysis of polychrome surfaces. *SPIE Proceedings, Optics for Arts, Architecture, and Archaeology, IV, 8790*, pp. 870091-9.

Daffara, C., & Fontana, R. (2011). Multispectral Infrared Reflectography to Differentiate Features in Paintings. *Microsc. Microanal., 17*, pp. 691-695.

Daffara, C., Pampaloni, E., Pezzati, L., Barucci, M., & Fontana, R. (2010). Scanning multispectral IR reflectography SMIRR: an advanced tool for art diagnostics. *Acc. Chem. Res., 43*, pp. 847-856.

Dai, F., Feng, Y., & Hough, R. (2014). Photogrammetric error sources and impacts on modeling and surveying in construction engineering applications. *Visualization in Engineering, 2*(2).

Dai, F., Rashidi, A., Brilakis, I., & Vela, P. (2013). Comparison of image-based and time-of-flight-based technologies for three-dimensional reconstruction of infrastructure. *Journal of Construction Engineering and Management, 139*(1), pp. 69-79.

De Luca, L., Busayarata, C., Stefania, C., Véronb, P., & Florenzano, M. (2011). A semantic-based platform for the digital analysis of architectural heritage. *Computers & Graphics, 35*(2), pp. 227–241.

De Ruggeri, M. B. (2002). Per una storia delle indagini scientifiche. In C. Falcucci, M. De Ruggeri, & M. Cardinali, *Diagnostica artistica. Tracce materiali per la storia dell'arte e per la conservazione*, pp. 41-94. Roma: Editore, Palombi.

Dey, T., & Giesen, J. (2002). Detecting undersampling in surface reconstruction. *Computational geometry*, pp. 257-263.

Diara, F. (2013). New software and technologies applied to documentation and communication of Cultural Heritage. *Conference on Cultural Heritage and New Technologies (CHNT).* Vienna.

Dietrich, D. (1997). On a Number of Things: Hanne Darboven's "Kulturgeschichte 1880–1983". *On paper, 2*(1), pp. 15-19. Retrieved from: http://www.jstor.org/stable/24554661

Eardley, W., Ashe, D., & Fletcher, B. (2016). An Ontology Engineering Approach to User Profiling for Virtual Tours of Museums and Galleries. *International Journal of Knowledge Engineering, 2*(2).

El-Hakim, S., Beraldin, J., Remondino, F., Picard, M., Cournoyer, L., & Baltsavias, M. (2008). Using terrestrial laser scanning and digital images for the 3D modelling of the Erechteion, Acropolis of Athens. *Proceedings of "Digital Media and its Applications in Cultural Heritage" (DMACH)*, pp. 3-16. Amman, Jordan.

Elnima, E. E. (2015, January). A solution for exterior and relative orientation in photogrammetry, a genetic evolution approach. *Journal of King Saud University - Engineering Sciences, 27*(1), pp. 108-113.

Eltner, A., & Schneider, D. (2015). Analysis of different methods for 3D reconstruction of natural surfaces from parallel-axes UAV images. *Photogramm. Rec., 30*, pp. 279-299.

Enhuber, M. (2015). Art, space and technology: how the digitisation and digitalisation of art space affect the consumption of art—a critical approach. *Digital Creativity, 26*(2), pp. 121-137.

Fassi, F., Achille, C., & Fregones, L. (2011). Surveying and modelling the main spire of Milan Cathedral using multiple data sources. *The Photogrammetric Record, 136*, pp. 462-487.

Feng, S., Shijie, C., & Mohammad-Djafari, A. (2008). Bayesian blind separation of mixed text patterns. *Proceedings of the 2008 International Conference on Audio, Language and Image Processing*, pp. 1373-1378.

Fischer, C., & Kakoulli, J. (2006). Multispectral and hyperspectral imaging technologies in conservation: current research and potential applications. *Rev. Conserv.*, pp. 3-16.

Fontana, R., Barucci, M., Carcagnì, P., Daffara, C., Pampaloni, E., & Pezzati, L. (2011). Autofocus laser system for multi-NIR scanning imaging of painting surfaces. *SPIE Proceeding, Optics for Arts, Architecture, and Archaeology*, *III*, pp. 8084051-9.

Fontana, R., Dal Fovo, A., Striova, J., Pezzati, L., Pampaloni, E., Raffaelli, M., & Barucci, M. (2015). Application of non-invasive optical monitoring methodologies to follow and record painting cleaning processes. *Applied Physics A*.

Fontana, R., Gambino, M., Greco, M., Marras, L., Materazzi, M., Pampaloni, E., Poggi, P. (2005). 2D imaging and 3D sensing data acquisition and mutual registration for painting conservation. *Proceedings SPIE Videometrics*, *VIII*, pp. 51-58.

Fontana, R., Pampaloni, E., & Pezzati, L. (2007). Tecniche ottiche per misurare la forma. In M. Martini, A. Castellano, & E. Sibilia, *Elementi di Archeometria. Metodi fisici per i beni culturali*, pp. 277-296. Milano: Egea.

Forte, M. (2004). Realtà virtuale, beni culturali e cibernetica: un approccio ecosistemico. In M. Cristofani, R. Francovich, & N. F. Moscati (ed.) (Ed.), *Archeologia e Calcolatori*, vol. XV, pp. 423-448. Borgo San Lorenzo: All’Insegna del Giglio.

Furlan, C. (2005). Giuseppe Fiocco e la fotografia. *Saggi E Memorie Di Storia Dell'Arte, 29*, pp. 291-298. Retrieved from: http://www.jstor.org/stable/43140165

Furukawa, Y., & Ponce, J. (2010). Accurate, dense, and robust multiview stereopsis. *IEEE transactions on pattern analysis and machine intelligence, 32*(8), pp. 1362-1376.

Girardeau-Montaut, D. (n.d.). *CloudCompare-3D point cloud and mesh processing software. Open Source Project.* Retrieved from: http://www.danielgm.net/cc/doc/qCC/Documentation_CloudCompare_version_2_1_eng.pdf

Goetz, A. (2009). Three decades of hyperspectral remote sensing of the Earth: a personal view. *Remote Sensing of Environment, 113*(Supplement 1), pp. S5-S16.

Guidi, G., Remondino, F., Russo, M., Menna, F., Rizzi, A., & Ercoli, S. (2010). A multiresolution methodology for the 3D modeling of large and complex archaeological areas. *International Journal of Architectural Computing, 7*(1), pp. 40-55.

Hage, J. (2016). *Atlas.* Retrieved from Gerhard Richter: https://www.gerhard-richter.com/en/art/atlas

Hart, K. (2011). Art Project, Powered by Google. *The Charleston Advisor, 13*(2), pp. 16-20.

Haykin, S. (1999). *Neural networks. A comprehensive foundation.* New Jersey, U.S: Prentice-Hall.

Hazan. (2007). A Crisis of Authority: New Lamps for Old. In F. Cameron, & S. Kenderdine, *Theorizing Digital Cultural Heritage. A critical discourse*, pp. 133-147. Boston: MIT Press.

Hazan, S., Hermon, S., Turra, R., Pedrazzi, G., Franchi, M., & Wallergard, M. (2014). *Theory Design – Deliverable report 3.1.* Retrieved from: http://www.v-must.net/sites/default/files/D3.1_update.pdf

Hoppe, H., DeRose, T., Duchamp, T., McDonald, J., & Stuetzle, W. (1992). Surface reconstruction from unorganized points. *SIGGRAPH, 26*(2).

Hoppe, H., DeRose, T., Duchamp, T., McDonald, J., & Stuetzle, W. (1992). Surface reconstruction from unorganized points. *ACM SIGGRAPH*, pp. 71-78.

Hu, Z., Xie, H., Lu, J., & Wang, H. (2011). Error evaluation technique for three-dimensional digital image correlation. *Applied Optics, 50*(33), pp. 6239-6247.

Huang, Q.-X., Flöry, S., Gelfand, N., & Hofer, M. (2006). Re-assembling fractured objects by geometric matching. *ACM Transactions on Graphics (Proceedings of ACM SIGGRAPH), 25(3),* pp. 569–578.

Huang, X. F.-C.-L. (2007). Optimal boundaries for. *Proceedings of the ACM Symposium on Solid and Physical Modeling*, pp. 35-40.

Huang, X., Fu, H., Au, O.-C., & Tai, C.-L. (2007). Optimal Boundaries for Poisson Mesh Merging. *Proceedings - SPM 2007: ACM Symposium on Solid and Physical Modeling*, pp. 35-40.

Huhtamo, E. (2010). On the origins of the Virtual Museum. In R. Parry, *Museums in a digital age*, pp. 121-135. London and New York: Routledge.

Huttenlocher, D., Klanderman, G., & Rucklidge, W. (1993). Comparing images using the Hausdorff distance. *IEEE Transactions on pattern analysis and machine intelligence*, pp. 850-863.

Ikeuchi, K., Oishi, T., Takamatsu, J., Sagawa, R., Nakazawa, A., Kurazume, R., Okamoto, Y. (2007). The Great Buddha Project: digitally archiving, restoring, and analyzing cultural heritage objects. *Int. J. Comput. Vis., 75*, pp. 189-208.

James, M., & Robson, S. Straightforward reconstruction of 3D surfaces and topography with a camera: Accuracy and geoscience application. *Journal of Geophysical Research, 117*(F3).

Karp , C. (2004). The Legitimacy of the Virtual Museum. *ICOM NEWS, 3*. Retrieved from: http://icom.museum/fileadmin/user_upload/pdf/ICOM_News/2004-3/ENG/p8_2004-3.pdf

Kazhdan, M., & Hoppe, H. (2013). Screened Poisson surface reconstruction. *ACM Trans Graph, 32*(29).

Kazhdan, M., Bolitho, M., & Hoppe, H. (2006). Poisson surface reconstruction. *Eurographics symposium on geometry processing*.

Kim, M., Harvey, T., Kittle, D., Rushmeier, H., Dorsey, J., Prum, R., & Brady, D. (2012). 3D Imaging Spectroscopy for Measuring Hyperspectral Patterns on Solid Objects. *ACM Transactions on Graphics, 31*(4:38).

Koch, R., Pollefeys, M., & Van Gool, L. (2000). Realistic surface reconstruction of 3D scenes from uncalibrated image sequences. *J. Visual. Comput. Animat., 11*, pp. 115-127.

Kohonen, T. (1990). The self-organizing map. *Proceedings of the IEEE, 78*(9), pp. 1464-1480.

Kozlowski, R. (1960). La Microstéréoradiographie. *Studies in Conservation, 5*(3), pp. 89-101.

Kubelka, P., & Munk, F. (1931). Ein Beitrag Zur Optik der Farbanstriche. *Zeitschrift fur technische Physik, 12*, pp. 593-601.

Kubik, M. (2007). Hyperspectral imaging: a new technique for the non-invasive study of. In *Physical Techniques in the Study of Art, Archaeology and Cultural Heritage* (vol. II). Amsterdam.

Kuncheva, L. (2004). *Combining pattern classifiers: Methods and algorithms*. New Jersey, U.S.: Wiley Interscience.

Lahanier, C., Aitken, G., Pillay, R., Beraldin, J., Blais, F., Borgeat, L., de Deyne, C. (2005). Two-dimensional multi-spectral digitization and three-dimensional modelling of easel paintings. *Proccedings of the 14th Triennal ICOM-CC Meeting, 1*. The Hague, Netherlands.

Legnaioli, S., Grifoni, E., Lorenzetti, G., Marras, L., Pardini, L., Palleschi, V., Tonazzini, A. (2013). Enhancement of hidden patterns in paintings using statistical analysis. *Journal of Cultural Heritage, 14*(3 SUPPL), S66-S70.

Legnaioli, S., Lorenzetti, G., Cavalcanti, G., Grifoni, E., Marras, L., Tonazzini, A., Palleschi, V. (2010). Recovery of archaeological wall paintings using novel multispectral imaging approaches. *Heritage Science, 1*(33).

Lettner, M., Kammerer, P., & Sablatnig, R. (2004). Texture analysis of painted strokes. *28th Workshop of the Austrian Association for Pattern Recognition (OAGM/AAPR), 179*, pp. 269-276. Schriftenreihe der OCG.

Levoy, M., Rusinkiewicz, S., Ginzton, M., Ginsberg, J., Pulli, K., Koller, D., Fulk, D. (2000). The Digital Michelangelo Project: 3D Scanning of Large Statues. *Proceedings of ACM SIGGRAPH*, pp. 131-144.

Lévy, P. (2010). Building a Universal Digital Memory. In R. Parry, *Museums in a digitale age*, pp. 107-116. London and New York: Routledge.

Lewis, P., Martinez, K., Abas, F., Fauzi, M., Chan, S., Addis, M., Grimwood, P. (2004). An integrated content and metadata based retrieval system for art. *IEEE Trans. Image Processing (Special Issue on Image Processing for Cultural Heritage)*, *13*, pp. 416-429.

Li, Q., He, X., Wang, Y., & Liu, H. (October 2013). Review of spectral imaging technology in biomedical engineering: achievements and challenges. *Journal of Biomedical Optics, 18*(10), pp. 1-28.

Li, X., Wan, W., Cheng, X., & Chi, B. (2010). An improved Poisson surface reconstruction algorithm. *IEEE.*

Liang, H. (2012). Advances in multispectral and hyperspectral imaging for archaeology and art conservation. *Applied Physics A, 106*(2), pp. 309-323.

Liang, H., Lange, R., Peric, B., & Spring, M. (2013). Optimum spectral window for imaging of art with optical coherence tomography. *Appl. Phys. B, 111*(4), pp. 589-602.

Liang, H., Lucian, A., Lange, R., Cheung, C., & Su, B. (2014). Remote spectral imaging with simultaneous extraction of 3D topography for historical wall paintings. *ISPRS Journal of Photogrammetry and Remote Sensing, 95*, pp. 13-22.

Liang, H., Saunders, D., & Cupitt, J. (2005). A new multispectral imaging system for examining paintings. *J. Imag. Sci. Technol., 49*(6), pp. 551-562.

Liritzis, I., Al-Otaibi, F., Volonakis, P., & A., D. (2015). *Mediterranean Archaeology and Archaeometry, 15*(3), pp. 313-332.

Liu, X.-J., Yang, J., Sun, J.-W., & Liu, Z. Image registration approach based on SIFT.

Liu, Y., Pu, Y., & Xu, D. (2013). Computer analysis for visual art style. *SIGGRAPH Asia 2013 Technical Briefs, SA 2013, art. no. 9.*

Loose, L. (1964). La stratiradiographie et la tirage cathodique. *Institut Royal du Patrimoine Artistique Bulletin, VII*, pp. 172-186.

Lowe, D. (2004). Distinctive Image Features from Scale-Invariant Keypoints. *International Journal of Computer Vision, 60*(2), pp. 91-110.

Luhmann, T., Robson, S., Kyle, S., & Boehm, J. (2013). *Close Range Photogrammetry and 3D Imaging*. De Gruyter.

Maiti, A., & Chak, D. (2016). Performance analysis of different surface reconstruction algorithms for 3D reconstruction of outdoor objects from their digital images. *SpringerPlus, 5:932*.

Malraux, A. (1936, September). Sur l'héritage culturel. *Commune, 37*(6).

Malraux, A. (1947). *Il museo dei musei. Le voci del silenzio*. Milano: Mondadori.

Manabe, Y., Kurosaka, S., & Chihara, K. (2000). Simultaneus Measurement of Spectral Distribution and Shape. *Pattern Recognition, 2000. Proceedings, 15th International Conference on, 3,* pp. 803-806.

Manferdini, A., & Remondino, F. (2012). A review of reality-based 3D model generation, segmentation and web-based visualization methods. *Int. Journal of Heritage in the Digital Era, 1*, pp. 103-124.

Mansouri, A., Marzani, F., Lathuiliere, A., Voisin, Y., & Gouton, P. (2007). Toward a 3D multispectral scanner: an application to multimedia. *IEEE Multimedia, 14*, pp. 40-47.

Marabelli, M. (2006). Il ruolo delle indagini scientifiche per il restauro e la conservazione secondo la Teoria di Cesare Brandi. In N. Editore (Ed.), *La Teoria del restauro nel Novecento. Da Riegl a Brandi. Atti del convegno internazionale (Viterbo, novembre 2003)*, pp. 269-275. Viterbo.

Marbs, A., Heinz , G., & Boehler, W. (2001). The potential of non-contact close range laser scanners for cultural heritage recording. *Proceedings of the CIPA international symposium*. Potsdam, Germany.

Marras S., G. F. (2010). *International Conference in Computer Graphics Theory and Applications. VISGRAPP*, pp. 104-110. Paris, France.

Martinez, K., Cupitt, J., & Saunders, D. (1993). High resolution colorimetric imaging of paintings. *Proceedings of the SPIE, 1901*, pp. 25-36.

Martinez, K., Cupitt, J., Saunders, D., & Pillay, R. (2002). Ten years of art imaging research. *Proceedings IEEE, 90*, pp. 28-41.

Matthias, A., Pedroso, J., van Eikema Hommes, M., Van der Snick, G., Tauber, G., Blaas, J., Janssens, K. (2013). A mobile instrument for in situ scanning macro-XRF investigation of historical paintings. *Journal of Analytical Atomic Spectrometry, 28*, pp. 760-767.

Mazzeo, R., Palazzi, C., Roccetti, M., & Sciutto, G. (2007). Computer-assisted pigment identification in artworks. *EurolMSA Proceedings of the Third IASTED European Conference on Internet and Multimedia Systems and Applications*, pp. 266-271. Chamonix, France.

Mazzucco, K. (2011). Mnemosyne, il nome della memoria. Bilderdemonstration, Bilderreihen, Bilderatlas: una cronologia documentaria del progetto warburghiano. *Quaderni del Centro Warburg Italia, III*, pp. 139-203.

Mazzucco, K. (2012). On the reverse. Some notes on photographic images from the Warburg Institute Photographic Collection. *Aisthesis. Pratiche, Linguaggi E Saperi Dell'Estetico, 5*(2), pp. 217-232.

McGlone, J. (2013). *Manual of Photogrammetry* (6th ed.). Americal Society for Photogrammetry.

Meersman, R., De Bruyne, S., & Stuer, P. (2001). The HyperMuseum Theme Generator System: Ontology-based Internet Support for the Active Use of Digital Museum Data for Teaching and Presentation. *Museums and the Web 2001: Proceedings*. Seattle, Washington, USA: Bearman, D., & Trant J.
Retrieved from:
http://www.archimuse.com/mw2001/papers/stuer/stuer.html.

Micheletti, N., Chandler, J., & Lane, S. (2015). Structure from Motion (SfM) Photogrammetry. In *Geomorphological Techniques*. British Society for Geomorphology.

Micheletti, N., Chandler, J., & Stuart, N. (2015). Structure from Motion (SfM) Photogrammetry. In L. Clarke, & J. Nield, *Geomorphological Techniques*, pp. 1-12. London.
Retrieved from:
https://dspace.lboro.ac.uk/dspace-jspui/bitstream/2134/17493/3/2.2.2_sfm.pdf

Mikhail, E., Bethel, J., & McGlone, J. (2001). *Introduction to Modern Photogrammetry*. Wiley.

Milazzo, M. (2007). Analisi XRF quantitativa nelle applicazioni archeometriche. In M. Martini, A. Castellano, & E. Sibilia, *Elementi* *di archeometria. Metodi fisici per i beni culturali*, pp. 124-153. Milano: Egea.

Mundy, J., & Zisserman, A. (1994). Repeated structures: Image correspondence constraints and ambiguity of 3D reconstruction. In J. Mundy, A. Zisserman, & D. Forsyth, *Applications of Invariance in Computer Vision*, pp. 89-106. Springer-Verlag.

Nauta, G. J., & Heuvel, W. v. (2015). *Survey Report on Digitisation in European Cultural Heritage Institutions 2015.* Retrieved from: http://pro.europeana.eu/files/Europeana_Professional/Projects/Project_list/ENUMERATE/deliverables/ev3-deliverable-d1.2-europeana-version1.1-public.pdf

Nguyen, A., & Le, B. (2013). 3D point cloud segmentation: A survey. *6th IEEE Conference on Robotics, Automation and Mechatronics (RAM)*, pp. 225-230.

Nieto, J., Monteiro, S., & Viejo, D. (2010). 3D geological modelling using laser and hyperspectral data. *Proceedings IEEE International Geoscience and Remote Sensing Symposium (IGARSS)*, pp. 4568-4571. Honolulu, HI.

Oniga, V., & Chirilă, C. (2003). Hausdorff distance for the differences calculation between 3D surfaces. *RevCAD, 15*, pp. 193-202.

Padfield, J. S. (2002). Improvements in the Acquisition and Processing of X-ray Images of Paintings. *National Gallery Technical Bulletin, 23*, pp. 62-75.

Parry, R. (2013). *Museums in a digital age.* London and New York: Routledge.

Pease, M. (1946). A Note on the Radiography of Paintings. *The Metropolitan Museum Bulletin, IV.*

Pelagotti, A., Del Mastio, A., Uccheddu, F., & Remondino, F. (2009). Automated multispectral texture mapping of 3D models. *17th European Signal Processing Conference (EUSIPCO)*, pp. 1215-1219. Glasgo, Scotland.

Pelagotti, A., Pezzati, L., Piva, A., & Del Mastio, A. (2006). Multispectral UV Fluorescence Analysis of painted surfaces. *14th European Signal Processing Conference (EUSIPCO 2006).* Florence, Italy.

Pierrot-Deseilligny, M., De Luca, L., & Remondino, F. (2011). Automated image-based procedures for accurate artifacts 3D modeling and orthoimage generation. *Geoinformatics FCE CTU, 6*, pp. 291-299.

Pinna, G. (2003). Museums and Intangible Heritage. *Intangible heritage in Museums in ICOM News. Newsletter of the International Council of Museums, 56*(4).

Poldi, G., & Villa, G. (2006). *Dalla conservazione alla storia dell'arte. Riflettografia e analisinon invasive per lo studiodei dipinti*. Pisa: Edizioni della Normale.

Proctor, N. (2011). The Google Art Project: A New Generation of Museums on the Web? *Curator. The Museum Journal, 54*(2), pp. 215-221.

Recine, F. (2006). *La documentazione fotografica dell'arte in Italia dagli albori all'epoca moderna*. Napoli: Scriptaweb. Retrieved from: https://books.google.it/books?id=nxjDXw-PWRwC&printsec=copyright&hl=it#v=onepage&q&f=false

Remondino, F. (2011). Heritage recording and 3D modeling with photogrammetry and 3D scanning. *Remote Sensing, 3*(6), pp. 1104-1138.

Remondino, F., & El-Hakim, S. (2006). Image-based 3D modelling: a review. *The Photogrammetric Record, 21*(115), pp. 269-291.

Remondino, F., & Fraser, C. (2006). Digital camera calibration methods: considerations and comparisons. *IAPRS, XXXVI, Part 5*, pp. 266-272. Dresden. Retrieved from: http://www.icsd.aegean.gr/lecturers/kavallieratou/vision_files/Remondino_Fraser_ISPRSV_2006.pdf

Remondino, F., & Menna, F. (2008). Image-based Surface measurement. *International Archives of Photogrammetry, Remote Sensing and Spatial Information Sciences, 37*(B5-1), pp. 199-206.

Remondino, F., Rizzi, A., Barazzetti, L., Scaioni, M., Fassi, F., Brumana, R., & Pelagotti, A. (2011). Review of Geometric and Radiometric Analyses of Paintings. *The Photogrammetric Record, 26*, pp. 439-461.

Ribés, A., Schmitt, F., Pillay, R., & Lahanier, C. (2005). Calibration and spectral reconstruction for cristatel: an art painting multispectral acquisition system. *J. Imaging Sci. Technol., 49*, pp. 563-573.

Romano, F., Caliri, C., Cosentino, L., Gammino, S., Giuntini, L., Mascali, D., Taccetti, F. (2014). Macro and Micro Full Field X-Ray Fluorescence with an X-Ray Pinhole Camera Presenting High Energy and High Spatial Resolution in Analytical chemistry. *Analytical Chemistry, 86*, pp. 10892-10899.

Romano, F., Caliri, C., Santos, H., Pappalardo, L., & Rizzo, F. (2016). Real-time elemental imaging of large area painted artworks with a novel mobile MA-XRF scanner. *EXRS 2016 - European Conference on X-ray Spectrometry*. Gotheborg.

Rothermel, M., Wenzel, K., Fritsch, D., & Haala, N. (2012). SURE: Photogrammetric Surface Reconstruction from Imagery. *Proceedings LC3D Workshop*. Berlin.

Roussou, M. (2002). Immersive Interactive Virtual Reality in the Museum. *TiLe*, p. 2. Athens: Foundation of The Hellenic World.

Roussou, M., & Drettakis, G. (2003). Photorealism and Non-Photorealism in Virtual Heritage Representation. In A. Chalmers, D. Arnold, & F. Niccolucci (Ed.), *Proceedings of the International Symposium on Virtual Reality, Archeology and Cultural Heritage*, p. 10. Brighton, United Kingdom: Eurographics.

Roy, M., Foufou, S., & Truchetet, F. (2002). Generic attribute deviation metric for assessing mesh simplication algorithm quality. *Proceedings of IEEE International Conference on Image Processing*, pp. 817-820.

Rusinkiewicz, S., & Levoy, M. (2001). Efficient variants of the ICP algorithm. *3-D Digital Imaging and Modeling, Proceedings. Third International Conference on*, pp. 145-152. IEEE.

Ruskin, J. (2000). *Le pietre di Venezia*. Milano: Mondadori.

Ruskin, J. (2010). Works. In A. Wedderburn, & E. T. Cook, *The Complete Works of John Ruskin*, vol. 3, p. 210. London: George Allan.

Salerno, E., Tonazzini, A., Grifoni, E., Lorenzetti, G., Legnaioli, S., Lezzerini, M., Palleschi, V. (2014). Analysis of Multispectral Images in Cultural Heritage and Archaeology. *ournal of Applied and Laser Spectroscopy JALS, 1*, pp. 22-27.

Scharstein, D., & Szeliski, R. (2002). A Taxonomy and Evaluation of Dense Two-Frame Stereo Correspondence Algorithms. *International Journal of Computer Vision, 47*(1), pp. 7-42.

Schmidt, R. (2010). Part-Based Representation and Editing of 3D Surface Models. *Ph.D. thesis, University of Toronto, Canada.*

Schmidt, R., & Singh, K. (2010, July). Meshmixer: an interface for rapid mesh composition. *ACM SIGGRAPH 2010 Talks*, p. 6.

Schnabel, R., Wessel, R., Wahl, R., & Klein, R. (2007). *Shape Recognition in 3D Point-Clouds*. Bonn.
Retrieved from:
http://cg.cs.uni-bonn.de/aigaion2root/attachments/cg-2007-1.pdf

Schoning, J., & Heidemann, G. (2015). Evaluation of multi-view 3D reconstruction software. *Computer Analysis of Images and Patterns (CAIP)*, pp. 450-461. Malta.

Schweibenz, W. (2004). Virtual Museums. The Development of Virtual Museums. *ICOM NEWS, 3*.
Retrieved from:
http://icom.museum/fileadmin/user_upload/pdf/ICOM_News/2004-3/ENG/p3_2004-3.pdf

Seccaroni, C., & Moioli, P. (2004). *Fluorescenza X. Prontuario per l'analisi XRF portatile applicata a superfici policrome*. Firenze: Nardini Editore.

Selvatico, P. (1852). L'Arte insegnata nelle Accademie secondo le norme scientifiche. *Atti dellAccademia di Belle Arti*, pp. 7-30. Venezia: Grimoldo.

Selvatico, P. (1859). Sui vantaggi che la fotografia può portare all'arte. In *Scritti d'arte di P. Selvatico Estense*, pp. 337-341. Firenze: Bordera Bianchi Editori.

Selvatico, P. (1870). *Proposta per la riproduzione fotografica dei principali monumenti d'Italia*. Biblioteca Civica di Padova. Padova: unpublished.

Serena, T. (1997). Pietro Selvatico e la musealizzazione della fotografia. *Annali della Scuola Normale Superiore di Pisa. Classe di Lettere e Filosofia, 2(1)*(serie iv), pp. 75-96.

Serena, T. (1997). Pietro Selvatico e la musealizzazione della fotografia, 2(1), serie iv, 75-96. *Annali Della Scuola Normale Superiore Di Pisa. Classe Di Lettere E Filosofia, 2*(1), pp. 75-96.
Retrieved from:
http://www.jstor.org/stable/24308220

Sharf, A., Blumenkrants, M., Shamir, A., & Cohen-Or, D. (2006). SnapPaste: An interactive technique for easy mesh composition. *The Visual Computer, 22*(9), pp. 835–844.

Sharma, N. (2014). A Survey on Surface Reconstruction Algorithms for 3-D Unorganized points. *International Journal of Advanced Research in Computer Science and Software Engineering (IJARCSSE), 4*(4), pp. 675-679.

Signore, O. (2008). The Semantic Web and cultural heritage: ontologies and technologies help in accessing Museum information. In K. Robering, & K. Robering (Ed.), *Information Technology for the Virtual Museum. Museology and the Semantic Web*, pp. 1-32. LIT Verlag.
Retrieved from:
http://www.weblab.isti.cnr.it/projects/archeomed/documents/ITVM.pdf

Signorini, R. (2007). *Alle origini del fotografico. Lettura di "The pencil of nature" (1844-1846) di William Henry Fox Talbot*. Bologna/Pistoia: CLUEB/Petit Pleiade.

Sitnik, R., Mczkowski, G., & Krzeslowski, J. (2010). Integrated shape, color, and reflectivity measurement method for 3D digitization of cultural heritage objects. *Proceedings of SPIE, 3D image Processing and Applications*, *7526*, pp. 75260 1–10. San Jose, CA, USA.

Smargiassi, M. (2015, January 5). *Fotocrazia. Evoluzione e rivoluzioni nel futuro, nel presente e nel passato del fotografico*.
Retrieved from: Smargiassi Michele Blogautore Repubblica: http://smargiassi-michele.blogautore.repubblica.it/2015/01/05/giotto-no-grazie-me-lo-vedo-in-foto/

Snavely, N., Seitz, S., & Szeliski, R. (2008). Modeling the World from Internet Photo Collections. *International Journal of Computer Vision, 80*.

Sonka, M., & Fitzpatrick, J. (2000). *Image Registration. Handbook of Medical Imaging*, vol. 2. (S. PRESS, Ed.) Washington: Bellingham D. L. G. Hill, C.R. Maurer Jr.

Sontag, S. (2004). *Sulla fotografia. Realtà e immagine nella nostra società*. Torino: Einaudi.

St. John, B. (2016, May 17). *An eye for detail: Zoom through 1,000 artworks thanks to the new Art Camera from the Google Cultural Institute.*
Retrieved from Google Official Blog: https://googleblog.blogspot.it/2016/05/art-camera-cultural-institute.html

Szeliski, R. (2010). *Computer vision: algorithms and applications.* Springer Science.

Taylor, J., Beraldin, J.-A., Godin, G., Cournoyer, L., & Domey, J. (2003). NRC 3D technology for museum and heritage applications. *J. Vis. Comput. Animat., 14*, pp. 121-138.

Tonazzini, A., Bedini, L., & Salerno, E. (2004). Independent component analysis for document restoration. *International Journal on Document Analysis and Recognition, 7*, pp. 17-27.

Tonazzini, A., Gerace, I., & Martinelli, F. (2010). Multichannel blind separation and deconvolution of images for document analysis. *IEEE Transactions on Image Processing, 19*(4), pp. 912-925.

Tonsho, K., Akao, Y., Tsumura, N., & Miyake, Y. (2001). Development of goniophotometric imaging system for recording reflectance spectra of 3d objects. *Proceedings of SPIE, Color Imaging: Device-Independent Color, Color Hardcopy and Applications*, *VII, 4663*, pp. 370-378.

Triggs, B., McLauchlan, P., Hartley, R., & Fitzgibbon, A. (2002). Bundle Adjustment — A Modern Synthesis. *Lecture Notes in Computer Science, 1883*, pp. 298-372.

Tsai, R. (1987). A versatile Camera Calibration Technique for High-Accuracy 3DMachine Vision Metrology Using Off-theShelf TV Cameras and Lenses. *IEEEJournal of Robotics and Automation, RA-3*(4), pp. 323-344.

Turk, G., & Levoy, M. (1994). Zippered polygon meshes from range images. *Proceedings of SIGGRAPH*, pp. 311-318.

Valery, P. (1964). The Conquest of Ubiquity. In P. Valery, *Aesthetics*, p. 225. New York: Pantheon Books.

van Asperen de Boer, J. (1968). Infrared reflectography: a method for the examination of paintings. *Appl. Opt., 7*, pp. 1711-1714.

Van Asperen de Boer, J. (1969). Reflectography of paintings using an infrared vidicon television system. *Studies in conservation, 14*(3), pp. 96-118.

Verhoeven, G. (2011). Taking computer vision aloft—Archaeological three-dimensional reconstructions from aerial photographs with PhotoScan. *Archaeol. Prospect., 18*, pp. 67-73.

Vermehren, A. (1952). Sulle possibilità stereo-strato-radiografiche di un nuovo tipo di apparecchio a raggi x in dotazione presso l'istituto centrale del restauro in Roma. *Bollettino dell'Istituto centrale del restauro* (11-12), pp. 121-133.

Villmann, T., Merényi, E., & Hammer, B. (2003). Neural maps in remote sensing image analysis. *Neural Networks, 16*(3-4), pp. 389-403.

Viola, P., & Wells, W. (n.d.). Alignment by maximization of mutual information. *IJCV, 24*, pp. 137-154.

Walsh, P. (2007). Rise and Fall of the Post-Photographic Museum: Technology and the Transformation of Art. In F. Cameron, & S. Kenderdine (Eds.), *Theorizing Digital Cultural Heritage: A Critical Discourse*, pp. 19-34. Cambridge: MIT Press.

Westoby, M., Brasington, J., Glasser, N., Hambrey, M., & Reynolds, J. (2012). 'Structure-from-Motion' photogrammetry: A low-cost, effective tool for geoscience applications, *179*, pp. 300-314.

Witcomb, A. (2007). The Materiality of Virtual Technologies: A New Approach to Thinking about. In F. Cameron, & S. Kenderdine, *Theorizing Digital Cultural Heritage. A critical discourse*, pp. 35-48. Boston: MIT Press.

Wold, S., Esbensen, K., & Geladi, P. (1987). Principal component analysis. *Chemometrics and Intelligent Laboratory Systems, 2*, pp. 1-3, 37-52.

Wolf, P., & DeWitt, B. (2000). *Elements of Photogrammetry* (3rd ed.). Boston: McGraw Hill.

Yanagi, H., & Chikatsu, H. (2016). Performance evaluation of 3D modeling software for UAV photogrammetry. *ISPRS - International Archives of the Photogrammetry, Remote Sensing and Spatial Information Sciences, XLI*(B5), pp. 147-152.

Yastikli, N. (2007). Documentation of cultural heritage using digital photogrammetry and laser scanning. *Journal of Cultural Heritage, 8*, pp. 423-427.

Yu, C.-H., & Hunter, J. (2013). Documenting and sharing comparative analyses of 3D digital museum artifacts through semantic web annotations, n. 18. *Journal of Computing for Cultural Heritage, 6*(4).

Yu, Y., Wu, Q., Khan, Y., & Chen, M. (2015). An adaptive variation model for point cloud normal computation. *Neural Computing and Applications, 26*(6).

Zia, A., Liang, J., Zhou, J., & Gao, Y. (2015). 3D Reconstruction from Hyperspectral Images. *WACV '15 Proceedings of the 2015 IEEE Winter Conference on Applications of Computer Vision*, pp. 318-325.

Acknowledgments

To Stefano, who engaged me with passion for our field. Without him this thesis would have never existed.

A very special thankfulness.

To every single person of the ICCOM group of Pisa that welcomed me and allowed me to spend the most intense years of my *not only working* life.

All my best appreciation.

To all my Comrades. Always close, always present.

All my most sincere esteem.

To Alessandro, who has been and is the most essential person to me.

A truly *immense* gratitude and love.

In the odious invasion of unreality, Art, which expresses reality, might represent almost the sole hope for the world.

The nature of Art is liberating and thus, in its effects, revolutionary.

E. Morante